THERE AND BACK AGAIN: DEVELOPING A XENOGRAFT MODEL OF SPORADIC INCLUSION BODY MYOSITIS FOR TRANSLATIONAL RESEARCH

by
Kyla A. Britson

A dissertation submitted to Johns Hopkins University in conformity with the requirements for the degree of Doctor of Philosophy.

Baltimore, Maryland
March 2020

© 2020 Kyla A. Britson
All Rights Reserved

Abstract

The absence of an animal model for sporadic Inclusion Body Myositis (IBM) has hindered progress in the field including an incomplete understanding of pathogenesis and a lack of effective therapies. We have developed a novel xenograft model of IBM in which human skeletal muscle is transplanted into immunodeficient NOD-Rag1^{null}IL2rγ^{null} mice. These grafts are spontaneously revascularized and innervated by the mouse host to form a fully functional human muscle ideal for modeling disease. At 4 months, xenografts from control and IBM patients both display robust regeneration, indicating that IBM patient satellite cells can proliferate and differentiate normally. In addition, pathological features of IBM are recapitulated within xenografts, including endomysial inflammation, primary invasion of non-necrotic fibers by CD3+ T cells, upregulation of MHC-I, and COX-deficient fibers. Ki-67 staining reveals that a majority of the CD8+ T cells within IBM xenografts are proliferative at 4 months, and T cell receptor sequencing shows that these T cells are oligoclonal. Removal of CD3+ T cells via treatment of mice with a monoclonal CD3 antibody (OKT3) does not significantly impact regeneration, indicating that myofiber regeneration is largely unaffected by T cells within xenografts. However, OKT3 significantly reduces the number of COX-deficient fibers suggesting that T-cell mediated inflammation drives mitochondrial pathology. Indeed, the number of COX-deficient fibers is significantly correlated with the number of CD3+ T cells in IBM xenografts but not in control myositis xenografts with comparable numbers of T cells. In addition to these inflammatory features, splicing defects due to loss of nuclear TDP-43 and rare fibers containing p62-positive aggregates are observed at later timepoints (8-10 months). Thus, this xenograft model of IBM shows both inflammatory and degenerative features of the human disease, and this model will be valuable for carrying out mechanistic studies and preclinical therapeutic testing in IBM.

Thesis Readers:

Primary Reader and Advisor:

Dr. Thomas E Lloyd, MD, PhD

Departments of Neurology and Neuroscience, Johns Hopkins University School of Medicine

Secondary Reader:

Dr. H. Benjamin Larman, PhD

Department of Pathology, Johns Hopkins University School of Medicine

Thesis Committee Members:

Dr. Thomas E Lloyd, MD, PhD (Thesis Advisor)

Dr. H. Benjamin Larman, PhD

Dr. Andrew L. Mammen, MD, PhD

Dr. Anthony Cammarato, PhD

Dr. Kathryn R. Wagner, MD, PhD (Chair)

Acknowledgements

First and foremost, I would like to thank my thesis advisor Dr. Tom Lloyd for his support throughout my thesis research. It is no small task for someone who has extensive experience in *Drosophila* research to mentor someone through a mouse project. When I joined the Lloyd lab in May of 2016, the ongoing projects in the lab were based largely on modeling degenerative neurological diseases in *Drosophila,* and the Xenograft Project was in its infancy. I spent my first year in lab splitting my time between a *Drosophila* model of IBMPFD and the Xenograft Project, but it was only a matter of time before the Xenograft Project demanded my full attention. Tom told me that the xenograft project was “high risk, but high reward” and time has shown that to be true. Tom’s passion for Inclusion Body Myositis is infectious, and I greatly appreciate that he gave me the opportunity to study the disease for my thesis research. The xenograft project will undoubtedly remain a foundation of the Lloyd Lab for years to come and that wouldn’t have been possible without Tom’s guidance.

A large part of the success of this project also lies in the hands of Dr. Kathryn Wagner—Chair of my thesis committee—and Dr. Aaron Black and Dr. Tracy Zhang of the Wagner Lab. With their help I was able to fully master the xenograft technique. In addition, Kathryn’s insight and suggestions during my thesis committee meetings were always incredibly valuable. I also want to thank my entire thesis committee—Dr. Ben Larman, Dr. Andy Mammen, and Dr. Anthony Cammarato—for guiding me throughout my thesis research. I’m still sorry that several of you got trapped in staircases of the Rangos Building on your way to my thesis committee meetings.

Dr. Debbie Andrew, Dr. John Meitzen and Dr. Mark Decker are three people I can never thank enough for their mentorship throughout my research career and the innumerable letters of recommendation they wrote on my behalf. John and Mark wrote the letters that helped me get all of my summer research internships and landed me the position in Debbie's lab after graduating from college. The three of them ensured my successful application to graduate school, and I know I wouldn't be where I am now without their enthusiastic support.

I want to thank Dr. Lyle Ostrow and Dr. Andrea Corse for their surgical expertise. Without them, we wouldn't have been able to carry out this Xenograft project, and I greatly appreciate their flexibility working with me as I added yet another complication to their busy surgical schedules.

To current and former members of the Lloyd lab, thank for you for making graduate school a far better experience than I could have ever hoped for. In particular, I would like to thank Mark Wilhem, Andrew Cheng, Kathryn Gallo, and Nicole Reed for their technical support, and Brian Woolums and Kathleen Cunningham, you were the best lab siblings I could have asked for.

I would like to thank the Cellular and Molecular Medicine program, especially Leslie Lichter-Mason and Colleen Graham for their administrative support, and director Dr. Rajini Rao.

Finally, I would like to thank my family for a lifetime of support. My parents Curt and Nancy were always there to remind me it's ok to take a break and that grades were only

grades. You can both finally say that all your kids have graduated from school. My brothers Derek and Jared heroically tried to understand my science, while I did the same for their jobs, and they were the best reality check I could have asked for when they thought I was getting too big for my britches. To my wonderful partner James, it is always a comfort to know at the end of any day in lab, good or bad, I always have you to tell about it and will for the rest of my life.

Dedication

This dissertation is dedicated to every patient who consented to be a participant in this Xenograft Project. As much as I contributed my metaphorical blood, sweat, and tears to this project, they truly gave a piece of themselves for this work, and I am forever grateful.

Contents

Abstract ii

Acknowledgements iv

Dedication vii

List of Tables ix

List of Figures x

Chapter 1: Introduction 1

1.1 History of Inclusion Body Myositis 1
1.2 The Presentation of Inclusion Body Myositis 3
1.3 Genetics of Inclusion Body Myositis 9
1.4 Current Treatments and Ongoing Clinical Trials 17
1.5 Laboratory Models of Inclusion Body Myositis 21

Chapter 2: Using Xenografts to Study Human Disease 25

2.1 The Use of Patient Derived Xenografts in Cancer 25
2.2 Using Xenografts to Study Muscle Disease 27

Chapter 3: A Surgical Description of the Xenograft Technique 30

3.1 Introduction 30
3.2 Protocol 31
3.3 Results 42
3.4 Discussion 45

Chapter 4: Methods 48

Chapter 5: A Xenograft Model of Inclusion Body Myositis 56

5.1 Overview and Aims 56
5.2 Inclusion criteria and patient characteristics 57
5.3 IBM xenografts regenerate robustly in NRG mice 59
5.4 IBM xenografts recapitulate disease pathology 61

Chapter 6: Preclinical Testing in the IBM Xenograft Model 71

6.1 Overview and Aims 71
6.2 Irradiation of IBM Xenografts 72
6.3 Depleting T cells in IBM Xenografts with monoclonal CD3 antibody OKT3 79

Chapter 7: Discussion and Future Directions 88

References 97

Curriculum Vita 114

List of Tables

Table 3.1 Materials for Xenograft Surgery. 39
Table 4.1 Primer Sequences for Cryptic Exon Detection 53
Table 5.1 Characteristics of xenograft study population 58
Table 6.1 Patient Characteristics - Irradiation Experiments 74
Table 6.2 Patient Characteristics - OKT3 Experiments 80

List of Figures

Figure 3.1 Xenograft Surgery 40
Figure 3.2 Xenograft Collection 41
Figure 3.3 Expected Positive and Negative Results 43
Figure 3.4 Representative Xenograft Regeneration 44
Figure 4.1 Protocol for Cryptic Exon Product Amplification 52
Figure 5.2 IBM xenografts show p62 aggregation and TDP-43 cryptic exon expression 63
Figure 5.3 IBM xenografts display mitochondrial pathology 65
Figure 5.4 Endomysial inflammation and primary invasion in IBM xenografts 68
Figure 5.5 T cells in IBM xenografts are proliferative, antigen experienced, and oligoclonal 69
Figure 6.1 Histological Features of Human Biopsies - Irradiation Experiments 75
Figure 6.2 Irradiation of xenografts severely impairs control regeneration and does not reduce inflammation. 77
Figure 6.3 Fiber Morphology and T cell quantification of 4-month Irradiated and Untreated xenografts. 78
Figure 6.4 Histological Features of Human Biopsies - OKT3 Experiments . 81
Figure 6.5 OKT3 eliminates T cells from IBM Xenografts 83
Figure 6.6 Myofiber regeneration is unaffected by T cells 84
Figure 6.7 The distribution of myofiber CSA is unchanged by OKT3 treatment 85
Figure 6.8 T cell-mediated inflammation drives mitochondrial pathology .. 87

Chapter 1: Introduction

“It’s not life-threatening, it’s life-changing.”

-Peter Frampton, 2019

When Peter Frampton publicly announced his diagnosis of Inclusion Body Myositis (IBM) in 2019, he shined a spotlight on this rare disease, which affects ~50 patients per million according to a recent meta-analysis study (Callan et al. 2017). IBM is a chronic disease of progressive skeletal muscle weakness with both degenerative and autoimmune pathological features. The field of IBM research faces many challenges, such as the uncertain pathogenesis, a struggle to develop effective treatments, and the lack of awareness in the general population as well as the medical community. A brief history of IBM, its clinical and pathological presentation, laboratory models, and treatment approaches for this life-changing disease are discussed below.

1.1 History of Inclusion Body Myositis

The first published description of IBM resides within a case study of a 66 year old man erroneously diagnosed with chronic polymyositis (PM) (Chou 1967). This patient presented with progressive weakness of all muscles over the course of 6 years, mild dysphagia, and muscle atrophy of the shoulder girdle and quadriceps. Of note, there was no significant elevation of creatine kinase (CK), whereas CK levels in PM patients are typically elevated 10-50 fold (Schmidt 2018). In hindsight, it is clear this study describes an IBM patient. A major novel finding of this study was the detection of filamentous aggregates via electron microscopy in both the sarcoplasm and nucleus of

patient myofibers. Based on the morphological similarity of the filaments to structures observed in cultured myxovirus-infected cells, it was hypothesized that the patient's disease was caused by a viral infection. In subsequent years, numerous studies have explored the association and potential contribution of viral infections to the development of IBM (Nishino, Engel, and Rima 1989; Kallajoki et al. 1991; Fox et al. 1996; Uruha et al. 2016).

A case study from 1971 is responsible for the etymology of 'Inclusion Body Myositis', although, this study actually described a patient that likely had limb-girdle muscular dystrophy (Yunis and Samaha 1971). It took an additional seven years for the first 'accurate ' clinical case study of IBM to be published (Carpenter et al. 1978). In this study, 6 patients were described showing progressive muscle weakness frequently involving distal muscles, a male predominance, and no improvement with corticosteroid treatment. Pathologically abnormal filaments could also be detected in the muscle using electron microscopy, and "hematoxylinophilic granules in "lined" vacuoles"—rimmed vacuoles—were described for the first time (Carpenter et al. 1978). This case study established IBM as a discrete entity within the group of idiopathic inflammatory myopathies (IIM). IIM is a heterogeneous group of diseases characterized by skeletal muscle weakness, and the intramuscular infiltration of immune cells (Dalakas 2015). Currently, this group also includes Dermatomyositis (DM), Polymyositis (PM), Immune Mediated Necrotizing Myopathy (IMNM), and non-specific myositis (Hoogendijk et al. 2004; Dalakas 2015). From these initial descriptions, the characteristics of IBM have been further researched and refined.

1.2 The Presentation of Inclusion Body Myositis

IBM patients have a heterogeneous presentation, and diagnosis is rarely straightforward with almost half of patients initially misdiagnosed with polymyositis, peripheral neuropathy, or motor neuron disease (Rose and ENMC 2013; Paltiel et al. 2015). Patients typically seek medical care when their muscle weakness limits the use of their hands or when they start to have difficultly climbing stairs or falls (Paltiel et al. 2015). The median time from symptom onset to diagnosis is between 5 to 6 years, and patients lose the ability to independently ambulate an average of 15 years after diagnosis (Needham, Corbett, et al. 2008; Molberg and Dobloug 2016). The diagnosis of IBM requires a careful assessment of a patient's clinical features, which commonly includes physical exam, electrodiagnostic testing, blood testing, and in some centers, MRI of affected muscle groups. In addition, a thorough pathological analysis of a skeletal muscle biopsy is typically an important component of the diagnostic process.

Clinical Presentation

IBM has a male predominance and usually affects individuals over the age of 45 with a mean age of symptom onset between 61-68 years (Molberg and Dobloug 2016; Suzuki et al. 2016; Greenberg 2019). The disease is characterized by chronic, slowly progressive asymmetric weakness of both proximal and distal muscles, with the finger flexors and quadriceps typically most affected (Griggs et al. 1995). Dysphagia is observed in more than half of patients, with some studies reporting an incidence of greater than 80% (Wintzen et al. 1988; Houser, Calabrese, and Strome 1998; Mohannak et al. 2019). Cardiac abnormalities in IBM patients have not been extensively explored, but several studies suggest that cardiac function is largely unaffected. (Cox et al. 2010;

Rosenbohm et al. 2020). However, patients with IBM may be predisposed to hypertension and show higher rates of myocardial infarction and congestive heart failure (Keshishian et al. 2018; Rosenbohm et al. 2020).

MRI studies of IBM patients show fatty infiltration and inflammation in affected muscles, especially in the flexor digitorum profundus (FDP), vastus medialis and lateralis, and gastrocnemius (Phillips et al. 2001; Cox et al. 2011; Guimaraes et al. 2017; Ansari et al. 2020). Assessment of FDP via MRI, electromyography (EMG), or ultrasonography may be particularly helpful in discriminating IBM from other IIMs and aid in diagnosis (Sekul, Chow, and Dalakas 1997; Hokkoku et al. 2012; Albayda et al. 2018). In contrast to the other forms of IIM, it is rare to observe a serum CK level more than 15 times the upper limit of normal (Rose and ENMC 2013). Another feature of IBM that distinguishes it from other IIMs are neurogenic findings in over 20% of IBM patients, including neuropathic-like recruitment patterns on EMG (Felice and North 2001; Hermanns, Molnar, and Schroder 2000). The most important clinical features in establishing a diagnosis are the history and pattern of weakness on physical exam, with finger flexor weakness greater than arm abductor weakness and knee extensor weakness greater than hip flexor weakness. In combination, these clinical features alone can be sufficient for a diagnosis of IBM by some diagnostic criteria. This has led some clinicians to question the necessity of a diagnostic open muscle biopsy, however, biopsies are routinely performed on IBM patients as they show several distinguishing pathological features and can be very helpful in confirming a diagnosis (Brady, Squier, and Hilton-Jones 2013).

Pathological Features

The pathological features of IBM are diverse and, although these features are shared with other disorders, in combination, they are highly specific for IBM. Histological features observed in IBM muscle biopsies include rimmed vacuoles, protein aggregates, cytochrome c oxidase (COX)-deficient fibers, upregulation of major histocompatibility complex class I (MHC-I) molecules, and an endomysial inflammatory infiltrate (reviewed in:Naddaf, Barohn, and Dimachkie 2018; Greenberg 2019). A considerable effort has been put forth by researchers to characterize the variety of aggregated proteins, and by 2010 more than 80 proteins had been reported as present within aggregates in IBM patient muscle, including ubiquitin, tau, and β-amyloid (Greenberg 2010b). In this overabundance of aggregated proteins, TDP-43 and p62 have been suggested to have high specificity for IBM and are seen aggregated in a high percentage of fibers (Dubourg et al. 2011; Hiniker et al. 2013).

Mitochondrial pathology has been recognized as a prominent feature of IBM, including myofibers that accumulate abnormal mitochondria, COX-deficient fibers, and mitochondrial DNA (mtDNA) deletions and depletion (Oldfors et al. 1993; Oldfors et al. 2006; Lindgren et al. 2015; Bhatt et al. 2019). While the number of COX-deficient fibers normally increases with age, the proportion of COX-deficient fibers is significantly higher in IBM patients (Oldfors et al. 1993). Electron microscopy of affected muscle shows enlarged mitochondria, loss of inner membrane cristae, and paracrystalline inclusions, although, is it important to note these changes are also associated with normal aging (Oldfors et al. 2006). Decreased transcript and protein levels of mitofusion-2 (MFN2) and optic atrophy 1 (OPA1)—genes involved in mitochondrial fusion—in IBM muscle suggest fusion is impaired and may partially explain this altered mitochondrial morphology

(Catalan-Garcia et al. 2016). In addition to these morphological changes, downregulated expression of complex I (NADH coenzyme Q oxidoreductase) and reduced COX activity indicates impaired oxidative phosphorylation in IBM muscle (Lindgren et al. 2015; Rygiel et al. 2015). Interestingly, positive correlations have been reported between the number of COX-deficient muscle fibers and the relative amount of mtDNA deletions as well as the severity of inflammation (Lindgren et al. 2015; Rygiel et al. 2015). These studies suggest that mitochondrial pathology may be mechanistically linked with inflammation. It is possible that inflammatory cells could trigger mtDNA damage, eventually leading to respiratory dysfunction and subsequent degeneration of muscle fibers.

The invasion of non-necrotic fibers by autoaggressive cytotoxic CD8+ T cells is a prominent feature of IBM muscle biopsies, and this inflammatory infiltrate has been a focus of numerous studies. T cell receptor (TCR) sequencing or spectratyping of cells from patient blood and muscle has shown these populations of T cells are clonally expanded, suggesting recognition of an unknown antigen is occurring (Amemiya 2000; Müntzing et al. 2003; Salajegheh et al. 2007). Recent microarray and mass cytometry studies have revealed a distinctive signature of T cell cytotoxicity in IBM muscle and blood in comparison to other muscle diseases and an abundance of highly differentiated CD8+ T-cell effector memory (TEMRA) cells and terminally differentiated effector cells (Greenberg et al. 2019; Dzangue-Tchoupou et al. 2019). This cytotoxic signature shows elevation of granzymes A, B, H, and K, perforin, and increased expression of KLRG1 (killer cell lectin-like receptor G1) and T-bet (T-box expressed in T cells) which are markers of highly differentiated CD8+ T cells. KLRG1 is an inhibitory T- and NK-cell receptor associated with increased cytotoxic activity, and high levels of T-bet are required for antigen-specific CD8+ response and cytotoxic function (Hruz et al. 2008;

Greenberg et al. 2019; Dzangue-Tchoupou et al. 2019). In particular, KLRG1+ cells were shown to be present in multifocal endomysial infiltrates and observed invading muscle cells. Taken together, KLRG1 and T-bet may serve as useful biomarkers for IBM, and it is hypothesized that therapeutic targeting of these highly differentiated cytotoxic T cell populations may be beneficial for the treatment of IBM.

Beyond cell-mediated immune responses, microarray analysis of IBM patient muscle has revealed an overabundance of immunoglobulin gene transcripts and intramuscular CD138+ plasma cells, suggesting a previously unappreciated role of humoral immune mechanisms in IBM (Greenberg et al. 2005). In 2011, the first circulating autoantibody in IBM was discovered, and shortly thereafter two groups independently identified cytosolic 5′-nucleotidase 1A (NT5C1A; cN1A) as the target of this circulating autoantibody (Salajegheh, Lam, and Greenberg 2011; Larman et al. 2013; Pluk et al. 2013). These initial studies showed that serum positivity of anti-NT5C1A was highly specific—90-95%--for the diagnosis of IBM. Further analysis of additional patient cohorts have supported this high specificity, but the sensitivity varies widely from 37% to 76% (Greenberg 2014; Lloyd et al. 2016; Amlani et al. 2019). Part of this variation could be explained by the different tests used to detect anti-NT5C1A, and the antibody has also been detected in other disorders such as systemic lupus erythematosus (SLE) and Sjögren's syndrome at varying levels of prevalence (Rietveld et al. 2018). Overall, serum negativity for anti-NT5C1A should not discourage a diagnosis of IBM, and more studies are needed to determine the diagnostic utility of anti-NT5C1A in IBM.

Diagnostic Guidelines

The first diagnostic criteria proposed by Griggs et al relied heavily on the pathological

features of IBM and divided patients into two categories: definite or possible IBM (Griggs et al. 1995). A definite diagnosis of IBM required muscle biopsies to show all the following: mononuclear cell invasion of non-necrotic muscle fibers, vacuoles, and amyloid deposits or 15-18 nm tubulofilaments. If a muscle biopsy showed these features the patient would be diagnosed with definite IBM regardless of any other clinical or laboratory features. If a patient biopsy only showed invasion of mononuclear cells, then a combination of clinical and laboratory features would allow a diagnosis of possible IBM. Understandably, these strict criteria lacked sensitivity as one or more of these pathological features are often missing in IBM biopsies (Chahin and Engel 2008; Ikenaga et al. 2017). Therefore, an international group of experts met to review and update diagnostic criteria for IBM and established the ENMC IBM Research Diagnostic Criteria 2011 (Rose and ENMC 2013).

The ENMC 2011 criteria divides IBM diagnosis into three classifications: clinico-pathologically defined IBM, Clinically defined IBM, or Probable IBM. Unlike the Griggs criteria, this updated classification considers the patient's clinical presentation. To be diagnosed with clinico-pathologically defined IBM patients must meet the following criteria: they must be over the age of 45, have a serum CK less than 15 times the upper limit of normal, with finger flexor and/or knee extension muscle weakness lasting more than a year, and muscle biopsies showing endomysial inflammation, rimmed vacuoles, and protein aggregation or 15-18nm filaments (Rose and ENMC 2013). Assessment of ENMC 2011 diagnostic criteria via machine learning approaches showed its "Probable IBM" classification performed the best with 90% sensitivity and 96% specificity (Lloyd et al. 2014). The Probable IBM classification requires patients to be over the age of 45, a serum CK less than 15 times the upper limit of normal, with finger flexor or knee

extension muscle weakness lasting more than a year, and muscle biopsies showing one or more of the following: endomysial inflammation, upregulation of MHC-I, rimmed vacuoles, or protein aggregation/15-18nm filaments (Rose and ENMC 2013).

More recently, the European League Against Rheumatism (EULAR) and the American College of Rheumatology (ACR) has developed a new classification criteria for IIMs (Bottai et al. 2017). When using muscle biopsy features in combination with clinical factors the EULAR/ACR criteria had high sensitivity (93%) and high specificity (88%), and by comparison the ENMC 2011 had low sensitivity despite its high specificity. Needless to say, as research progresses new criteria will continue to be proposed with the goal of improving the diagnostic process for both patients and clinicians.

1.3 Genetics of Inclusion Body Myositis

This section is adapted from Britson, K.A., Yang, S.Y., and Lloyd, T.E. New Developments in the Genetics of Inclusion Body Myositis. Curr Rheumatol Rep. 2018 Apr 2;20(5):26. doi: 10.1007/s11926-018-0738-0 (Britson, Yang, and Lloyd 2018).

Introduction

In 1990, IBM was referenced in 11 citations in the PubMed database maintained by the United States National Library of Medicine at the National Institutes of Health (Pubmed 2020). Over the last decade the average number of citations has risen to 85 per year. Part of this growth can be attributed to the increasing number of sequencing studies performed on IBM patient samples, which has been made possible by a concerted effort by several international groups to develop patient biospecimen banks and databases of

clinical information. Two groups that have been instrumental in these efforts are the Myositis Genetics Consortium (MYOGEN) and the International IBM Consortium Genetic Study (IIBMCGS).

At this point, it is crucial to draw a distinction between IBM and hereditary Inclusion Body Myopathies (HIBMs). The latter is a group of genetic muscle disorders with either autosomal recessive or dominant inheritance, and includes Glucosamine (UDP-N-acetyl)-2-epimerase/N-acetylmannosamine kinase gene (GNE) myopathy, hereditary inclusion-body myopathy with Paget's disease of the bone and frontotemporal dementia (IBMPFD), and HIBM with congenital joint contractures and external ophthalmoplegia (Broccolini and Mirabella 2015). Although rare patients with genetic muscle disease have been reported with clinical phenotypes indistinguishable from IBM (Roda et al. 2014), HIBMs typically present at a younger age than IBM (before age 40), lack inflammation, and display different patterns of muscle weakness (Leung et al. 2014; Broccolini and Mirabella 2015). For example, GNE myopathy—also called HIBM2—is caused by autosomal recessive inheritance of mutations in the GNE gene, the quadriceps is typically spared, and biopsy shows rimmed vacuoles and protein inclusions but lacks inflammation (No et al. 2013; Huizing et al. 2014; Carrillo, Malicdan, and Huizing 2018). Thus, mutations in known HIBM genes cause syndromes that share degenerative features on biopsy but otherwise are clinically distinct from IBM. However, classic IBM can occasionally be present within multiple family members (“familial IBM”) strongly supporting a role for genetic risk factors in the development of IBM (Sivakumar, Semino-Mora, and Dalakas 1997; Ranque-Francois et al. 2005). The advent of high-throughput sequencing technologies and the efforts of genetic consortiums have begun to shed light on the complex genetic landscape of IBM.

HLA Locus: the strongest risk alleles for IBM

Robust, unbiased genome-wide association studies (GWAS) have not yet been completed in IBM due to the rarity of the disease, though a large multinational effort is underway (Gang, Bettencourt, Houlden, et al. 2015). Nonetheless, since first described by Garlepp et al in 1994, the Human Leukocyte Antigen (HLA) locus has been shown repeatedly to contain the strongest risk alleles for the development of IBM (Garlepp et al. 1994; Rojana-udomsart et al. 2012; Johari et al. 2017; Rothwell et al. 2017). Recently, the Myositis Genetics Consortium (MYOGEN) analyzed immune-related genes in 252 Caucasian IBM patients and 1,008 ethnically-matched controls from 11 countries using the Illumina Immunochip array (Rothwell et al. 2017). Variants within the HLA locus were the only single-nucleotide polymorphisms (SNPs) to reach genome-wide significance ($p < 5 \times 10^{-8}$). HLA-DRB1*03:01 showed the most significant association with IBM ($p = 5.77 \times 10^{-34}$), followed by HLA-DRB1*01:01 ($p = 1.57 \times 10^{-16}$), and HLA-DRB1*13:01 ($p = 3.28 \times 10^{-8}$). This finding is consistent with prior HLA-association studies identifying an association of IBM with the 8.1 ancestral MHC haplotype (8.1 AH) (Garlepp et al. 1994; Badrising et al. 2004; Mastaglia 2009; Needham, James, et al. 2008). Contrary to previous results that HLA-DRB4 is protective and ameliorates the risk effect of HLA-DRB1*03:01 (Rojana-udomsart et al. 2012), no HLA alleles were found to modify disease onset or severity of IBM in this study. Furthermore, in agreement with a study performed in an Australian cohort, there was no distinct HLA association with anti-cytosolic 5'-nucleotidase 1A (anti-NT5C1A) positivity (Rothwell et al. 2017; Limaye et al. 2016).

To investigate whether the risk associated with these HLA-DRB1 alleles could be explained by specific amino acid positions shared between alleles, amino acid

imputation was performed. A tyrosine residue at position 26 was found to be more strongly associated with IBM ($p < 5.22 \times 10^{-43}$) than the HLA-DRB1 allele alone, and an additional independent effect was seen at position 11 ($p < 3.8 \times 10^{-13}$) for serine. Of note, previous studies have associated positions 11 and 26 with other autoimmune diseases such as systemic lupus erythematosus (Kim et al. 2014). Both of these residues are located within the β-sheet floor of DR β-chain 1 that forms part of the peptide-binding groove and may influence peptide binding and predispose individuals to autoimmunity (Rothwell et al. 2017). Interestingly, although HLA-DRB1*03:01 is also a significant risk factor for Polymyositis (PM) and Dermatomyositis (DM), amino acid position 74 explains almost all of the risk within the allele for PM and DM (Rothwell et al. 2016).

NOTCH4, a previously identified risk gene within the HLA locus (Scott et al. 2012), was not explicitly examined in this study due to its strong linkage disequilibrium with the 8.1 AH. Three regions outside of the HLA locus that almost reached the level of genome-wide significance ($p < 2.25 \times 10^{-5}$) included a known frameshift mutation in CCR5 that causes a nonfunctional receptor (Rothwell et al. 2017). CCR5 (C-C Chemokine Receptor type 5) is an important regulator of T-cell migration, suggesting a potential role for chemokines in the pathogenesis of IBM. A recent case-control study analyzing whole exome sequencing data on 30 Finnish IBM patients identified seven SNPs found at >2-fold higher frequency in IBM, and in addition to the HLA locus, implicated genes that regulate sphingolipid transport as potential IBM risk factors (Johari et al. 2017). Overall, these recent studies have confirmed that variants within the HLA locus are risk factors for developing IBM

Genetic Variants Identified in Pathways Related to Proteostasis

As mentioned previously, both IBM and HIBM syndromes share degenerative myopathic features on biopsy including rimmed vacuoles, ubiquitinated protein aggregates, and 15-18 nm tubulofilamentous “inclusions” observed with electron microscopy. A known cause of this pathology shared with many degenerative diseases is disruption of protein homeostasis, or proteostasis, as can be caused by impairment of the proteasome or autophagy (reviewed in: Klaips, Jayaraj, and Hartl 2018). For example, IBMPFD is a multisystem degenerative disease caused by autosomal dominant inheritance of missense mutations in valosin-containing protein (VCP) (Watts et al. 2004). VCP, also called p97 or cdc48, is a highly conserved homohexameric ATPase that functions as a “segregase” to remove ubiquitinated proteins from macromolecular complexes, and thus plays an important role in proteostasis (Meyer and Weihl 2014).

Intriguingly, rare VCP variants have recently been implicated in IBM as well as multiple neurodegenerative diseases including Frontotemporal Dementia (FTD), Parkinson’s Disease, Amyotrophic Lateral Sclerosis (ALS), and Charcot-Marie Tooth Disease (Johnson et al. 2010; Koppers et al. 2012; Majounie et al. 2012; Spina et al. 2013; Gonzalez et al. 2014). Rare mutations in other genes, including HNRPA1, HNRPA2B1, and SQSTM1 have also been found to cause similar autosomal dominantly inherited degenerative diseases affecting muscle, bone, and brain, and have been termed “multisystem proteinopathy”, or MSP (Benatar et al. 2013). As with HIBM, MSP patients usually present before age 40 without the typical IBM pattern of weakness, and affected muscles in MSP display rimmed vacuoles and protein inclusions but lack inflammation. However, recent findings suggest that rare variants in these MSP genes may increase the risk for developing IBM.

Using targeted next generation sequencing, Weihl et. al. screened a cohort of 79 IBM patients for variants in 38 genes associated with muscular dystrophies, myopathies, ALS, and dementia (Weihl et al. 2015). This candidate-based approach uncovered an increased frequency of rare variants in multiple genes including VCP, SQSTM1, FLNC, ZASP, and BAG3 as well as a novel variant in HNRPA2B1. FLNC, SQSTM1, ZASP, and BAG3 are known to be mutated in rare inherited vacuolar myopathies and also play integral roles in the autophagy pathway (Ruparelia et al. 2016; Behl 2011; Baixauli, López-Otín, and Mittelbrunn 2014). SQSTM1 (Sequestosome 1, also known as p62) is a ubiquitin-binding autophagic adaptor that has been shown to label protein inclusions in IBM muscle (Nogalska et al. 2009; Dubourg et al. 2011; Ikenaga et al. 2017). The two rare variants identified in VCP were previously reported as putative disease-associated variants (Majounie et al. 2012; Kimonis et al. 2008; Rohrer et al. 2011), and expression of these variants in cell culture causes an accumulation of the autophagosome markers p62 and LC3-II, suggestive of a disruption in autophagy (Ju et al. 2009). Similarly, other candidate-based whole exome sequencing (WES) approaches have also identified rare VCP variants in IBM in addition to SQSTM1 (Gang et al. 2016) and ZASP (Cai et al. 2012). The majority of these variants are in evolutionarily conserved regions, suggesting that they may have functional consequences and increase risk for disease. However, given the selection bias inherent in candidate-based approaches, further studies are necessary to determine whether these variants significantly alter protein function and play a role in IBM pathogenesis.

Rather than starting with genes previously implicated in muscle disease, Guttsches et. al. performed an unbiased proteomics approach to identify proteins enriched in rimmed

vacuoles (RVs) (Guttsches et al. 2017). This method led to the identification of 213 proteins, 40 of which had been previously described in IBM including VCP and p62, validating this approach. Interestingly, proteins involved in protein quality control were among the most abundantly overrepresented proteins. To look for novel genetic contributors to IBM, WES was used to identify variants in genes encoding proteins found in RVs. When comparing the burden of these variants to an ALS cohort, only variants in the FYCO1 gene were statistically enriched in IBM patients (11.3% vs. 2.6% in controls). FYCO1 has been implicated in microtubule transport of autophagosomes, consistent with a role for autophagy impairment in the pathogenesis of IBM (Pankiv et al. 2010).

Large Deletions in Mitochondrial DNA and Related Genetic Variants

Using real-time PCR, COX-deficient fibers from IBM patients were shown to have higher mitochondrial DNA (mtDNA) deletion loads when compared to COX-normal fibers (Lindgren et al. 2015). In addition, it has been reported that the amount of mtDNA is reduced in IBM muscle in comparison to controls (Catalan-Garcia et al. 2016). Interestingly, the fraction of COX-deficient fibers correlated with the amount of infiltrating T lymphocytes, suggesting an interaction between the mitochondrial defect and the autoimmune component of IBM (Rygiel et al. 2015).

Another mitochondrial protein that has been investigated in IBM is the Translocase of Outer Mitochondrial Membrane 40 (TOMM40). TOMM40 lies adjacent to apolipoprotein E (ApoE) in the genome, and thus ApoE and TOMM40 alleles are co-inherited. Prior studies have shown that the ApoE and TOMM40 genotype combination can be used as a predictor of age-dependent risk in Alzheimer's Disease (AD) (Roses et al. 2013). Given reported β-amyloid deposition in both IBM and AD, Mastaglia et al investigated

ApoE and TOMM40 polymorphisms in IBM (Mastaglia et al. 2013). In a study of 90 Caucasian patients, they found that carriers of APOE ε3 who also contained the very long (VL) poly-T repeat allele of TOMM40 had a reduced risk of developing IBM as well as a later age of onset. Recently, Gang et. al. investigated this further in a larger cohort of 158 IBM patients obtained through the International IBM Genetics Consortium (Gang, Bettencourt, Machado, et al. 2015). In contrast to the previous study, they did not find an association between any particular APOE-TOMM40 genotype and the risk of developing IBM, but did find that individuals carrying the VL TOMM40 allele had a later age of onset (Gang, Bettencourt, Machado, et al. 2015). Since both studies found that the TOMM40 VL allele delays IBM disease onset, these findings suggest that further investigation into how the VL allele alters TOMM40 and mitochondrial function may shed insight into IBM pathogenesis.

Conclusion

New high-throughput sequencing methods have revolutionized genetic analyses of complex diseases, allowing for identification of genetic variants that are associated with an increased risk of developing IBM. Recent studies have confirmed and refined the major role the HLA locus plays in IBM susceptibility, strongly implicating autoimmunity in disease pathogenesis. In addition, multiple studies have identified rare variants within genes known to regulate protein quality control including autophagy, suggesting that one's ability to prevent protein aggregate formation may partially underlie disease risk. While intriguing, the rare nature of IBM and the presence of most of these variants at low levels in the population make the significance of these findings unclear. However, the identification of both immune and proteostasis-related genes in disease susceptibility of IBM further implicates both processes in IBM pathogenesis.

1.4 Current Treatments and Ongoing Clinical Trials

Regrettably, there are no clinically effective treatments that have been shown to improve muscle weakness or halt its progression for IBM patients. The standard of care for IBM patients includes nonpharmacological management such as physical and occupational therapy, education on fall prevention, and the use of medical devices to improve mobility such as braces for foot drop and wheelchairs. Interventions to improve dysphagia in IBM patients are also common as dysphagia is associated with increased mortality and morbidity due to malnutrition, dehydration, and aspiration pneumonia (Oh et al. 2007; Mohannak et al. 2019). There are both non-invasive (e.g. lingual strengthening programs) and invasive approaches (e.g. balloon dilation, botulinum toxin injection, and cricopharyngeal myotomy) for treating dysphagia. These invasive approaches have been found to be more effective, and in one study, approximately 60% of patients with dysphagia benefitted at least temporarily from undergoing cricopharyngeal myotomy (Mohannak et al. 2019).

Exercise in IBM

Although previously it had been thought that exercise did not significantly alter the natural history of IBM, several studies suggest beneficial effects of exercise in IBM patients (Spector et al. 1997; Arnardottir et al. 2003; Johnson et al. 2009; Alexanderson and Lundberg 2012; Alexanderson 2018). A variety of exercise paradigms have been tested in small IBM cohorts, including home exercise programs, resistance strength training, and blood-flow restriction training. Importantly, several of these studies assessed the effect exercise had on the patient's immune system and endomysial inflammation. Serum CK levels were unaffected by exercise and in studies where

participants underwent repeated muscle biopsies, changes in the number of degenerating fibers or inflammatory cells were not observed (Spector et al. 1997; Johnson et al. 2009; Arnardottir et al. 2003). IBM patients undergoing blood-flow restriction training did show increased endomysial infiltration of CD3-CD8+ expressing natural killer cells, but populations of T cells and macrophages were unchanged (Jensen et al. 2019). The main conclusions from these studies were that exercise is well tolerated by IBM patients and the exercise arms frequently showed modest improvements in aerobic capacity, or improved strength from baseline (Spector et al. 1997; Johnson et al. 2009). These studies are encouraging, but large, randomized trials examining the potential benefits of exercise for IBM patients are still needed.

Clinical Trials

A modest number of clinical trials—both open-label and blinded placebo-controlled trials—have been carried out with IBM patients to test potential pharmaceutical therapies targeting immune modulation, the myostatin pathway, or proteostasis (reviewed in: Greenberg 2019; Glaubitz, Zeng, and Schmidt 2020). Broad lymphocytic depletion treatment strategies tested in IBM patients include antithymocyte globulin (ATG), methotrexate, intravenous or subcutaneous immunoglobulin, and alemtuzumab. Most of these treatments have shown minimal or no treatment efficacy (Glaubitz, Zeng, and Schmidt 2020). For instance, a double-blinded, placebo-controlled study with methotrexate showed no difference in progression and muscle strength over 48 weeks, although a pilot trial of alemtuzumab in 13 IBM patients suggested reduced progression of weakness, and post-treatment biopsies showed reduced endomysial lymphocytes (Badrising et al. 2002; Dalakas et al. 2009). It is also worth noting studies have found that intravenous immunoglobulin (IVIG) may be beneficial for patients with dysphagia

(Dalakas et al. 1997; Dobloug et al. 2012).

As therapies targeting inflammatory pathways have only been moderately efficacious at best, researchers have been exploring a number of other treatment avenues. A small study showed that the myostatin inhibitor Bimagrumab could improve skeletal muscle mass in 14 IBM patients (Amato et al. 2014). This was followed by a large randomized, placebo-controlled trial of Bimagrumab in 240 patients using a 6-minute walk test as the primary outcome, which was not significantly changed compared to the placebo-controlled group (Hanna et al. 2019).

Recently, a study evaluated the therapeutic potential of targeting protein aggregation in IBM with Arimoclomol (Ahmed et al. 2016). Arimoclomol is a small molecule thought to upregulate chaperone expression in stressed cells, thereby reducing the formation of protein aggregates (Kieran et al. 2004; Douglas and Cyr 2010). In cultured myoblasts and mice expressing mutant VCP protein, Arimoclomol improved IBM-like pathology, and in a small proof-of-concept clinical study, there was a trend toward reduced decline in muscle strength and physical function in IBM patients taking Arimoclomol compared to placebo (Ahmed et al. 2016) . A multisite phase II clinical trial (NCT02753530) began in 2018 to evaluate the efficacy of this drug in IBM and the study is predicted to conclude in December of 2021.

Recent success in clinical trials of gene therapy in Spinal Muscular Atrophy (SMA), an inherited motor neuron disease (Mendell, Al-Zaidy, et al. 2017; Finkel et al. 2017; Ramdas and Servais 2020), in addition to excitement around using genome editing technologies such as CRISPR for treating muscle diseases (Bengtsson et al. 2017;

Amoasii et al. 2018; Jin et al. 2019), has led to the consideration of gene therapy for IBM. Since muscle atrophy is a major part of IBM pathology, researchers have analyzed the myostatin signaling pathway in IBM muscle. Myostatin is a tumor growth factor beta (TGF-β) family member that has a well-defined role as a negative regulator of muscle mass, making it a promising therapeutic target for muscle wasting disorders (Elkina et al. 2011). In particular, gene therapy using follistatin, a natural inhibitor of the myostatin receptor, has been reported to be safe and causes muscle hypertrophy in mice and primates (Kota et al. 2009). Since the myostatin signaling pathway was reported to be upregulated in IBM (Amato et al. 2014), follistatin gene therapy has been tested to determine if it improves muscle strength and function in IBM.

In a recent phase 1/2a clinical trial, adeno-associated viral (AAV) delivery of follistatin isoform 344 (FS344) via intramuscular quadriceps injection was reported to modestly improve the distance traveled for a 6 minute walk test (6MWT) in a small cohort of Becker muscular dystrophy (BMD) patients (Mendell et al. 2015). Promising histological changes were also observed including reduced endomysial fibrosis, fewer centralized nuclei, and normalization of fiber size. In a 'proof-of-principle' trial, 6 male IBM patients received bilateral intramuscular quadriceps injections of AAV1 vectors carrying FS344 (Mendell, Sahenk, et al. 2017). One noteworthy change from the BMD study is that the IBM study included an exercise regimen for each participant as it had been demonstrated that exercise increased plasma levels of follistatin (Hansen et al. 2011). This study observed an improvement in the distance traveled for a 6MWT, and all post-treatment biopsies showed increased number of muscle fibers (Mendell, Sahenk, et al. 2017). However, significant concerns have been raised in regards to the design of this trial and the authors' claim of efficacy (Greenberg 2017). Most importantly, the lack of a

control group makes it difficult to determine how much of the improvement was a result of exercise and/or placebo effect.

1.5 Laboratory Models of Inclusion Body Myositis

To date, the xenograft model described below in Chapter 5 is the only comprehensive animal model of IBM. A plethora of laboratory models have been developed for various forms of HIBM, such as transgenic mutant VCP mouse models (Weihl et al. 2007; Custer et al. 2010), a knock-in mutant VCP model (Nalbandian et al. 2013), GNE myopathy models (reviewed in:Pogoryelova et al. 2018), and various *Drosophila* models (Ritson et al. 2010; Chang et al. 2011; Wang et al. 2012; Li et al. 2016). However, to reiterate, while HIBMs share some pathological features with IBM, they are clinically distinct from sporadic IBM in that they lack inflammation (which is prominent in sporadic IBM), have a much earlier age of onset, and have a different pattern of muscle involvement.

Outside of the HIBM models, several labs have developed animal models that recapitulate specific characteristics of IBM (reviewed in: Afzali et al. 2017). The majority of these models involve using either pharmacologic or transgenic means to drive β-amyloid (Aβ) aggregation in skeletal muscle. One group performed intraperitoneal injections of Wistar rats with chloroquine diphosphate: an anti-malaria drug that can cause a vacuolar myopathy (Ikezoe et al. 2009). Prior to rimmed vacuole formation at 7 weeks post-treatment, they observed increased levels of LC3-II—indicating increased autophagy—and Aβ in skeletal muscle followed by an elevated unfolded protein response (UPR). The authors hypothesized that Aβ accumulation may be driving ER

stress in their model eventually leading to degeneration of myofibers (Ikezoe et al. 2009). Interestingly, when this chloroquine rat model was challenged with resistance exercise—rats climbed a ladder with weight attached to their tails 9 weeks after starting treatment—it was found that exercise reduced Aβ accumulation, which rescued muscle atrophy and increased expression of key regulators of mitochondrial biogenesis (Koo, Kang, and Cho 2019). Another group generated a transgenic animal model in which human wild-type (WT) β-amyloid precursor protein (βAPP) was expressed in fast-twitch (type II) skeletal muscle (Moussa et al. 2006). Hemizygous transgenic mice showed increased levels of βAPP and Aβ in skeletal muscle fibers, and they became significantly weaker with age in comparison to nontransgenic littermates. In addition, dissociated muscle fibers from transgenic mice exhibited a 2-fold increase in resting calcium and membrane depolarization compared with nontransgenic littermates (Moussa et al. 2006). These latter characteristics may explain the persistent muscle weakness in IBM, however, the potential contribution of βA and βAPP in the pathogenesis of IBM remains controversial (Greenberg 2009; Fergusson 2009).

A striking feature of IBM biopsies is the dramatic sarcoplasmic and sarcolemmal upregulation of MHC-I, and several groups have developed models to explore this characteristic. First, a conditional mouse model was developed where overexpression of MHC-I (mouse H-2K^{b}) was driven by a muscle-specific promoter repressible with doxycycline (Nagaraju et al. 2000). After doxycycline was removed at 4 weeks, these transgenic mice showed specific upregulation of MHC-I, impaired locomotor activity, and increased serum levels of CK and glutamic-oxaloacetic transaminase, indicating ongoing muscle damage compared to littermates. By 3.5 months, skeletal muscles showed myopathic features including internalized nuclei and degenerating fibers as well as

macrophage infiltration. Readministration of doxycycline for 5 months after 4 months of transgene expression was unable to rescue these phenotypes, and expression of MHC-I remained elevated, indicating the persistent, uncontrollable nature of this inflammatory response once initiated (Nagaraju et al. 2000). Another group used this model to assess the impact of this MHC-I overexpression in young muscle tissue and reported a more severe phenotype when doxycycline was removed immediately after weaning (Li et al. 2009). Gene expression analysis of these mice revealed up-regulation of genes involved in protein transportation, folding, processing, and glycosylation such as Hsp40 chaperones and derlin proteins (Li et al. 2009). In addition, several significantly over-expressed genes were part of the UPR, such as Armet, a clear parallel to the chloroquine rat model discussed above. The UPR is activated to handle misfolded or overexpressed proteins and is characterized by the expression of ER chaperones, reduced protein synthesis, and enhanced degradation of misfolded proteins by the ubiquitin-proteasome system and ER-associated degradation. Interestingly, when MHC-I is overexpressed in the skeletal muscle of immunodeficient, alymphoid mice, proteomic analysis also shows upregulation of the UPR indicating this process is intrinsic to myofibers and can occur independently from involvement with the adaptive immune system (Freret et al. 2013). It is important to note that MHC-I staining is also commonly seen in muscle biopsies from patients diagnosed with non-inflammatory myopathies and neurogenic disorders, whereas MHC-II staining is more specific to inflammatory myopathies (Rodriguez Cruz et al. 2014). Therefore, it would be informative to explore the effect of conditionally overexpressing MHC-II in skeletal muscle.

To explore the involvement of anti-NT5C1A in IBM pathology, a passive in-vivo immunization model has been developed by injecting mice with immunoglobulin (IgG)

samples from IBM patients with and without NT5C1A antibodies. Mice injected with anti-NT5C1A positive patient serum showed myopathic features (e.g. fiber size variation), p62 aggregates in muscle, and macrophage infiltration (Tawara et al. 2017). As a next step, this group has also developed an active immunization mouse model using NT5C1A peptides (Chinoy and Lilleker 2019: P131). Of the three different peptide sequences injected into mice, autoantibodies recognizing the injected NT5C1A peptides were detected in the sera of all the mice (5 per group). Two of the peptide-injected groups showed a significant decrease in motor activity, and one group also showed increased expression of p62 and LC3-II in muscle lysates as detected via western blot (Chinoy and Lilleker 2019: P131). These models show that mice immunized passively or actively to develop antibodies to NT5C1A can mimic some pathological features of IBM; however, more research is needed to understand the of role anti-NT5C1A in IBM.

While the models described above are useful tools to elucidate the basic biology underlying discrete elements of IBM pathology, none of them could be described as a comprehensive laboratory model showing the full spectrum of pathological features. Increasingly, xenograft models of disease —where human tissue is transplanted in immunocompromised mice—have proven to be valuable tools for rare or sporadic diseases that often lack laboratory models and they have propelled therapeutic development, especially in oncology.

Chapter 2: Using Xenografts to Study Human Disease

2.1 The Use of Patient Derived Xenografts in Cancer

The first immortal human cell line was created in Dr. George Gey's laboratory by the technician Mary Kubicek who successfully cultured cells from a sample of Henrietta Lacks' cervical cancer at Johns Hopkins Hospital (Scherer, Syverton, and Gey 1953). This HeLa cell line has had an immeasurable impact on human medicine, and it is only natural that *in vitro* cell culture models dominated cancer research for decades. In 2012 the Cancer Cell Line Encyclopedia (CCLE) compiled gene expression, chromosomal copy number, and parallel sequencing data from 947 human cancer cell lines to aid in predictions of drug sensitivity (Barretina et al. 2012). In a recent amendment, the number of lines rose to 1,072 and the characterization of the cell lines expanded to include data on RNA splicing, DNA methylation, and histone H3 modification among other characteristics (Barretina et al. 2019). This vast array of cancer cell lines have been used for both *in vitro* and *in vivo* studies, in particular, the most frequently used models for preclinical therapeutic testing have historically been xenograft models generated by injecting these cells into immunodeficient mice (Jung, Seol, and Chang 2018). While such models are easy to generate, they have a number of limitations. Most importantly these models do not recapitulate the heterogenous population of cells found within the tumor microenvironment, and they typically fail to predict drug efficacy in patients. To overcome these shortcomings, researchers have turned to patient-derived tumor xenografts (PDX).

The first successful PDX model was developed by subcutaneously transplanting tissue from a metastatic adenocarcinoma into athymic, nude mice (Rygaard and Povlsen 1969). Although the xenografts regressed in control mice, they showed rapid growth in nude mice, and 40 days after transplantation the tumor mass more than doubled. More than five decades have passed since this initial study, and PDX models have been developed for the majority of solid tumors including urothelial and renal cell carcinomas, prostate cancer, and glioblastomas (Namekawa et al. 2019; Lee et al. 2019; Tracey et al. 2020). One clear issue that can arise when using PDX models is tissue availability as not all universities or laboratories have ready access to patient samples. However, numerous serially transplantable PDX models have been established to address this issue of accessibility (Dobrolecki et al. 2016; Navone et al. 2018). To date, the Jackson Laboratory's Mouse Models of Human Cancer Database (MMHCDB), a compendium of mouse models of human cancer, lists over 400 patient-derived xenograft (PDX) models (Krupke et al. 2017).

It is clear that PDXs models have been successfully utilized to develop laboratory models and treatments for common cancers, including multiple myeloma, as well as personalized therapies for individual patients (Kim et al. 2005; Rubio-Viqueira and Hidalgo 2009; Sako et al. 2010; Roberts et al. 2014; Izumchenko et al. 2017). Although some characteristic hallmarks of cancer—uncontrollable proliferation and tissue invasion—undoubtably predispose the success of PDX models in oncology, researchers have expanded the use of xenografts to successfully study other diseases including disorders of skeletal muscle (Fouad and Aanei 2017).

2.2 Using Xenografts to Study Muscle Disease

The most frequently used method for producing skeletal muscle xenografts is the injection of myogenic cells (e.g. satellite cells, iPSCs, or myoblasts) into immunodeficient mice following preinjury of the injection site via cardiotoxin, cryodamage, or irradiation to create a favorable niche for engraftment (reviewed in: Mueller and Bloch 2019). This process creates a chimeric muscle within the host mouse containing both murine and human myofibers. Originally nude or SCID mice were preferred hosts as these mice lack T cells or all lymphocytes, respectively, which make them permissive for xenograft studies. However, improved immunocompromised mouse models have been developed in recent years. In particular, NOD-Rag1 (null) strains carrying the IL2rγ (null) mutation, such as NSG and NRG mice, more readily support engraftment of human tissue (Silva-Barbosa et al. 2005; Maykel et al. 2014).

Three major obstacles to successful engraftment of myogenic precursors are early progenitor cell death, limited cell proliferation, and poor migration within engrafted muscle (Riederer et al. 2012). In addition, the injection of a homogenous population of cells does not fully recapitulate the heterogenous population of cells found within the skeletal muscle niche. For instance, fibro-adipogeneic progenitors (FAPs) massively proliferate in skeletal muscle following muscle injury and their intercellular interactions drive satellite cell activation and promote efficient regeneration (Farup et al. 2015; Malecova et al. 2018; Biferali et al. 2019). In a mouse model of limb girdle muscular dystrophy 2B, progressive accumulation of Annexin A2—a calcium-dependent phospholipid-binding protein involved in exocytosis—in the myofiber matrix causes FAPs to preferentially differentiate into adipocytes driving fatty replacement of myofibers

(Hogarth et al. 2019). These data implicate FAPs in the adipogeneic replacement of myofibers commonly seen in muscle diseases, including IBM, and showing the importance of cells beyond myogenic precursors in skeletal muscle regeneration.

Another approach to generate human skeletal muscle xenografts is to transplant whole muscle grafts into immunodeficient host mice. The first proof-of-principal study that unintentionally tested this approach involved the transplantation of muscle from dystrophic mdx mice to control mice sharing the same genetic background (Morgan, Coulton, and Partridge 1989). While the goal of this study was to demonstrate that the mdx mutation caused a muscle intrinsic primary myopathy, it also revealed that whole muscle grafts could regenerate in host mice and maintain their original genetic profile (Watt et al. 1987; Morgan, Coulton, and Partridge 1989).

More recently, whole muscle xenografts have been used to develop a model of fascioscapulohumeral muscular dystrophy (FSHD) (Zhang et al. 2014). In this model, human muscle biopsy specimens are transplanted into the hindlimbs of immunodeficient NRG mice to form xenografts. The transplanted human myofibers die, but human satellite cells present in the xenograft subsequently expand and differentiate into new human myofibers which repopulate the engrafted human basal lamina. Therefore, the regenerated myofibers in these xenografts are entirely human and are spontaneously revascularized and innervated by the mouse host. Importantly, FSHD patient muscle tissue transplanted into mice recapitulates key features of the human disease, namely expression of the DUX4 transcription factor (Zhang et al. 2014). FSHD is caused by overexpression of DUX4, which is epigenetically silenced in normal muscle tissue (Gabellini, Green, and Tupler 2002; Lemmers et al. 2010). In the FSHD xenograft model,

treatment with a DUX4-specific morpholino has been shown to successfully repress DUX4 expression and function and may be a potential therapeutic option for FSHD patients (Chen et al. 2016).

These studies demonstrate that human skeletal muscle xenografts are a promising approach to model muscle disease and test potential therapies in mice. In a novel application of this methodology, this study demonstrates that human skeletal muscle xenografts can be used to model acquired, inflammatory muscle diseases, such as IBM.

Chapter 3: A Surgical Description of the Xenograft Technique

This is adapted from Britson, K. A., Black, A. D., Wagner, K. R., Lloyd, T. E. Performing Human Skeletal Muscle Xenografts in Immunodeficient Mice. J. Vis. Exp. (151), e59966, doi:10.3791/59966 (2019) (Britson et al. 2019). Reprinted in this dissertation with permission from the Journal of Visual Experiments, pursuant to their Author License Agreement.

3.1 Introduction

It has been reported that only 13.8% of all drug development programs undergoing clinical trials are successful and lead to approved therapies (Wong, Siah, and Lo 2019). While this success rate is higher than the 10.4% previously reported (Hay et al. 2014), there is still significant room for improvement. One approach to increase the success rate of clinical trials is to improve laboratory models used in preclinical research. The Food and Drug Administration (FDA) requires animal studies to show treatment efficacy and assess toxicity prior to Phase 1 clinical trials. However, there is often limited concordance in treatment outcomes between animal studies and clinical trials (Perel et al. 2007). In addition, the need for preclinical animal studies can be an insurmountable barrier for therapeutic development in diseases that lack an accepted animal model, which is often the case for rare or sporadic diseases.

One way to model human disease is by transplanting human tissue into immunodeficient mice to generate xenografts. There are three key advantages to xenograft models: First, they can recapitulate the complex genetic and epigenetic abnormalities that exist in human disease that may never be reproducible in other animal models. Second, xenografts can be used to model rare or sporadic diseases if patient samples are available. Third, xenografts model the disease within a complete *in vivo* system. For these reasons, we hypothesize that treatment efficacy results in xenograft models are more likely to translate to trials in patients. Here, we describe in detail the surgical method for creating human skeletal muscle xenografts in immunodeficient mice.

3.2 Protocol

All use of research specimens from human subjects was approved by the Johns Hopkins Institutional Review Board (IRB) to protect the rights and welfare of the participants. All animal experiments were approved by the Johns Hopkins University Institutional Animal Care and Use Committee (IACUC) in accordance with the National Institutes of Health (NIH) Guide for the Care and Use of Laboratory Animals. 8 to 12-week-old male NOD-Rag1^{null} IL2rγ^{nul}l (NRG) host mice (Jackson Laboratory, 007799) are used to carry out xenograft experiments. These mice are housed in ventilated racks and are given HEPA-filtered, tempered, and humidified air as well as reverse osmosis filtered hyperchlorinated water. Mice are provided water and an irradiated antibiotic diet (Envigo, TD.06596) ad libitum, and the facility provides 14 hours of light to 10 hours of dark as controlled by central timer.

1. Equipment preparation

1.1. Acquire NOD-Rag1null IL2rγnull (NRG) mice, 8-12 weeks of age.

1.2. Autoclave surgical equipment: scissors, forceps, needle holder, surgical stapler (Table 3.1), wound clips, surgical wipes (**Table 3.1**), and beaker.

1.3. Prepare 50 mL of muscle media (20% fetal bovine serum, 2% chick embryo extract, 1% antibiotic/antimycotic in Hams F10 Medium). Keep all chemicals/drugs/solutions used for surgery at room temperature unless stated differently in the protocol.

1.4. Prepare a 1 mL syringe with a 26-gauge needle that is 3/8 inches long containing 2 mg/mL analgesic (**Table 3.1**), and place on ice. The analgesic can be diluted to the proper concentration using sterile phosphate buffered saline (PBS).

2. Surgical preparation

2.1. Obtain a human muscle biopsy under an IRB-approved protocol from patients whose muscles display strength > 4-/5 on the MRC (Medical Research Council) scale (MRC 1976). Place the research specimen in a 100 mm x 15 mm Petri dish containing muscle media.

> NOTE: The MRC scale is used in clinical practice as an assessment of muscle strength with 0 showing no contraction, 5 showing normal power, and 4 (4- to 4+) showing movement against resistance (MRC 1976). We have found that muscles with mild to moderate weakness (MRC > 4-/5) typically show disease pathology but are not extensively replaced by fatty tissue or fibrosis, both of which impede xenograft regeneration. In the case of autopsy tissue where a recent MRC score is not available, muscle quality can be accessed via gross observation. Muscle biopsies that are pale pink in appearance or have large areas of fatty tissue are not likely to xenograft successfully.

2.2. Remove any remaining fascia or fatty tissue from the specimen with surgical scissors using a stereo microscope and light source to assist visualization.

2.3. Dissect the muscle biopsy into approximately 7 mm x 3 mm x 3 mm pieces with surgical scissors using the stereo microscope and a light source. Ensure fibers are arranged longitudinally within the specimen.

2.4. Place the Petri dish containing dissected muscle on ice. On average, the xenografts are kept in media for 4 hours while surgeries are being performed. However, biopsies have been stored in media for 24 hours prior to xenografting, and this delay did not appear to negatively impact transplantation or regeneration.

2.5. Place synthetic, non-absorbable sutures (**Table 3.1**) in a 100 mm x 15 mm Petri dish containing 70% ethanol.

2.6. Set up a dual procedure anesthesia circuit: arrange the Mapleson E breathing circuit on the stereo microscope and place the induction chamber in a biosafety cabinet.

2.7. Obtain the weight of the NRG mouse by placing in an autoclaved beaker on a scale, and transfer to the induction chamber. Induce anesthesia under 3% isoflurane. Once the appropriate anesthetic depth is achieved—as assessed by observation of respiratory rate, muscle relaxation, and lack of voluntary movement—reduce the vaporizer setting to 1.5% for the remainder of the surgery.

2.8. Transfer the mouse from the induction chamber to the Mapleson E breathing circuit and apply ophthalmic ointment to eyes.

2.9. Remove hair overlying the tibialis anterior (TA) from ankle to knee with a trimmer, followed by a 1-minute treatment with hair removal lotion (**Table 3.1**) (**Figure 3.1**).

2.10. Disinfect the surgical site by swabbing the leg with povidone-iodine solution. Then wash away the remaining povidone-iodine with 70% ethanol.

2.11. Inject the mouse subcutaneously with analgesic (**Table 3.1**) at a dose of 5 mg/kg.

3. Xenograft surgery

3.1. Tape down the leg and make a straight incision over the tibialis anterior (TA) muscle with scissors and iris forceps originating at the distal tendons and terminating below the knee (**Figure 3.1A, B**).

3.2. Separate skin from muscle using blunt dissection with surgical scissors.

3.3. Cut through the epimysium of the TA muscle with scissors starting at the tendon and ending at the knee.

> NOTE: This is a very superficial cut (less than 0.5 mm; **Figure 3.1B**, black dashed line), and the underlying TA should not be damaged in the process as this would make removal more challenging. When performed correctly, the muscle fibers will visibly relax.

3.4. Cut the distal tendon of the TA with scissors, grab the tendon with iris forceps, and pull the TA up toward the knee (**Figure 3.1C**).

3.5. Cut the distal tendon of the extensor digitorum longus (EDL) with scissors and pull the EDL up toward the knee (**Figure 3.1D**). Once the proximal tendon of the peroneus longus (PL) muscle is visible, remove the EDL with scissors (**Figure 3.1D**, green dashed line).

3.6. Remove the TA with scissors (**Figure 3.1D**, blue dashed line) and use a surgical wipe wetted with PBS and slight pressure to achieve hemostasis (**Figure 3.1E**).

3.7. Thread a suture through proximal peroneus longus (PL) tendon and trim, leaving approximately 1.5 inch of thread on either side of the tendon (**Figure 3.1F**).

3.8. Perform the first half of a two-hand surgical square knot, but do not tighten: this will form a circle. Place a xenograft in this circle and tighten the loop to secure the xenograft. Complete the other half of the square knot (**Figure 3.1G, H**). This will suture the xenograft to the proximal tendon of the PL.

NOTE: The medial tarsal artery and vein can lie close to or on top of the distal tendon of the PL. Do not place sutures through or around these vessels. It is easy to tell if a suture has been improperly placed as vessels will blanch or bleed. If this occurs, remove the suture and place in a different location.

3.9. Thread suture through distal PL tendon and repeat the square knot technique from step 3.8 to tie the xenograft to the distal tendon (**Figure 3.1H, I**).

3.10. Pull skin over xenografted muscle, seal with surgical glue, and place 2-3 surgical staples over the incision (**Figure 3.1J**).

3.11. Place mouse in a clean cage on a heated pad to recover. Monitor mouse until fully conscious and periodically over the next few days for signs of local systemic infection and to ensure the surgical site is not reopened.

4. Xenograft collection

NOTE: Xenografts are typically collected between 4 to 6 months post-surgery. However, collections have been performed up to 12 months post-surgery.

4.1. Place a covered beaker containing 200 mL of 2-methylbutane in a box containing dry ice for a minimum of 30 minutes before xenograft collection.

4.2. Induce anesthesia under 3% isoflurane in induction chamber. Once the appropriate anesthetic depth is achieved, reduce the vaporizer setting to 1.5% for the remainder of the surgery.

4.3. Transfer the mouse from the induction chamber to the Mapleson E breathing circuit arranged on a stereo microscope.

4.4. Remove hair overlying the tibialis anterior from ankle to knee with a trimmer and hair removal lotion. The sutures holding the xenograft in place can be seen through the skin (**Figure 3.2A**).

4.5. Tape down the leg and use scissors and iris forceps to open skin over the xenograft until both sutures are visible (**Figure 3.2B**). Skin overlying the xenograft can be removed as shown to make removal of the xenograft easier (**Figure 3.2C**).

4.6. Use a scalpel to cut between the PL muscle and the gastrocnemius muscle (**Figure 3.2D, E**, incision along epimysium labeled with arrow). The PL will be removed with the xenograft.

4.7 Use a scalpel to cut between the xenograft and the tibia (**Figure 3.2E**, arrow denotes initial site and direction of incision).

4.8. Cut below the distal suture and through the distal tendon of the PL (**Figure 3.2F**, the arrow indicates where the tendons are cut).

4.9. Remove the xenograft and PL by grabbing the suture with iris forceps and deflecting it toward the knee while using scissors to cut it away from the underlying muscle (**Figure 3.2J**).

4.10. Cut above the proximal suture with scissors to remove the xenograft and PL (**Figure 3.2J**, cut along dotted line).

4.11. Place the specimen on a small piece of cardboard or plastic, and pin as close to the sutures as possible. While pinning the specimen, gently stretch the muscle to ensure that the fiber orientation is maintained during the snap freezing process. After the pins are securely in place, slide the muscle up the pins so it rests just above the cardboard.

NOTE: Alternatively, one end of the xenograft can be mounted in tragacanth on a cork, or it can be submerged entirely in optimal cutting temperature (O.C.T.) compound in a cryomold. With care, muscle conformation can be retained with both methods.

4.12. Snap freeze the xenograft in pre-cooled 2-methylbutane.

4.13. Store xenograft at -80 °C.

4.14. Immediately following xenograft collection, euthanize mice in accordance with American Veterinary Medical Association guidelines:

4.14.1. Place mice in a sealed chamber with an appropriate waste gas scavenging system. Use isoflurane at a concentration of 3-4% to induce anesthesia.

4.14.2. Once the appropriate anesthetic depth is achieved—as assessed by observation of respiratory rate, muscle relaxation, and lack of voluntary movement—increase the vaporizer setting to 5% to induce death. Leave the mice in the chamber for an additional 2 minutes after breathing has ceased. Death is verified by observing that the mice fail to recover within 10 minutes after overdose of isoflurane.

4.14.3. Finally, perform cervical dislocation on the mice.

NOTE: In the case of bilaterally xenografted mice, the contralateral xenograft can be saved for a later collection. To perform a survival collection, open the skin overlying the xenograft with a single straight cut with surgical scissors, and remove the xenograft as described in steps 4.6 to 4.10. Then close the skin over the empty tibial compartment using surgical glue and staples. Treat the mouse with analgesic as described in step 2.11 and place the mouse in clean cage on heated pad to recover. Monitor the mouse

until fully conscious and periodically over the next few days for signs of local systemic infection and to ensure the surgical site is not reopened.

Table 3.1 Materials for Xenograft Surgery. A summary of all equipment and reagents necessary to carry out the xenograft surgical technique.

Name of Material/ Equipment	Company	Catalog Number
2-Methylbutane	Fisher	O3551-4
Animal Weighing Scale	Kent Scientific	SCL- 1015
Antibiotic-Antimycotic Solution	Corning, Cellgro	30-004-CI
AutoClip System	F.S.T	12020-00
Castroviejo Needle Holder	F.S.T	12565-14
Chick embryo extract	Accurate	CE650TL
Dissection Pins	Fisher Scientific	S13976
Dry Ice - pellet	Fisher Scientific	NC9584462
Dual Procedure Circuit	VetEquip	921400
Ethanol	Fisher Scientific	459836
Fetal Bovine Serum	GE Healthcare Life Sciences	SH30071.01
Fiber-Lite MI-150	Dolan-Jenner	Mi-150
Forceps	F.S.T	11295-20
Hams F-10 Medium	Corning	10-070-CV
Histoacryl Blue Topical Skin Adhesive	Tissue seal	TS1050044FP
Iris Forceps	F.S.T	11066-07
Irradiated Global 2018 (Uniprim 4100 ppm)	Envigo	TD.06596
Isoflurane	MWI Veterinary Supply	502017
Kimwipes	Kimberly-Clark	34155
Mobile Anesthesia Machine	VetEquip	901805
NAIR Hair remover lotion/oil	Fisher Scientific	NC0132811
NOD-*Rag1* ^{null} *IL2rg* ^{null} (NRG) mice	The Jackson Laboratory	007799
O.C.T. Compound	Fisher Scientific	23-730-571
Oxygen	Airgas	OX USPEA
PBS (phosphate buffered saline) buffer	Fisher Scientific	4870500
Petri dish	Fisher Scientific	FB0875712
Povidone Iodine Prep Solution	Dynarex	1415
Puralube Ophthalmic Ointment	Dechra	17033-211-38
Rimadyl (carprofen) injectable	Patterson Veterinary	10000319
Scalpel Blades - #11	F.S.T	10011-00
Scalpel Handle - #3	F.S.T	10003-12
Stereo Microscope	Accu-scope	3075
Suture, Synthetic, Non-Absorbable	Covidien	VP-706-X
Syringe (27G)	BD Biosciences	329412
Trimmer	Kent Scientific	CL9990-KIT
Vannas Spring Scissors	F.S.T	15009-08
VaporGaurd Activated Charcoal Filter	VetEquip	931401
Wound clips	F.S.T	12022-09

Figure 3.1 Xenograft Surgery

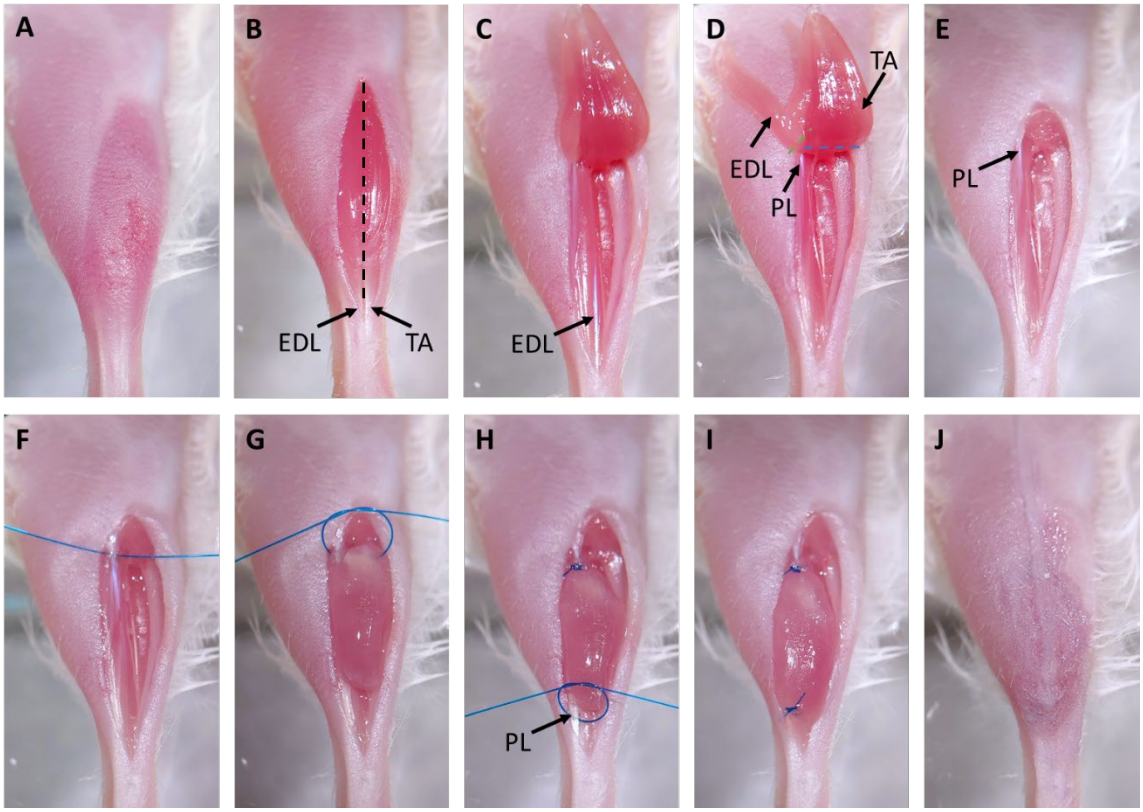

Figure 3.1 A) Hair is removed from surgical site. B) An incision is made over the tibialis anterior (TA). The distal tendons of the TA and extensor digitorum longus (EDL) are marked with arrows. The black dashed line indicates where the epimysium will be cut in step 3.3. C) The distal tendon of the TA is cut and the muscle is pulled up to the knee. D) The tendon of the EDL is cut and the EDL is pulled up to the knee. This exposes the proximal tendon of the peroneus longus (PL) marked with an arrow. Dashed lines indicate where to cut with scissors to remove the EDL (green) and PL (blue). E) The EDL and TA are removed. F) A suture is placed through the proximal tendon of the PL. G) The xenograft is placed in the empty tibial compartment and sutured to the proximal PL tendon using a two-hand surgical square knot. H) A suture is placed through the distal tendon of the PL, marked with an arrow, and another two-hand surgical square knot is used to suture the xenograft to the distal tendon. I) The xenograft is fully transplanted and sutured to the PL. J) The skin is closed with surgical glue.

Figure 3.2 Xenograft Collection

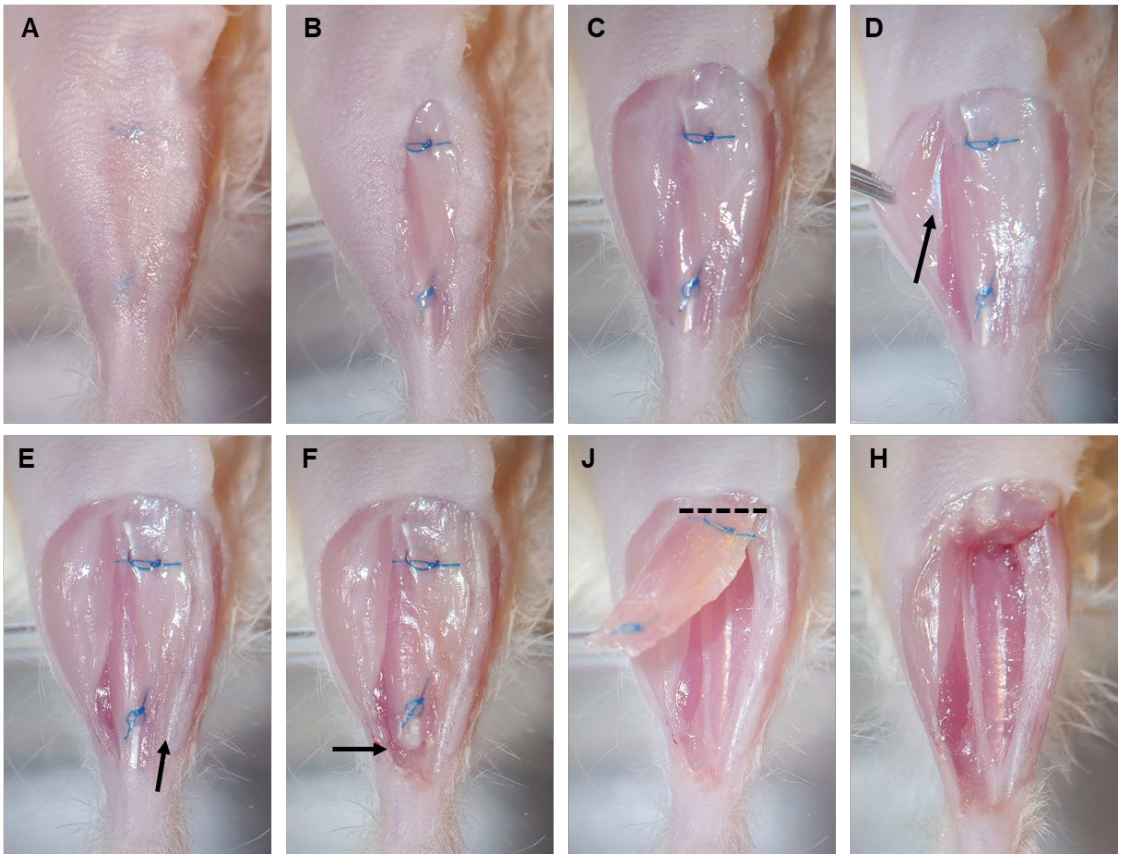

Figure 3.2 A) Hair is removed from surgical site. Sutures are visible under skin. **B**) An incision is made over the top of the xenograft. **C**) The skin overlying the xenograft is removed. **D**) By pulling the gastrocnemius muscle to the side, a faint white line of epimysium separating the peroneus longus (PL) muscle and the gastrocnemius becomes visible (shown by the arrow). Use the scalpel to cut along this line to separate the PL from the other leg muscles. **E**) Starting at the ankle, a scalpel is used to cut along the tibia and free the xenograft. The arrow shows the beginning of the incision along the tibia. **F**) The right side of the xenograft, and the PL are now free from the other muscles in the leg and are ready for removal. The arrow indicates where the tendons are cut with surgical scissors to start removing the xenograft and PL. **J**) After cutting below the distal suture, deflect the xenograft toward the knee. The dashed line indicates where to cut with surgical scissors to remove the xenograft and PL from the tibial compartment. **F**) The empty tibial compartment with the xenograft and PL successfully removed.

3.3 Results

As demonstrated by Yuanfan Zhang et al., this surgical protocol is a straightforward method to produce human skeletal muscle xenografts (Zhang et al. 2014). Regenerated xenografts become spontaneously innervated and display functional contractility. In addition, muscle xenografted from FSHD patients recapitulates changes in gene expression observed in FSHD patients (Zhang et al. 2014).

In our experience, approximately 7 out of 8 xenografts performed from control patient specimens will show successful muscle engraftment. A successful xenograft shows robust regeneration of human myofibers as identified with human specific antibodies (**Figure 3.3**). Positive embryonic myosin staining within a proportion of myofibers indicates that the regeneration process is still ongoing. In contrast, poor surgical technique or an inadequate specimen may lead to poor regeneration of muscle fibers (**Figure 3.3**).

Xenografts performed from a patient diagnosed with an idiopathic inflammatory myopathy (IIM) show moderate numbers of regenerated human myofibers at 4- and 6-month collections, and embryonic myosin staining persists at 6 months (**Figure 3.4A**). Inflammatory cells are present in the xenograft as shown by H&E staining (**Figure 3.4A**), and have been confirmed with CD3, CD68, and other immunological markers (data not shown). Xenografts are stable within the mouse, and up to 12-month collections have been performed. Individual myofiber size is comparable between the 4- and 6-month IIM xenografts and the original IIM patient biopsy (**Figure 3.4B**). Rare fibers showing a cross sectional area (CSA) greater than 3500 μm^2 are observed in xenografts but not in the

IIM biopsy, indicating that some myofibers in the xenografts can regenerate to a CSA comparable in size to healthy myofibers (**Figure 3.4B**).

Figure 3.3 Expected Positive and Negative Results

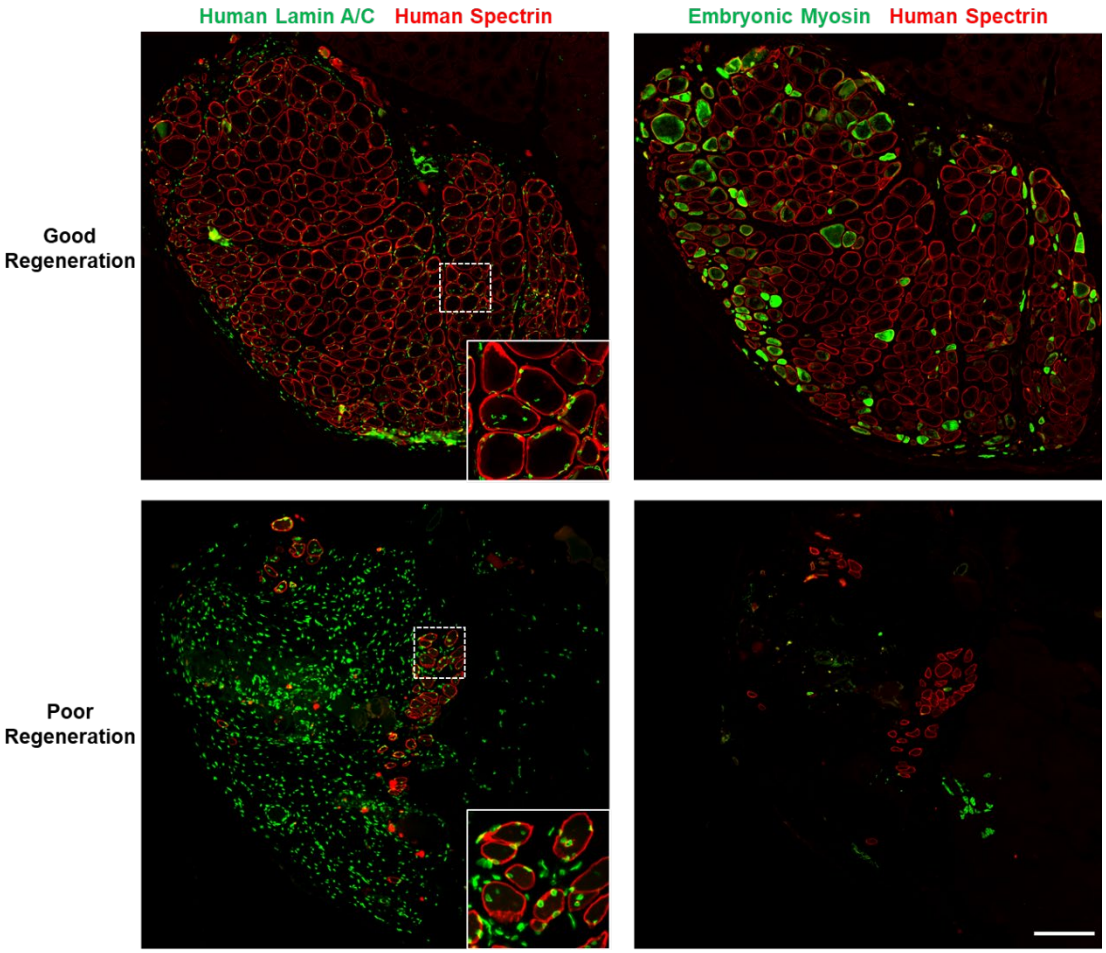

Figure 3.3 Xenografts collected 4-months post-surgery showing good or poor regeneration are stained with human-specific lamin A/C (1:50) and human-specific spectrin (1:20) and embryonic myosin (1:10) (Table 3.1). Regions indicated by the white dashed boxes are shown as higher magnification inserts. Scale bar: 200 μm.

Figure 3.4 Representative Xenograft Regeneration

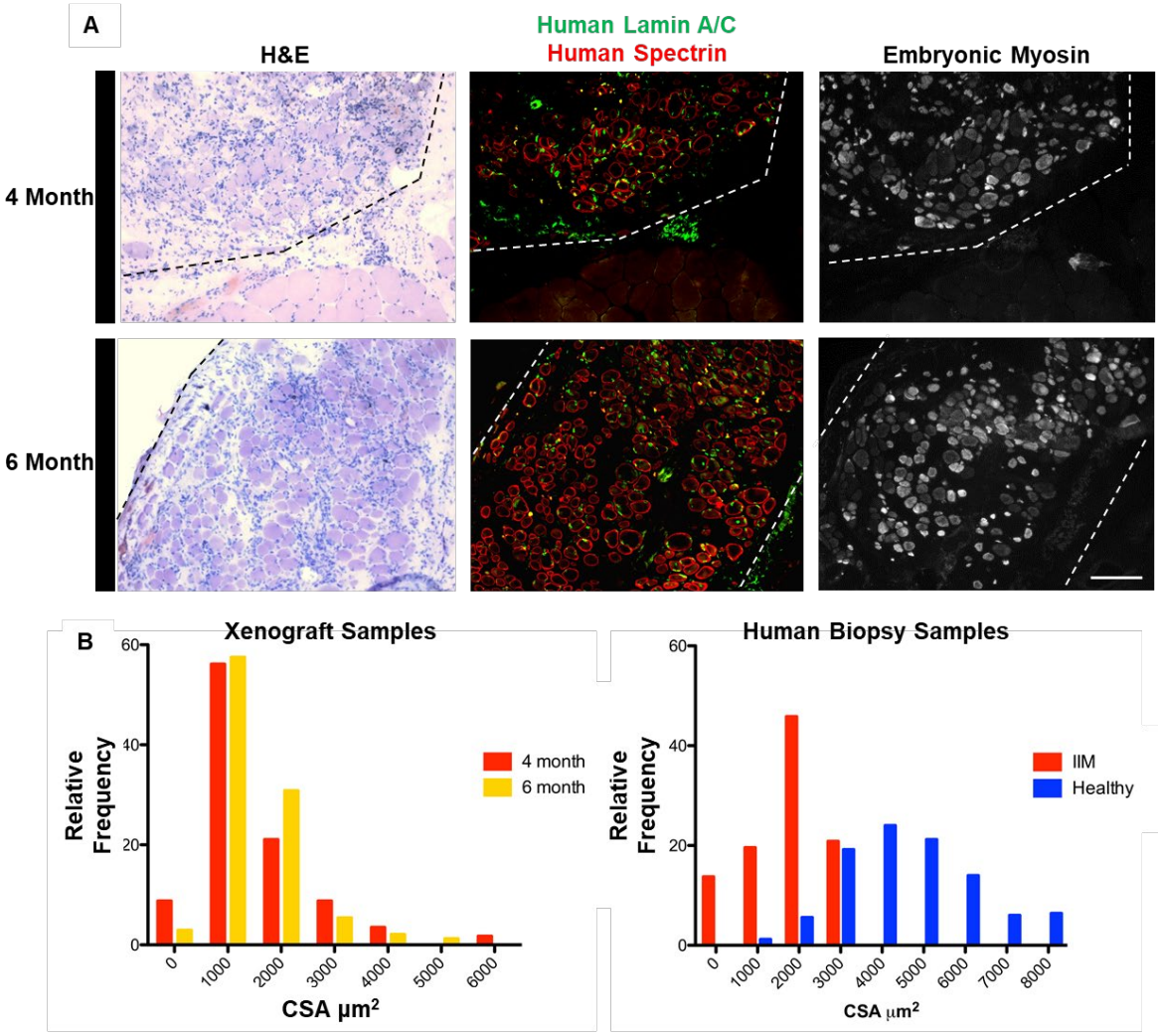

Figure 3.4 A) Xenografts (outlined with dashed lines) performed from a patient diagnosed with an idiopathic inflammatory myopathy (IIM) stained with Hematoxylin and Eosin (H&E), human specific Lamin A/C, and human specific spectrin, show myofiber formation within NRG mice at both 4- and 6-month time points. Embryonic myosin staining demonstrates that regeneration is still ongoing at both time points. Scale bar: 200 µm. B) Histograms depicting cross sectional area (CSA) of myofibers from 4- and 6-month xenografts and human biopsies from one patient diagnosed with an idiopathic inflammatory myopathy (IIM) and one healthy control patient.

3.4 Discussion

Patient-derived xenografts are an innovative way to model muscle disease and carry out preclinical studies. The method described here to create skeletal muscle xenografts is rapid, straightforward, and reproducible. Unilateral surgeries can be performed in 15 to 25 minutes, or bilaterally in 30 to 40 minutes. Bilateral xenografts can provide additional experimental flexibility. For instance, researchers can perform localized treatment of one xenograft, with the other left as a control. The NRG mice are resistant to surgical site infection when housed in a pathogen-free facility; in our experience performing more than 300 xenografts, we have never had a mouse acquire a surgical infection. In addition, host mice tolerate the removal of the TA and EDL very well. Within an hour post-surgery, unilaterally and bilaterally xenografted mice will be active and walking around their cage, and even standing up on their hindlimbs. Occasionally we observe some foot drop in host mice, but usually only after a period of inactivity, such as if recently awoken, and within minutes of waking leg use will be normal.

There are several critical steps in the protocol. First, during removal of the EDL and TA, it is very important to not injure the adjacent PL muscle or its tendons. This can be avoided by carefully and correctly identifying the placement of all distal tendons after the initial incision over the TA is performed. In addition, the proximal tendon of the PL should be identified and clearly visible before removal of the EDL (**Figure 3.1D**). Second, sutures must be placed through tendons and tightened fully in a proper two-hand surgical square knot. Xenografts regenerate more robustly under tension, and this is only obtainable if the xenograft is tethered to the PL tendons and if the sutures do not loosen post-operatively. Finally, it is important to not damage or sever any major blood

vessels supplying the foot. In particular, the medial tarsal artery and vein can lie close to or on top of the distal tendon of the PL. Do not place sutures through or around these vessels. It is easy to tell if a suture has been improperly placed as vessels will blanch or bleed. If this occurs, remove the suture and place in a different location.

This method does have several limitations. It is not amenable to standard functional assays used in mouse models of muscle disease, such as grip strength or treadmill endurance. However, electrophysiological assessments of xenograft function can still be performed. Evoked force measurements can be recorded from collected xenografts, and single enzymatically isolated myofibers from xenografts loaded with ratiometric calcium dyes and electrically stimulated can be used to study calcium dynamics (Zhang et al. 2014). Another inherent challenge in this model is that acquiring and working with human tissue can be difficult. Not all laboratories will have easy access to fresh muscle biopsies, but it has been shown that xenografts performed from autopsy tissue approximately 48 hours post-mortem can successfully engraft, and this tissue may be easier to obtain for some laboratories (Zhang et al. 2014). It is also challenging to manipulate gene expression in human tissue, whereas researchers using standard mouse models of disease can readily use the plethora of mouse genetic tools available.

A strength of this xenograft model is that it allows researchers to study human muscle *in vivo*. Tissue culture has been used extensively to study the cell and molecular biology of human muscle. Yet, these short-term, *ex vivo* studies do not always approximate functional muscle *in vivo*. However, one caveat is that it is challenging to determine how closely xenograft biology and function approximates human muscle due to the contribution of components from the host mouse during the regenerative process. For

instance, human and mouse neuromuscular junctions (NMJs) are morphologically distinct, and there is significant divergence between the synaptic proteome of human and mouse NMJs (Jones et al. 2017). As xenografts are innervated by the mouse host, this may result in biological changes unique to the human xenografts.

In future studies, this skeletal muscle xenograft method could be used to better understand human muscle cell biology and to develop novel models for rare or acquired muscle diseases that currently lack animal models. We anticipate that this will have a significant beneficial impact on therapeutic development for these diseases.

Chapter 4: Methods

Human Muscle Biopsy

All use of research specimens from human subjects was approved by the Johns Hopkins Institutional Review Board (IRB) to protect the rights and welfare of the participants. Patients with putative Inclusion Body Myositis (IBM) or other forms of myositis provided informed consent prior to recruitment and then were screened for participation in this study. More specifically, for inclusion in this study, IBM cases met ENMC 2011 criteria for clinically or clinico-pathologically defined IBM (Rose and ENMC 2013). Control samples were selected from age-matched non-IBM patients, including dermatomyositis, polymyositis, immune-mediated necrotizing myopathy, as well as patients with normal biopsies or non-inflammatory pathological features. Patient samples with excessive fibroadipose replacement or in poor condition were excluded. During a required diagnostic biopsy, individuals included in the study donated an extra muscle sample for use in xenograft surgeries. Under sterile conditions in the operating room, approximately one gram of tissue was removed from muscles having strength of ≥4 (MRC scale (MRC 1976)). This tissue was then dissected into approximately 7 x 3 x 3mm strips of longitudinal fibers and taken immediately to the animal suite for xenografting.

Irradiation of Muscle Biopsy

Human biopsies treated with irradiation were dissected into two pieces, placed in separate 50mL conical tubes containing 10mL of primary muscle media (20% fetal bovine serum, 2% chick embryo extract, 1% antibiotic/antimycotic in Hams F10 Medium), and one tube was treated with a 6.5 Gy dose of ionizing radiation using a Cs-

137 irradiator. This dose was selected based on several studies demonstrating this dose was myeloablative, but not likely to severely impact satellite cell activation and thus xenograft regeneration (Gulati 1987; Masuda et al. 2015; Giebel et al. 2014; Paix et al. 2018). This irradiated and untreated muscle was immediately taken to the animal suite and xenografted into 8- to 12-week NRG mice.

Animal Husbandry

All animal experiments were approved by the Johns Hopkins University Institutional Animal Care and Use Committee (IACUC) in accordance with the National Institutes of Health (NIH) Guide for the Care and Use of Laboratory Animals. Male NOD-Rag1[null] IL2rγ[null] (NRG) mice (The Jackson Labs, stock 007799) were used for all experiments. Mice were housed in ventilated racks and were given HEPA-filtered, tempered, and humidified air as well as reverse osmosis filtered hyperchlorinated water. Mice were provided water and an irradiated antibiotic diet (Envigo, TD.06596) ad libitum, and the facility provided 14 hours of light to 10 hours of dark as controlled by central timer. For xenografted mice treated with 10mg/kg OKT3 (Fisher, 50561956), stock OKT3 was diluted with sterile PBS and injected intraperitoneally immediately after the xenograft surgery and once weekly until xenograft collection was performed. This dose was chosen based on previous studies that demonstrated a dose of 10mg/kg delivered intraperitoneally could effectively eliminate $CD45^{+}CD3^{+}$ cells in the peripheral blood of humanized mice (Wunderlich et al. 2014). Control “untreated” mice in OKT3 experiments were injected with sterile PBS following the same treatment regimen.

Xenograft Surgery

For a detailed protocol please refer to Chapter 3. Briefly, 8- to 12-week NRG mice were

anaesthetized with 1.5% isoflurane, and 0.1mg/kg Buprenorphine (ZooPahrm) was administered subcutaneously for pre-emptive analgesia. A vertical incision was made to open the skin above the tibial compartment. The tibialis anterior and extensor digitorum longus muscles were removed, and pressure applied to achieve hemostasis. A 7 x 3 x 3mm strip of dissected human muscle was placed in the tibial compartment and ligated with non-absorbable suture (6-0 Surgipro, Covidien) to the tendons of the peroneus longus muscle. The incision was closed with surgical glue (Histoacryl, Tissue seal) and stainless-steel wound clips (AutoClip System, F.S.T). The analgesic Carprofen (Rimadyl, Patterson Veterinary) was given subcutaneously after the surgery at a dose of 5mg/kg.

Xenograft Collection and Processing

For a detailed protocol please refer to Chapter 3. Briefly, NRG host mice were anesthetized with 1.5% isofluorane, and the leg was shaved. The skin overlying the xenograft was opened by a longitudinal incision from ankle to knee, and the location of the graft was determined by the position of the non-absorbable sutures. The xenograft was then removed, snap-frozen in 2-methylbutane (Fisher, 03551), and sectioned at 10 μm using a cryostat (Leica, CM1860 UV). Following collection, the NRG host mice were euthanized consistent with AVMA guidelines.

Hematoxylin and Eosin (H&E) Staining

Fresh, 10μm sections were rehydrated through an ethanol dilution series: three 3-minute washes in 100% ethanol (Fisher, BP2818100), a 3-minute wash in 95% ethanol, and a 3-minute wash in 80% ethanol). Following a 5-minute wash in distilled water (dH_2O), slides were placed in Hematoxylin (Poly Scientific, s212A) for 3 minutes, washed quickly in dH_2O, and placed in Tap water for 5 minutes to allow stain to develop. Slides were

dipped 12 times in acid ethanol (1 mL concentrated Hydrochloric Acid (Fisher, SA48) in 400mL 70% ethanol), rinsed twice in Tap water for 1 minute, and placed in dH_2O for 5 minutes. Slides were then placed in Eosin (Poly Scientific, s176) for 30 seconds, and dehydrated in ethanol. Slides were cleared in xylene (Fisher, X5) and mounted using Permount (Fisher, SP15).

Cytochrome C Oxidase/Succinate Dehydrogenase (COX/SDH) Stain

10μm cryostat sections were obtained and dual-stained for COX/SDH as previously described (Loughlin 1993). Briefly, after slides were sectioned, they were immediately placed in COX incubating solution. Slides incubated for 2 hours at room temperature, and then were rinsed with distilled water. Next, the slides were placed in SDH incubating solution and incubated at 37°C for 2 hours, rinsed in distilled water, dehydrated in ethanol (80%, 95%, and 100% Ethanol 5 minutes each), cleared in xylene, and mounted using Permount.

Immunohistochemistry

10μm fresh frozen sections were fixed with ice-cold methanol (Fisher, A412) for 10 minutes and blocked with anti-mouse IgG (MKB-2215, Vector Laboratories) or with a blocking solution consisting of 2% normal goat serum in PBS. The primary antibodies used were: anti-human spectrin (NCL-SPEC1, Leica, 1:50), anti-human lamin A/C (Abcam, Ab40567, 1:50), anti-human MHC-1 (SC-32235, Santa Cruz, 1:300), anti-human p62 (SC-25575, Santa Cruz, 1:250), anti-embryonic Myosin (eMHC, MYH3) (F1.652, DSHB, 1:10), anti-CD3 mouse (M725401-2 ,DAKO, 1:60), anti-CD3 rabbit (A0452, DAKO, 1:60), anti-human CD4 (ab133616, abcam, 1:100), anti-CD8 (M710301-2,DAKO, 1:60), anti-Ki-67 (ab92742, abcam,1:60), anti-CD20 (M0755, DAKO, 1:200),

anti-CD68 (M0718, DAKO, 1:60), anti-CD138 (M7228, DAKO, 1:100). The secondary antibodies used were AlexaFluor 488 goat anti-mouse IgG1, AlexaFluor 594 goat anti-mouse IgG2b, and AlexaFluor 594 goat anti-mouse IgG1a (all Life technologies, 1:500). Biotinylated Goat Anti-Rabbit IgG Antibody (BA-1000, Vector Laboratories, 1:100) and Biotinylated Goat Anti-Mouse IgG Antibody (BA-9200, Vector Laboratories, 1:100) were used for DAB peroxide staining (SK-4100, Vector Laboratories). Where applicable, nuclei were labeled with DAPI in mounting medium (P36931, Invitrogen).

TDP-43 Cryptic Exon Detection

RNA was extracted from xenograft samples and human biopsies using TRIzol (Fisher Scientific, 15596018). A cDNA library was prepared using Protoscript II First Strand cDNA synthesis kit with random primers (NEB, E6560L), and cryptic exons were PCR amplified using the Dreamtaq Kit (Fisher, K1081P) following the protocol described in Figure 4.1. Primer sequences for TDP-43 target genes are summarized in Table 4.1. PCR products were visualized via gel electrophoresis on a 2% agarose (Fisher, 17850) gel containing 0.5µg/mL Ethidium bromide (Fisher, A25645).

Figure 4.1 Protocol for Cryptic Exon Product Amplification

Temperature	Duration	
95°C	60 s	
95°C	30 s	40X
64°C	15 s	
72°C	45 s	
72°C	7 min	
4°C	∞	

Table 4.1 Primer Sequences for Cryptic Exon Detection

Target Gene	Primer Sequences (5' => 3')	Product Length
GPSM2	F- AGTGGACATGTGGTGGTAAGAA R- GCTTCAAAGAATGACACGCCA	199bp
ACSF2	F- TGGTCAGACACAAACCTGG R- ACCGAGATGACTGTGGTCAG	169bp
HDGFRP2	F- CTGCGCTAAAGATGTCGGTCT R- TGCTTCCCTCCCTTCTGATGC	263bp

T cell Receptor Sequencing

T cell Receptor (TCR) Sequencing experiments were performed in collaboration with the laboratory of Dr. H. Benjamin Larman using the Framework Region 3 (FR3) AmplifiKation sequencing ("FR3AK-seq") method (Montagne et al. 2018). Briefly, RNA was TRIzol extracted from human biopsies and xenograft samples, and then reverse transcribed using a TCR beta (TCRB) chain constant region reverse primer with Superscript III First-Strand Synthesis System (Invitrogen). Primers to FR3 were used to PCR amplify all human TCR beta V alleles with KAPA2G Fast Multiplex Mix (Roche). Sequencing was performed on a HiSeq 2500, and results were analyzed using MiXCR v2.1.11 software (Bolotin et al. 2015)

Flow Cytometry

Flow Cytometry experiments were performed in collaboration with the laboratory of Dr. Armando Villalta as previously described (Villalta et al. 2014). To eliminate non-muscle

residing immune cells, mice were perfused with PBS and lymph nodes were removed. Single-cell suspensions were prepared from the isolated xenografts and incubated with anti-CD16/32 (clone 2.4G2) to block Fc receptors. These suspensions were then stained with human antibodies for CD3, CD4, CD8, CD28, CD57, and DAPI or Blue-Fluorescent Reactive Dye (Invitrogen Life Technologies) to assess cell viability. Analysis was performed on live cells on a BD LSRII flow cytometer with FACSDiva software (BD Bioscience). Post-acquisition analysis was performed with Flowjo software version 9.1.

Microscopy and Image Analysis

Fluorescent and transmitted light microscopy was carried out at the Johns Hopkins NINDS Multiphoton Imaging Core on a Keyence (BZ-X700) widefield, inverted microscope. Image analysis was performed in Fiji (Schindelin et al. 2012). Analysis of fiber cross-sectional area was semi-automated using MuscleJ (Mayeuf-Louchart et al. 2018).

Statistical analysis

All statistical analyses were performed using GraphPad Prism version 8.3.1 for Windows, GraphPad Software, La Jolla California USA, www.graphpad.com.
One-way ANOVA was used for comparisons between multiples groups, followed by a post hoc Tukey test to determine significance of differences between two groups. Alternatively, If the standard deviations between the groups were different, one-way Brown-Forsythe and Welch ANOVA test was used with the Dunnett's T3 test for multiple comparisons. The nonparametric Mann-Whitney test was used also used to determine significance between two groups where noted. Data are presented as means +/- SD unless otherwise indicated in figure legends. Significance markers on figures are from

post hoc analysis (ns, not significant; *p ≤ 0.05, **p ≤ 0.001; ***p ≤ 0.001; ****p ≤ 0.00001) with values of $p \leq 0.05$ considered significant.

Chapter 5: A Xenograft Model of Inclusion Body Myositis

5.1 Overview and Aims

The pathogenesis of IBM has eluded researchers for decades, and is an area of considerable debate (Benveniste et al. 2015; Weihl and Mammen 2017; Keller, Schmidt, and Lünemann 2017; Greenberg 2019). The presence of highly differentiated CD8+ T-cells invading healthy-appearing myofibers, the association of IBM with specific HLA loci and other autoimmune disorders, and the presence of autoantibodies in IBM support an autoimmune basis for the disease. However, the fact that immunosuppression has failed to show clinical benefit, the presence of protein aggregates (e.g. p62 and TDP-43) commonly found in neurodegenerative diseases, and the association with aging suggest the possibility that IBM is primarily a degenerative disease. Taken together, the pathogenesis of IBM is likely multifactorial with contributions from aging, genetic background, and environmental factors, and thus may be a combination of autoimmune and degenerative pathophysiologic processes. The absence of an animal model for IBM has hindered our progress in understanding the pathogenesis of IBM, and this study aims to establish and characterize the first animal model of IBM.

5.2 Inclusion criteria and patient characteristics

Patients with putative IBM or other forms of myositis or myopathy provide informed consent prior to recruitment and then are screened for participation in this study (**Table 5.1**). Older patients undergoing muscle biopsy were preferentially recruited for this study to increase the likelihood of obtaining age-matched controls. IBM cases meet ENMC 2011 criteria for clinically or clinico-pathological defined sporadic IBM (Rose and ENMC 2013). Control samples are selected from non-IBM patients, including dermatomyositis, polymyositis, immune-mediated necrotizing myopathy, as well as patients with normal biopsies or mild, non-inflammatory pathological features. Patient samples with excessive fibroadipose replacement or in poor condition are not used for xenograft surgeries. Control patients are divided into non-myositis or myositis groups based on the absence or presence of T cells within the diagnostic biopsy respectively. The typical pathologic diagnoses of “non-myositis control” (NMC) biopsies include normal muscle, mild myopathic features (e.g. scattered internalized nuclei), mild neurogenic atrophy, and/or mitochondrial abnormalities. The “myositis control” (MC) biopsies show perifascicular inflammation, mild necrosis, myophagocytosis, and/or fasciitis. The IBM biopsies show characteristic features of IBM, including endomysial inflammation, primary invasion of myofibers by CD3+ T cells, COX-deficient fibers, and/or rimmed vacuoles. The sex and disease duration of the patients as well as the strength of the biopsied muscle are not significantly different between control and IBM patients (**Table 5.1**). However, the IBM patient population is significantly older than both control groups (non-myositis controls (NMC) vs IBM, $p = 0.0125$; myositis controls (MC) vs IBM, $p = 0.0088$) (**Table 5.1**). The majority of skeletal muscle biopsies used in xenograft surgeries were obtained from the biceps (46.15%) or rectus femoris (30.77%).

Table 5.1 Characteristics of xenograft study population

	Entire Population (n=26)	Non-myositis Controls (n=6)	Myositis Controls (n=6)	IBM (n=14)	p-value NMC vs IBM	p-value MC vs IBM
Sex (male), n (%)	17 (65.38%)	3 (50%)	3 (50%)	11 (78.57%)	0.3027	0.3027
Age (yrs.), mean ± SD	64.27 ± 10.23	58.5 ± 10.9	57.3 + 9.58	69.7 + 7.13	0.0125*	0.0088**
Disease duration (yrs.), mean ± SD	4.77 ± 5.98	5.67 ± 4.84	6.50 ± 11.57	3.64 ± 2.27	0.4503	0.3313
Biopsy location, n (%)						
- Biceps	12 (46.15%)	3 (50%)	1 (16.67%)	8 (57.14%)		
- Rectus femoris	8 (30.77%)	2 (33.33%)	3 (50%)	3 (21.43%)		
- Vastus lateralis	3 (11.54%)	1 (16.67%)	1 (16.67%)	1 (7.12%)		
- Deltoid	3 (11.54%)	0 (0%)	1 (16.67%)	2 (14.28%)		
Number of Xenografts	229	48	42	139		
Histological features of biopsy	----	Normal muscle, mild myopathic features, mild neurogenic atrophy, and/or mitochondrial abnormalities	Perifascicular inflammation, mild necrosis, myophagocyt-osis, and/or fasciitis	Endomysial inflammation, primary invasion, COX-deficient fibers, and/or rimmed vacuoles		

Table 5.1 A summary of clinical, demographic, and biopsy details of patients involved used in this study. The disease duration was determined from the time of symptom onset—according to the patient's medical records—to the time the diagnostic biopsy was performed. The strength of the biopsied muscle was based on the Medical Research Council (MRC) scale out of five (MRC 1976). Mann-Whitney test was used to determine significance for the following features: age, disease duration, and strength of biopsied muscle. Fisher's exact test was used to determine significance for the sex ratio of the patient population (Non-myositis control (NMC); Myositis control (MC)). In all cases, $p \leq 0.05$ was considered significant.

5.3 IBM xenografts regenerate robustly in NRG mice

Our data demonstrate that IBM xenografts successfully regenerate comparably to both non-myositis and myositis control xenografts (**Figure 5.1**). Histological and immunofluorescent stains both show numerous regenerated human fibers (**Figure 5.1A**), and there are no significant differences in the number of regenerated fibers between any of the three groups (**Figure 5.1B**). In addition, the percent of embryonic myosin (eMHC) positive fibers is unchanged, indicating that the process of myofiber maturation as assessed by the turnover of eMHC is unaffected (Schiaffino et al. 2015) (**Figure 5.1D**). There is a moderate increase in myofiber density, as determined by the percent of the xenograft area covered by myofibers, observed in IBM xenografts in comparison to non-myositis control xenografts ($p = 0.0315$) (**Figure 5.1C**). This can be explained by a corresponding increase in the median cross-sectional area (CSA) of IBM xenografts in comparison to both non-myositis control ($p < 0.0001$) and myositis control xenografts ($p = 0.0420$) (**Figure 5.1E**). Overall, these data show that IBM patient muscle is capable of forming robust human xenografts, even from patients showing moderate to severe IBM pathology. This is important on two fronts: first and foremost, this demonstrates feasibility of this model, and second, it demonstrates that IBM muscle is capable of robust regeneration which shows promising potential for therapeutic testing.

Figure 5.1 IBM muscle regenerates robustly in NRG mice

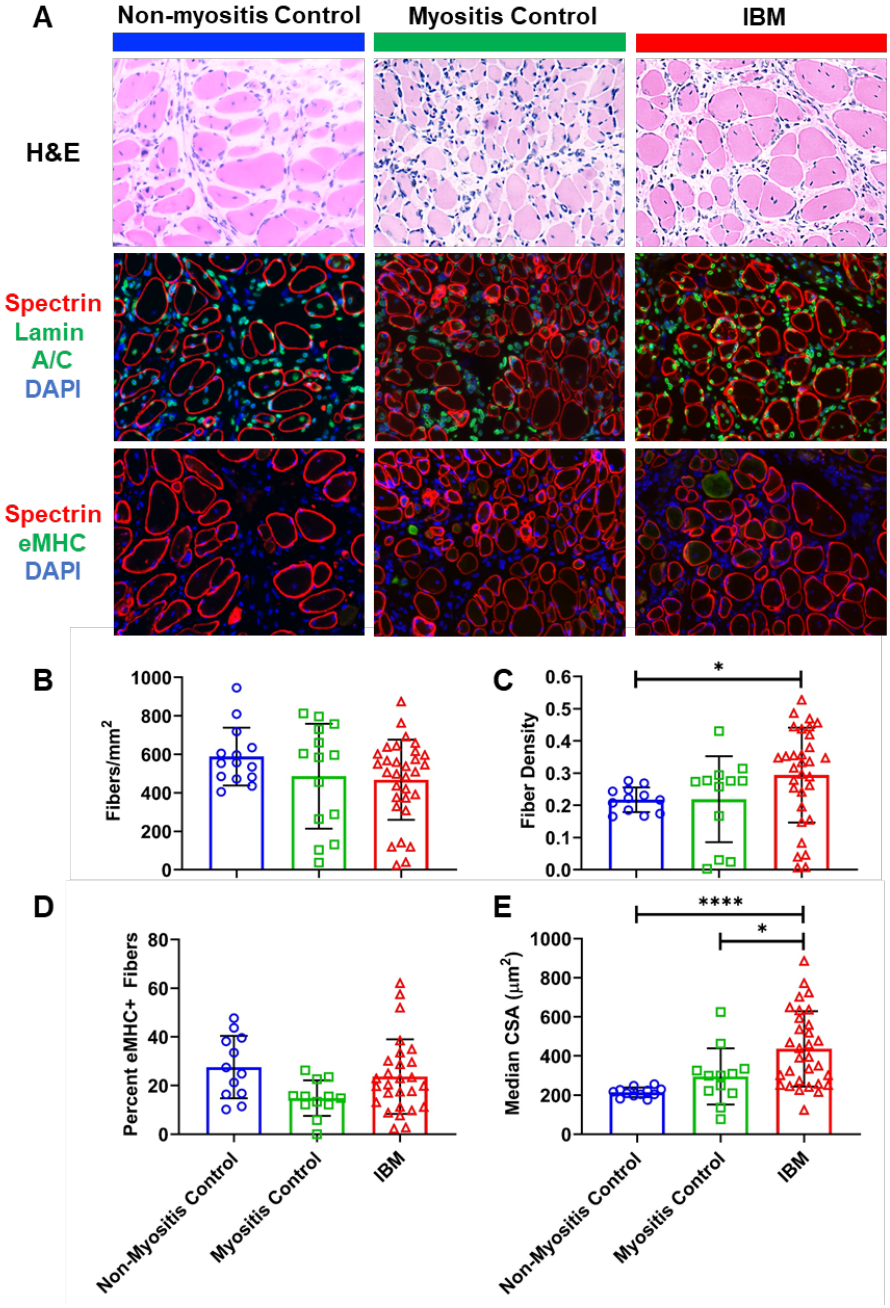

Figure 5.1 (A) Representative images of non-myositis control, myositis control, and IBM xenografts stained with H&E, human spectrin (red), human lamin A/C (green), embryonic myosin (eMHC) (green), and DAPI (blue). Quantification of the number of fibers over the xenograft area **(B)**, the fiber density of the xenografts as determined by the percentage of the xenograft area covered by myofibers **(C)**, the percent of eMHC+ fibers (**D**), and the median cross-sectional area (CSA) of myofibers within the xenografts **(E)**. For all graphs, each point denotes one xenograft (non-myositis control, n=14; myositis control, n=14; IBM xenografts, n=31) and for all p-values determined by Dunnett's T3 test following one-way Brown-Forsythe and Welch ANOVA: *p ≤ 0.05.

5.4 IBM xenografts recapitulate disease pathology

Once it was established IBM muscle could regenerate in host mice, the next step was to assess these xenografts for features of IBM pathology. Namely, we examined xenografts for degenerative features such as protein aggregation and mislocalization as well as inflammatory features such as endomysial inflammation and primary invasion of non-necrotic fibers.

Protein aggregation and mislocalization

To assess the IBM xenografts for degenerative features of disease we first performed immunostaining for p62, an autophagic adaptor that binds to ubiquitinated protein aggregates and is commonly seen aggregated in IBM muscle (Hiniker et al. 2013). We found positive staining at 10-months within IBM xenografts, but not myositis controls (**Figure 5.2A**). These p62-positive fibers are rare and have not been observed in earlier collections. Another degenerative feature observed in IBM patient muscle is the sarcoplasmic mislocalization and aggregation of TAR DNA-binding protein 43 (TDP-43) (Salajegheh et al. 2009; Hiniker et al. 2013). One of the essential nuclear functions of TDP-43 is to act as a splice repressor of cryptic exons (Jonathan P. Ling 2015). When TDP-43 is mislocalized from the nucleus, these cryptic exon sequences are included in mRNA transcripts and can be detected via RT-PCR using primers designed to the junctions between cryptic exons and adjacent exons (**Figure 5.2B**). We tested non-myositis, myositis, and IBM patient biopsies for cryptic exon expression from three TDP-43 target genes: GPSM2, ACSF2, and HDGFRP2 (**Figure 5.2C**). The majority (9 out of 11, 81.82%) of the IBM patient biopsies showed cryptic exon expression, and none (0 out of 7, 0%) of the control patients showed cryptic exon expression (**Figure 5.2C**). In

addition, we have detected GPSM2 and ACSF2 cryptic exon expression within 8-month and 10-month IBM xenografts from three different IBM cases, but not in non-myositis control xenografts (**Figure 5.2D,E**). Cryptic exon expression in IBM xenografts always corresponds to the patient biopsy; i.e. only human biopsies showing cryptic exon expression result in xenografts with cryptic exon expression. Examining cryptic exon expression longitudinally within one case reveals that although cryptic exon expression cannot be detected at 4-months (0/2 xenografts), by 8-months expression can be detected (3/4 xenografts) (**Figure 5.2E**), which suggests that this feature of IBM xenografts develops over time. Of note, we have not observed an obvious mislocalization and aggregation of TDP-43 in the sarcoplasm of IBM xenografts. However, these data show that TDP-43 nuclear function is likely impaired, and the protein is likely mislocalized in IBM xenografts, but not to the same extent as observed in IBM patient biopsies.

Figure 5.2 IBM xenografts show p62 aggregation and TDP-43 cryptic exon expression

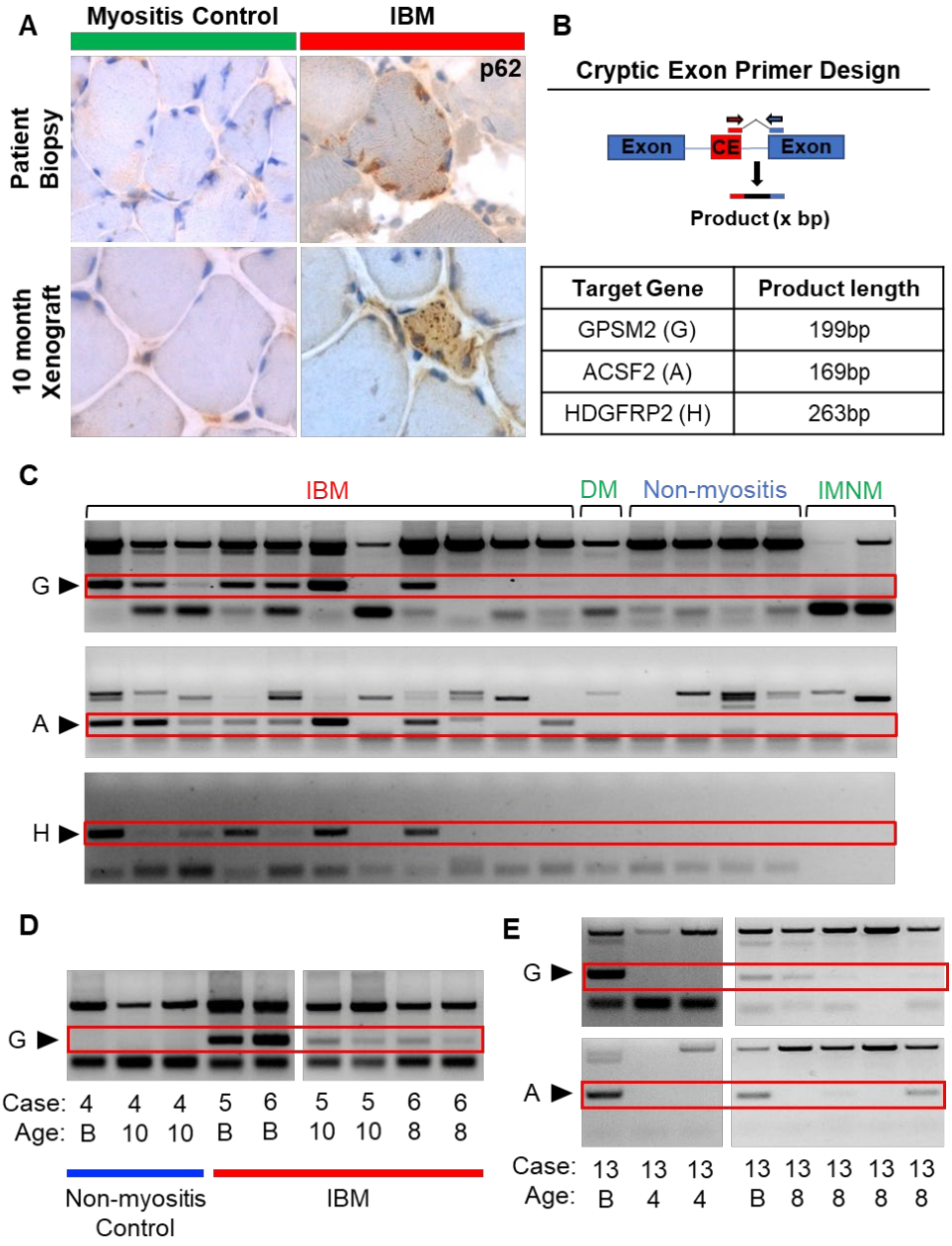

Figure 5.2 (**A**) Staining of autophagic adaptor p62 within patient biopsies and 10-month xenograft collections from myositis control and IBM xenografts. (**B**) Using primer pairs (arrows) designed to the junction of cryptic exon (CE) sequences, cryptic exon expression from TDP-43 target genes can be detected using RT-PCR. (**C**) Cryptic exon expression from TDP-43 target gene GPSM2 (G), ACSF2 (A), and HDGFRP2 (H) detected in IBM patient biopsies. No cryptic exon expression was detected in biopsies from non-myositis controls patients, or myositis control patients diagnosed with Dermatomyositis (DM) or immune mediated necrotizing myopathy (IMNM). (**D**) Cryptic exon expression from GPSM2 (G) detected in IBM patient biopsies and xenografts, but not non-myositis control biopsy or xenografts (B = patient biopsy). (**E**) Cryptic exon expression from TDP-43 target gene GPSM2 (G) and ACSF2 (A) detected in IBM xenografts at 8-months, but not 4-month collections (B = patient biopsy).

Mitochondrial Pathology

Mitochondrial abnormalities are a widely underappreciated feature of IBM pathology, and are not included in most diagnostic criteria for IBM. However, scattered cytochrome c oxidase (COX)-deficient fibers can be seen in the vast majority of patient muscle biopsies (Dahlbom, Lindberg, and Oldfors 2002; Joshi et al. 2014; Catalan-Garcia et al. 2016). To assess IBM xenografts for this pathological feature, we carried out dual COX and succinate dehydrogenase (SDH) histological stains on 4-month non-myositis, myositis, and IBM xenografts. We find that the number of COX-deficient fibers is significantly increased in IBM xenografts in comparison to both non-myositis control xenografts ($p = 0.0010$) and myositis control xenografts ($p = 0.0256$) (**Figure 5.3A,B**). These findings indicate that this feature of IBM pathology is also recapitulated in our IBM xenograft model.

Figure 5.3 IBM xenografts display mitochondrial pathology

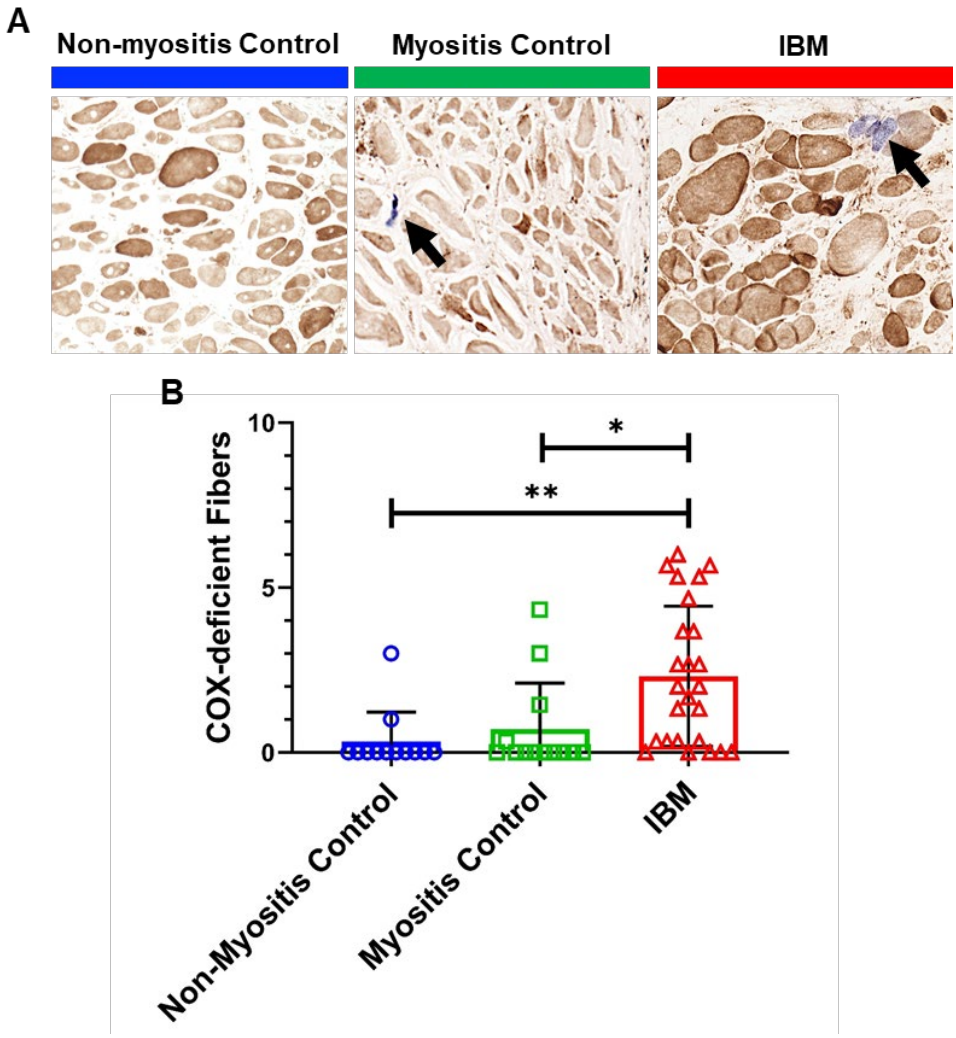

Figure 5.3 (A) Representative images of dual COX/SDH stains of 4-month non-myositis control, myositis control, and IBM xenografts. **(B)** Quantification of the number of COX-deficient fibers in each group; each point denotes one xenograft (non-myositis control n = 12, myositis control n= 13, IBM n = 25). Groups were compared using Brown-Forsythe and Welch one-way ANOVA with Dunnett's T3 multiple comparison test to determine all p-values: *p ≤ 0.05, **p ≤ 0.01.

Endomysial inflammation and primary invasion in IBM xenografts

In addition to these degenerative characteristics, several inflammatory features of IBM are also recapitulated in IBM xenografts (**Figure 5.4**). Non-myositis and myositis control xenografts show typical MHC-I staining around capillaries; however, IBM xenografts show a dramatic sarcoplasmic upregulation of MHC-1 (**Figure 5.4A**). We find that this upregulation corresponds to the presence of CD3+ T cells within IBM xenografts (**Figure 5.4A**). In comparison to non-myositis control xenografts, both myositis control xenografts ($p < 0.0001$) and IBM xenografts ($p < 0.0001$) show significantly higher levels of CD3+ T cells (**Figure 5.5B**). Despite the similar levels of inflammation in both IBM and myositis control xenografts, examples of primary invasion of non-necrotic fibers are only observed in IBM xenografts (**Figure 5.5C**). Further staining shows a variety of different human immune cells persist within IBM xenografts, including helper (CD4+) and cytotoxic (CD8+) T cells, in addition to B cells (CD20+), macrophages (CD68+), and rare plasma cells (CD138+) (**Figure 5.4D**).

Remarkably, the majority of CD8+ T cells within IBM xenografts were found to be proliferative at 4-months, and this proliferation is significantly reduced by 6-months ($p < 0.0001$) and remains low at 8.5-months ($p < 0.0001$) (**Figure 5.5A,B**). The nature of the immune cells present with IBM patient muscle has been the focus of numerous studies. The majority of IBM muscle biopsies show oligoclonal populations of T cells, indicating that recognition of an unknown antigen is likely occurring (O'Hanlon et al. 1994; Lindberg, Oldfors, and Tarkowski 1994; Fyhr et al. 1997; Salajegheh et al. 2007). These clonal population of T cells persist over time, experience repeated antigen stimulation indicated by their loss of CD28 expression, and become highly differentiated and

cytotoxic as shown by the expression of markers such as CD57 and KLRG1 (Müntzing et al. 2003; Pandya et al. 2010; Greenberg et al. 2016; Greenberg et al. 2019).

To better characterize the human immune cells within IBM xenografts, we have performed flow cytometry and T cell receptor (TCR) sequencing. Flow cytometry experiments have shown increased numbers of human CD45+ lymphocytes in an IBM xenograft in comparison to a myositis control xenograft (**Figure 5.5C**). The IBM xenograft had high levels of both CD4+ T cells and CD8+ T cells whereas the myositis control only had very low numbers of CD8+ cells (**Figure 5.5C**). Finally, many CD4+ and CD8+ T cells in the IBM xenografts were CD57+, and some of the CD8+ cells were CD28-CD57+ indicating they were antigen experienced, which was not the case in the myositis control xenograft (**Figure 5.5C**). These populations of cells mirror what has been found in IBM patient biopsies.

To examine whether the T cells in IBM xenografts are oligoclonal, we used Framework Region 3 AmplifiKation sequencing (FR3AK-seq), a multiplex PCR-based approach to determine TCR repertoires (Montagne et al. 2018). This technique revealed that T cells within IBM xenografts are clonally restricted and contain hyperexpanded populations of T cells (**Figure 5.5D**). In addition, T cells within two xenografts showed restricted J gene (TRBJ2-3*01) usage, which was also observed three IBM patients (**Figure 5.5E**). Taken together, these data indicate that potentially disease relevant immune cells persist in IBM xenografts, and, as this model recapitulates the inflammatory and degenerative features of IBM, it provides a platform for therapeutic testing.

Figure 5.4 Endomysial inflammation and primary invasion in IBM xenografts

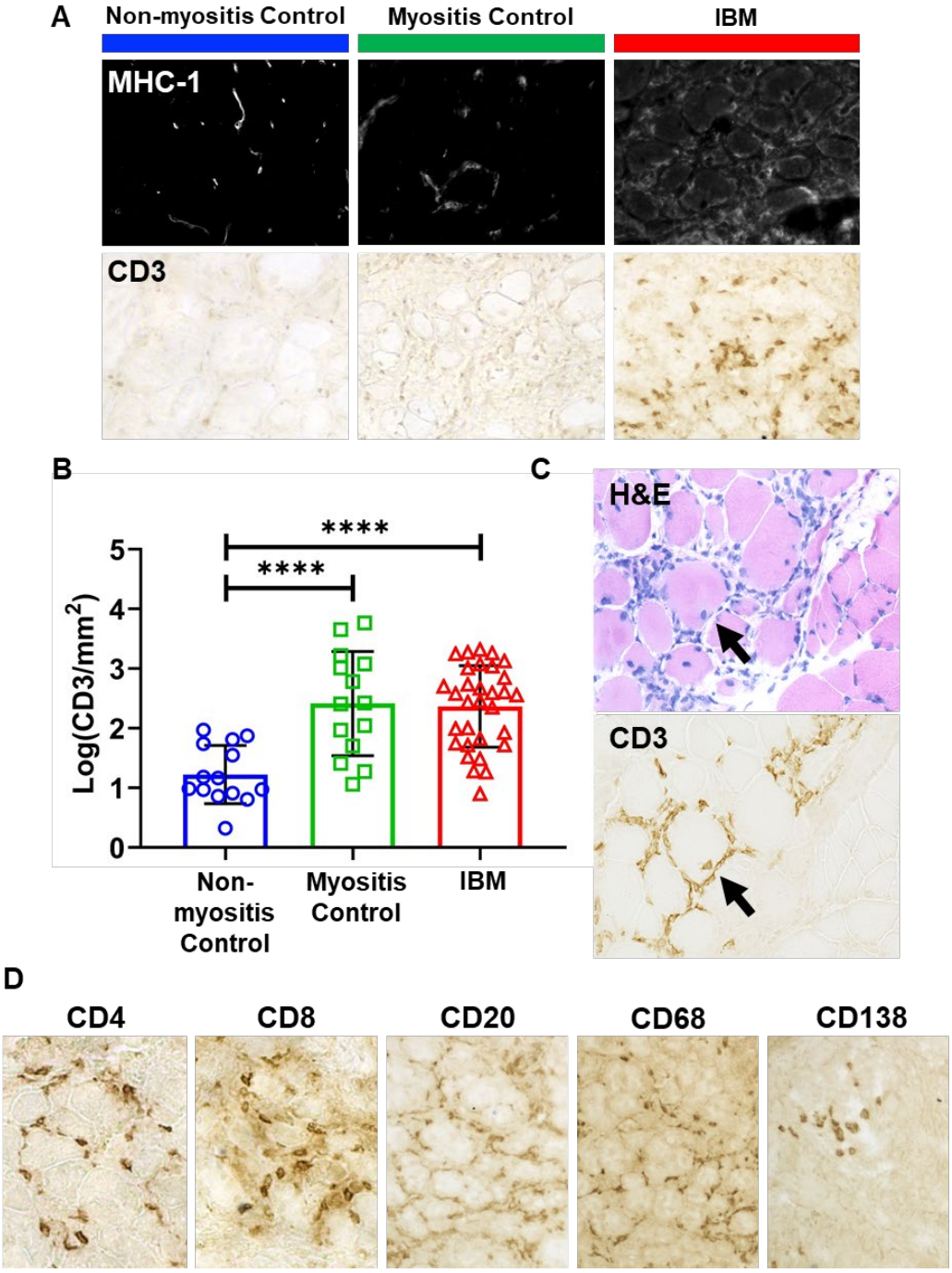

Figure 5.4 (**A**) Representative MHC-I and CD3 stains of 4-month non-myositis control, myositis control, and IBM xenografts. (**B**) Quantification of the number of CD3+ T cells over the xenograft area. Each point denotes one xenograft (non-myositis control, n=14; myositis control, n=14; IBM xenografts, n=31), and one-way ANOVA with Tukey's multiple comparison test was used to determine p-values (****p<0.0001). (**C**) H&E and CD3 stains showing an example of primary invasion of a non-necrotic fiber in a 4-month IBM xenograft. (**D**) Representative stains of CD4, CD8, CD20, CD68, and CD138 from a 4-month IBM xenograft.

Figure 5.5 T cells in IBM xenografts are proliferative, antigen experienced, and oligoclonal

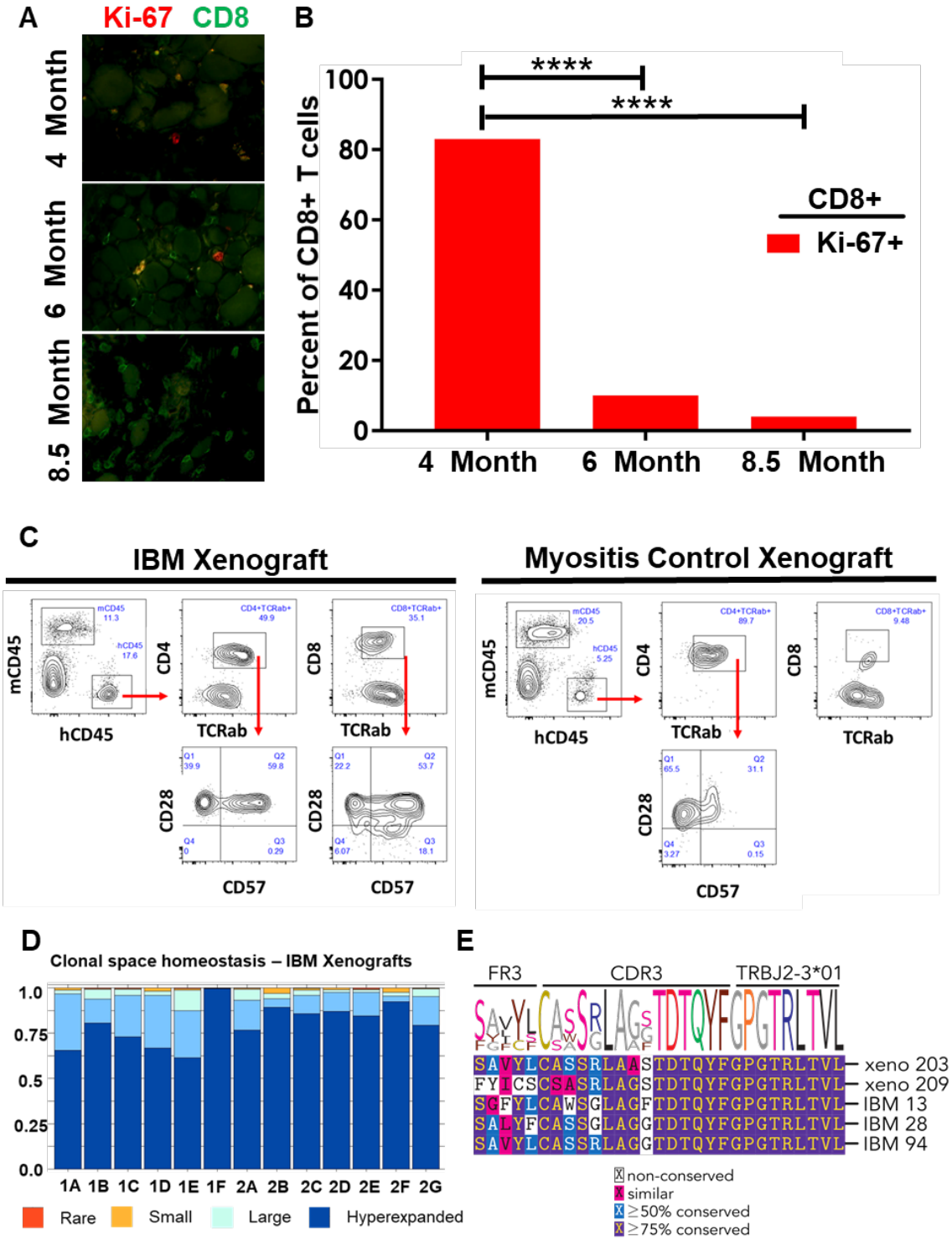

Figure 5.5 (A) Ki-67 (red) and CD8 (green) staining of 4-month, 6-month, and 8.5-month IBM xenografts. **(B)** Quantification of the percent of CD8+ T cells that show positive Ki-67 staining in

4-month, 6-month, and 8.5-month IBM xenografts. Fisher's exact test was used to determine significance (****$p < 0.0001$). (**C**) Flow cytometry experiments comparing a myositis control xenograft and an IBM xenograft using human specific CD45 (hCD45) to analyze CD4+ and CD8+ populations of human T cells in xenografts. CD28 and CD57 populations were also examined (**D**) Analysis of TCR repertoire of 14 IBM muscle biopsies shows that most have primarily "large or "hyperexpanded" T cell clones. 5 xenografts samples from case 1 (1A-1F) and 7 samples from case 2 (2A-2G) from 3-11 month timepoints all show primarily hyperexpanded T cell clones. (**E**) Multiple sequence alignment (by MUSCLE) of a TCR clone found in xenografts from 2 patients ("xeno") and 3 IBM biopsies ("IBM") showing restricted usage of TRBJ2-3*01.

.

Chapter 6: Preclinical Testing in the IBM Xenograft Model

6.1 Overview and Aims

A fundamental stumbling block to the development of therapies for IBM has been the lack of an animal model: a problem we have aimed to address with our IBM xenograft model. The second goal of this project is to determine the feasibility of using this model to carry out preclinical studies. A central question in IBM is whether inflammation drives degeneration or is secondary to it. Recently, highly differentiated effector CD8+ T cells present in IBM muscle have been suggested to be refractory to conventional immunotherapy, and several companies are developing targeted approaches to deplete this subpopulation of T cells for therapeutic development in IBM (Greenberg et al. 2016; Greenberg et al. 2019). Our xenograft model may be an ideal model to test this hypothesis in vivo. If depleting T cells rescues degenerative pathological features, this would provide direct evidence that T cells are necessary for myofiber degeneration in IBM. In contrast, if depleting T cells (including the putative refractory highly-differentiated subset) has no effect on degenerative pathology, this would suggest that this is unlikely to be a successful therapeutic approach. If these experiments are successful, they hold promise for directing therapeutic development in IBM.

6.2 Irradiation of IBM Xenografts

Our initial studies involved the use of *ex vivo* irradiation to eliminate immune cells within the human biopsy. Ionizing radiation causes double-strand breaks in DNA either directly or indirectly via reactive oxygen species (ROS). DNA repair mechanisms for correcting double-strand breaks are error-prone and typically result in chromosomal aberrations and rearrangements that can be observed in the first metaphase after irradiation (Hall and Kereiakes 2001). When cells attempt to proliferate in the face of this DNA damage, they enter cell cycle arrest, and, if the DNA damage cannot be repaired, apoptosis or other cell death pathways are triggered and the cells are eliminated (Mladenov et al. 2016). In particular, T cells are moderately radiosensitive and typically die via necrosis when challenged with a dose over 2 Gy (Falcke et al. 2018). We hypothesize that low dose radiation may deplete inflammatory cells without inhibiting proliferation of muscle stem cells (satellite cells), and thereby allow us to test our central hypothesis that T cells drive degenerative pathology in IBM.

Patient Characteristics

To carry out these experiments, muscle biopsy specimens from six patients (4 IBM, 2 controls (**Table 6.1**)) were treated with a 6.5 Gy dose of ionizing radiation. This dose was selected based on several studies demonstrating that this dose was myeloablative, without severely impacting satellite cell activation (Gulati 1987; Masuda et al. 2015; Giebel et al. 2014; Paix et al. 2018; Falcke et al. 2018). All IBM patients met ENMC 2011 criteria for clinico-pathologically or clinically defined IBM (Rose and ENMC 2013). The IBM biopsies showed characteristic pathological features including endomysial inflammation and primary invasion as well as vacuoles and mitochondrial pathology

(**Table 6.1, Figure 6.1**). The control case 14 biopsy showed scattered myofiber degeneration and necrosis (**Figure 6.1E**), and rare scattered inflammatory cells (**Figure 6.1H**). There were no examples of primary invasion, and the GT stain did not show red-rimmed vacuoles or ragged-red fibers (**Figure 6.1K**). The control case 15 biopsy showed rare angular atrophic fibers indicating mild neurogenic atrophy, and there was no myofiber degeneration, regeneration, or necrosis and no inflammatory cells were present (**Figure 6.1C,F,I,L**).

Table 6.1 Patient Characteristics - Irradiation Experiments

Case	Patient Sex	Age	Clinical Diagnosis	Biopsy Location (MRC)	Histological Features of Biopsy
5	Male	77	sIBM	Biceps (5)	Moderate inflammatory myopathy with myofiber degeneration, MHC-I upregulation, necrosis, regeneration, endomysial inflammatory cells, and frequent red rimmed vacuoles. In addition, there is mild neurogenic atrophy and 2 dozen COX-negative fibers.
6	Male	74	sIBM	Vastus lateralis (5)	Chronic inflammatory myopathy with red rimmed vacuoles, myofiber degeneration, endomysial inflammation and primary invasion, numerous COX-negative fibers, and mild neurogenic atrophy.
19	Female	66	sIBM	Biceps (4+)	Severe, chronic inflammatory myopathy with myofiber degeneration, necrosis, regeneration, endomysial inflammation and primary invasion, and vacuoles. There is also mild neurogenic atrophy and several COX-negative fibers.
20	Male	66	sIBM	Biceps (5)	Moderate inflammatory myopathy with myofiber degeneration, necrosis, regeneration, endomysial inflammation and primary invasion, and frequent vacuoles. In addition, there is mild neurogenic atrophy and innumerable COX-negative fibers.
14	Female	64	HMGCR-myopathy	Biceps (5)	Mild necrotizing myopathy and mild type 2 atrophy. There is scattered myofiber degeneration and necrosis, rare scattered inflammatory cells and no primary inflammation.
15	Female	64	Putative metabolic myopathy	Rectus Femoris (5)	Mild Neurogenic atrophy. No myofiber degeneration, regeneration, or necrosis, and no inflammatory cells are present.

Table 6.1 A summary of clinical demographics, histological features, and clinical diagnosis of patients involved in irradiation experiments. The average age of the IBM patients was 70.25 years and the average age of controls was 64 years. One of the four IBM patients was female, and both control patients were female. The majority of the muscle biopsies were taken from the biceps. One IBM patient had a vastus lateralis biopsy, and one control had a rectus femoris biopsy. The biopsy location is followed in parentheses by the strength of the biopsied muscle based on the Medical Research Council (MRC) scale out of five (MRC 1976). The IBM biopsies showed characteristic pathological features including endomysial inflammation and invasion as well as rimmed vacuoles. One control showed a mild necrotizing myopathy with limited immune cells, and the other control showed mild neurogenic atrophy and an absence of immune cells.

Figure 6.1 Histological Features of Human Biopsies - Irradiation Experiments

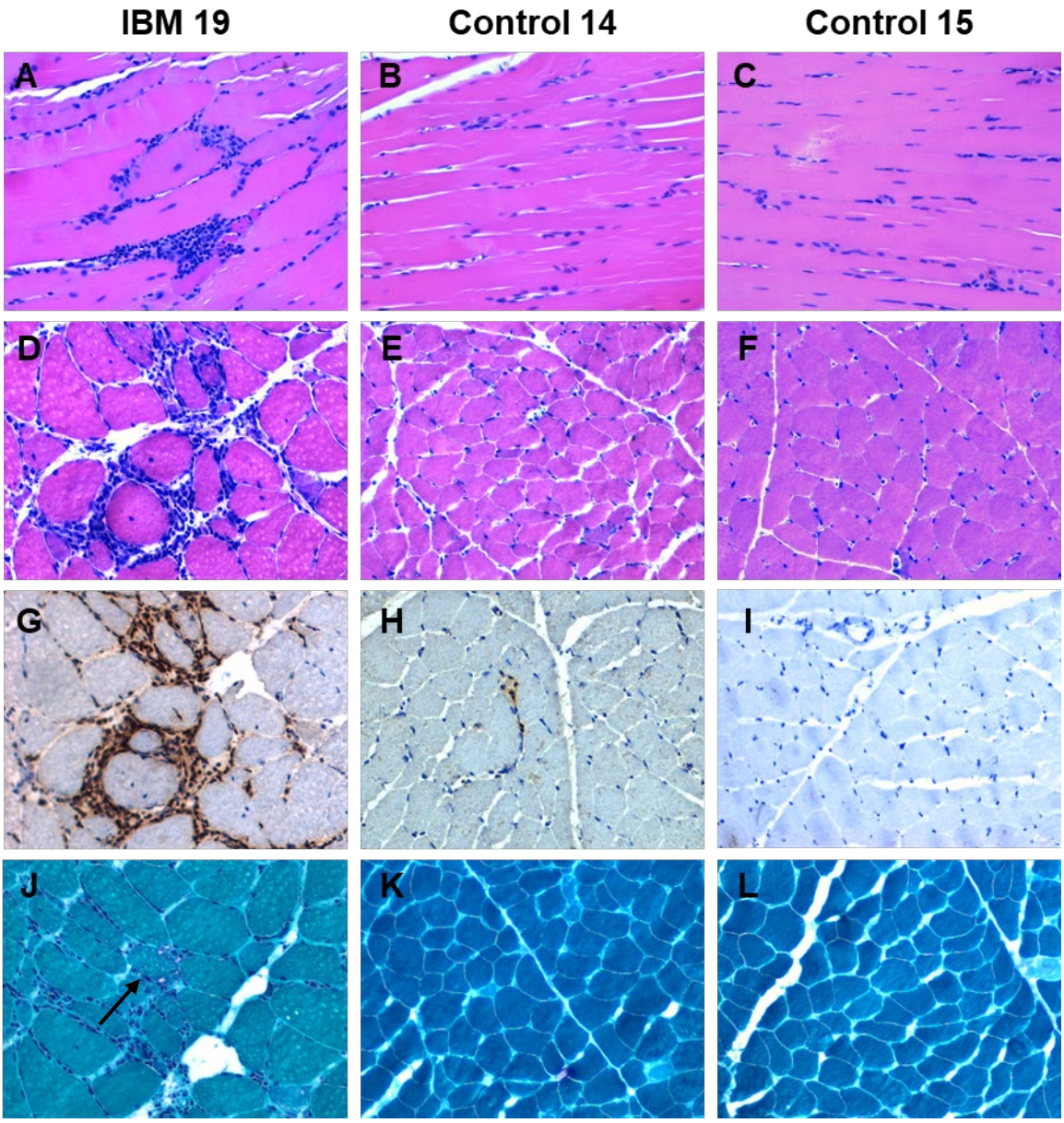

Figure 6.1 Paraffin (**A-C**), H&E (**D-F**), CD3 (**G-I**), and gomori trichrome (GT) (**J-L**) stains showing representative histology from IBM case 19, and control cases 14 and 15. The IBM case 19 biopsy shows severe endomysial inflammation and primary invasion of non-necrotic fibers (**A,D,G**), and vacuoles (**J, arrow**). The control case 14 biopsy shows scattered myofiber degeneration and necrosis (**E**), and rare scattered inflammatory cells (**H**). There is no primary invasion, and the GT stain does not show vacuoles or ragged-red fibers (**K**). The control case 15 biopsy shows rare angular atrophic fibers (**F**) indicating mild neurogenic atrophy. There is no myofiber degeneration, regeneration, or necrosis, and no inflammatory cells are present (**C,F,I,L**).

Irradiation of xenografts severely impairs control regeneration and does not significantly reduce inflammation

At 4 months, irradiated IBM xenografts show moderately improved regeneration ($p = 0.0309$), but no significant reduction in the number of CD3+ T cells (**Figure 6.2, Figure 6.3A,B**). Interestingly, while the regeneration of control xenografts was severely impaired by irradiation ($p = 0.0004$) (**Figure 6.2D, Figure 6.3A**), irradiation led to a small but significant improvement in muscle regeneration in IBM xenografts. Similarly, while there is also a reduction in the median CSA of regenerated myofibers in the irradiated control xenografts ($p = 0.0023$), there is no effect of radiation on myofiber size in IBM xenografts (**Figure 6.3C**). These data demonstrate that even low dose irradiation can impair regeneration of control xenografts, likely by impacting proliferating satellite cells. It is interesting that IBM xenografts appear to be resistant to this irradiation-induced impairment in myoregeneration. It has been reported that the number of satellite cells is increased in IBM patient muscle, and expression of MyoD is reduced whereas Myogenin is strongly upregulated (Hollemann et al. 2008). MyoD is a transcription factor that drives proliferation of satellite cells and, conversely, the transcription factor Myogenin drives differentiation (Zammit 2017). Taken together, this describes an increased population of satellite cells primed for differentiation instead of proliferation, which may explain why IBM xenografts were not negatively impacted by irradiation and instead showed moderate improvement in the number of regenerated fibers. The number of control (n=2) and IBM (n=4) patients used in these studies was small, however, this may be an interesting area for future investigation. In addition, despite the small patient population, the inability of irradiation to significantly reduce T cell number in xenografts suggests that a more targeted approach is needed to test the effects of T cells on IBM pathology.

Figure 6.2 Irradiation of xenografts severely impairs control regeneration and does not reduce inflammation.

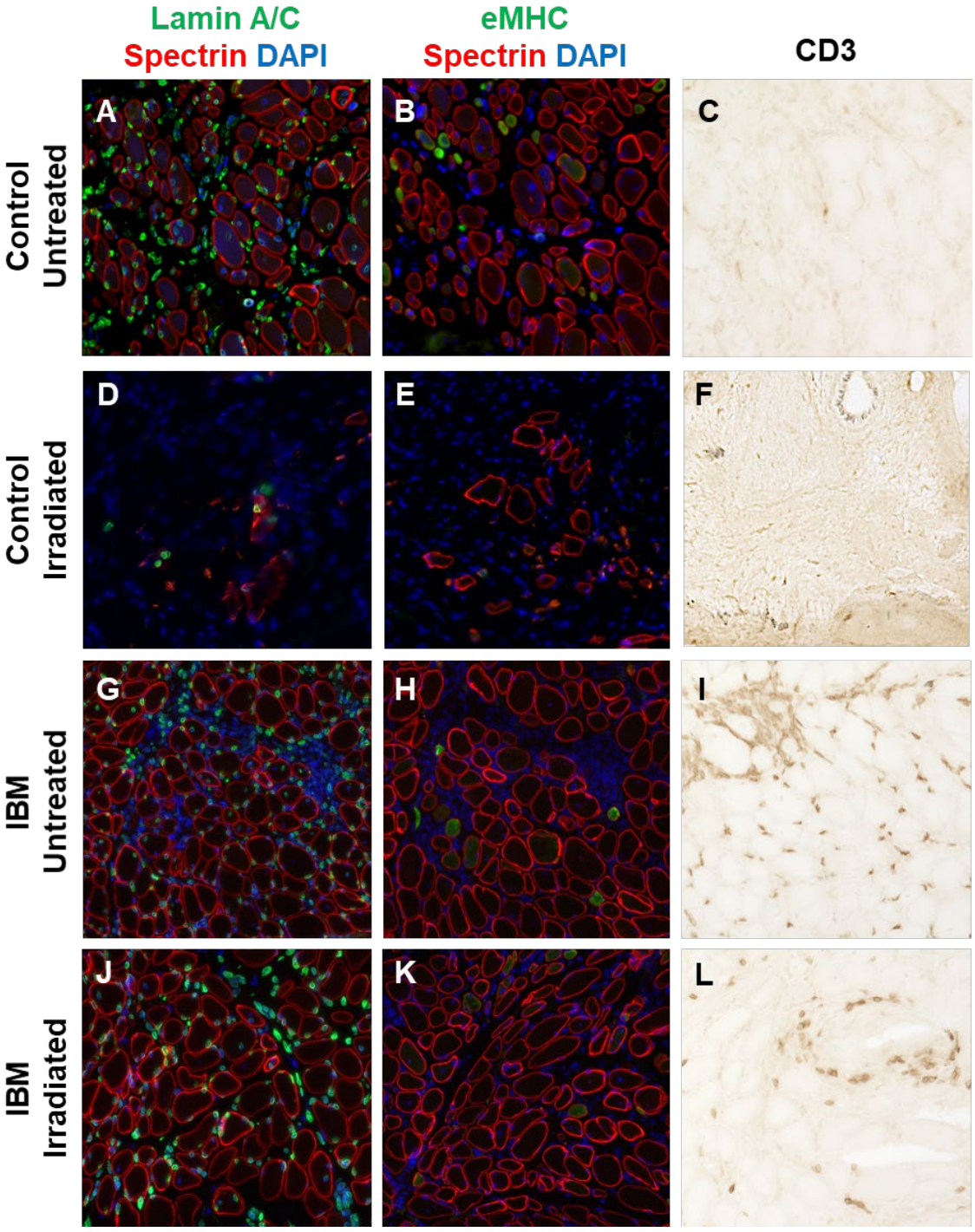

Figure 6.2 Lamin A/C (green), spectrin (red), eMHC (green), DAPI (blue), and CD3 staining of control untreated xenografts (**A-C**), control irradiated xenografts (**D-F**), IBM untreated xenografts (**G-I**), and IBM irradiated xenografts (**J-L**). All xenografts were collected at 4 months.

Figure 6.3 Fiber Morphology and T cell quantification of 4-month Irradiated and Untreated xenografts.

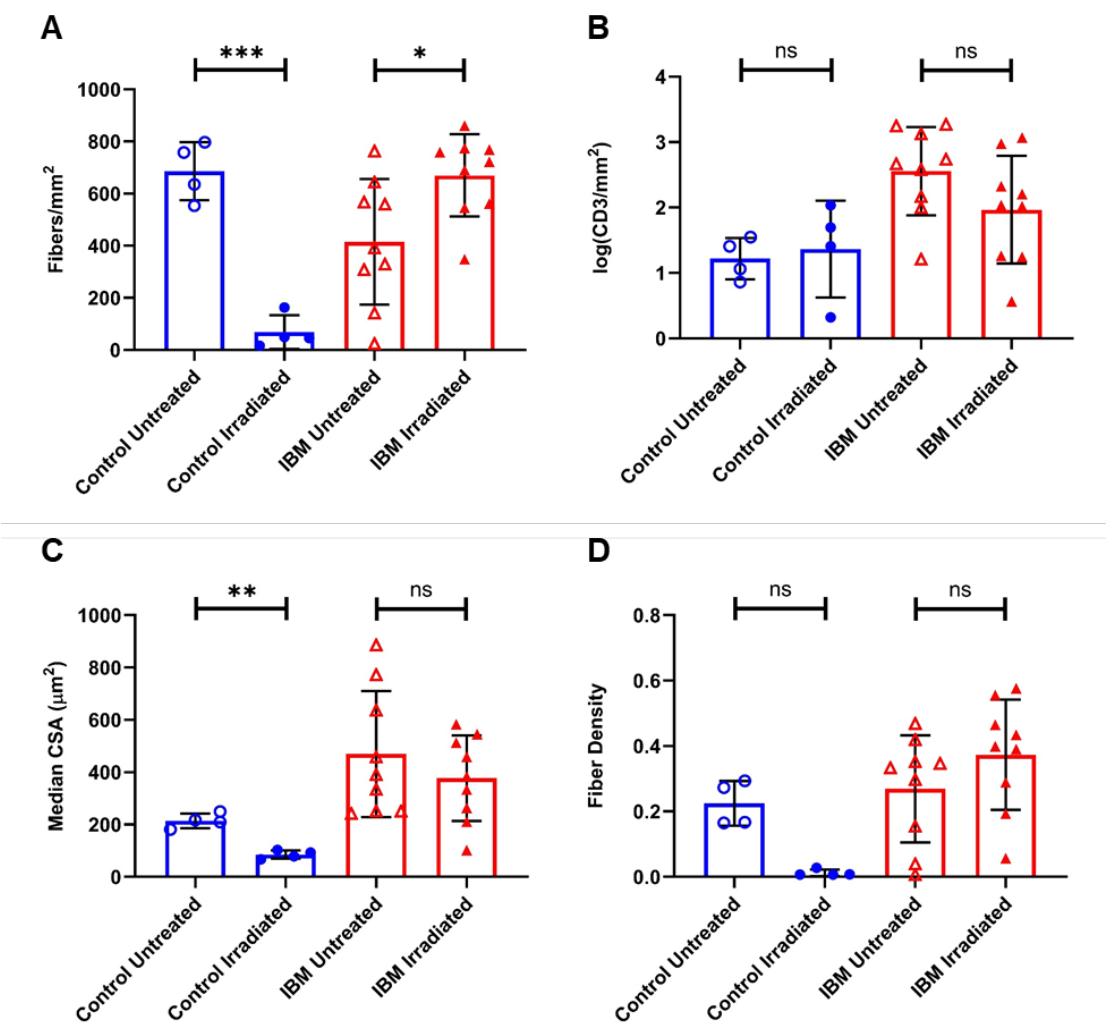

Figure 6.3 Quantification of the number of fibers over the xenograft area **(A)**, the number of CD3+ T cells over the xenograft area **(B)**, the median cross sectional area (CSA) of myofibers within the xenografts **(C)**, and the fiber density of the xenografts as determined by the percent of the xenograft area covered by myofibers **(D)**. For all graphs, each point denotes one xenograft (control untreated n =4, control irradiated n = 4, IBM untreated n = 9, IBM irradiated n = 9) and p-values determined were determined by Tukey's multiple comparisons test: ns, not significant; *p ≤ 0.05; **p ≤ 0.01; ***p ≤ 0.001.

6.3 Depleting T cells in IBM Xenografts with monoclonal CD3 antibody OKT3

A monoclonal antibody is produced by a single B cell targeting one specific antigen, and this specificity has been adapted for clinical use in the form of chimeric and humanized monoclonal antibodies (Zhang et al. 2018). Monoclonal antibodies can be used to deplete specific immune cells via induction of apoptosis or by antibody-dependent cell-mediated cytotoxicity (ADCC). One of the first human monoclonal antibodies created was OKT3 (generic name: Muromonab-Cd3), which recognizes a nonpolymorphic subunit of the human TCR: CD3ε (Kung et al. 1979; Kjer-Nielsen et al. 2004). OKT3 was the first monoclonal antibody approved by the US FDA for therapy in humans to prevent acute rejection in organ transplant patients by blocking cytotoxic T cell function (Zhang et al. 2018). In addition, OKT3 treatment can prevent graft-versus-host disease (GVHD) by ablating human T cells in mice engrafted with human hematopoietic cells (Wunderlich et al. 2014). We hypothesized that treating xenografted mice with OKT3 would specifically eliminate T cells within the grafts, which would enable us to study the effect T cells may be exerting on xenograft regeneration and determine if aspects of IBM degenerative pathology are dependent on T cells.

Patient Characteristics

Muscle biopsies from three patients with clinico-pathologically or clinically defined IBM were used to carry out these OKT3 experiments (**Table 6.2**). All IBM patient biopsies showed moderate to severe endomysial inflammation, numerous examples of primary invasion of non-necrotic fibers, and mitochondrial pathology (**Figure 6.4**). Of note, IBM case 36 did not have rimmed vacuoles, but studies have found that up to 20% of

patients with typical clinical features of IBM do not have rimmed vacuoles (Chahin and Engel 2008; Ikenaga et al. 2017).

Table 6.2 Patient Characteristics - OKT3 Experiments

Case	Patient Sex	Age	Clinical Diagnosis	Biopsy Location (MRC)	Histological Features of Biopsy
23	Male	64	sIBM	Biceps (4+)	Severe, chronic inflammatory myopathy with myofiber degeneration, necrosis, regeneration, and rimmed vacuoles. There is diffuse endomysial inflammation and many examples of primary invasion. MHC-1 is upregulated and innumerable COX-negative fibers.
26	Male	75	sIBM	Biceps (4)	Moderate inflammatory myopathy with endomysial and perivascular inflammation, examples of primary invasion, many COX-negative fibers, MHC-1 is diffusely upregulated, red-rimmed vacuoles, and neurogenic atrophy.
36	Male	64	sIBM	Rectus Femoris (5)	Moderately severe, chronic inflammatory myopathy with myofiber degeneration, necrosis, and regeneration. There are numerous foci of endomysial inflammation, primary invasion, and. Particularly striking are mitochondrial abnormalities with innumerable COX-negative fibers and several ragged red fibers. There were no vacuoles seen, and there is mild acute neurogenic atrophy

Table 6.2 A summary of clinical demographics, histological features, and clinical diagnosis of IBM patients involved in OKT3 experiments. The average age of the IBM patients was 67.667 years.

Figure 6.4 Histological Features of Human Biopsies - OKT3 Experiments

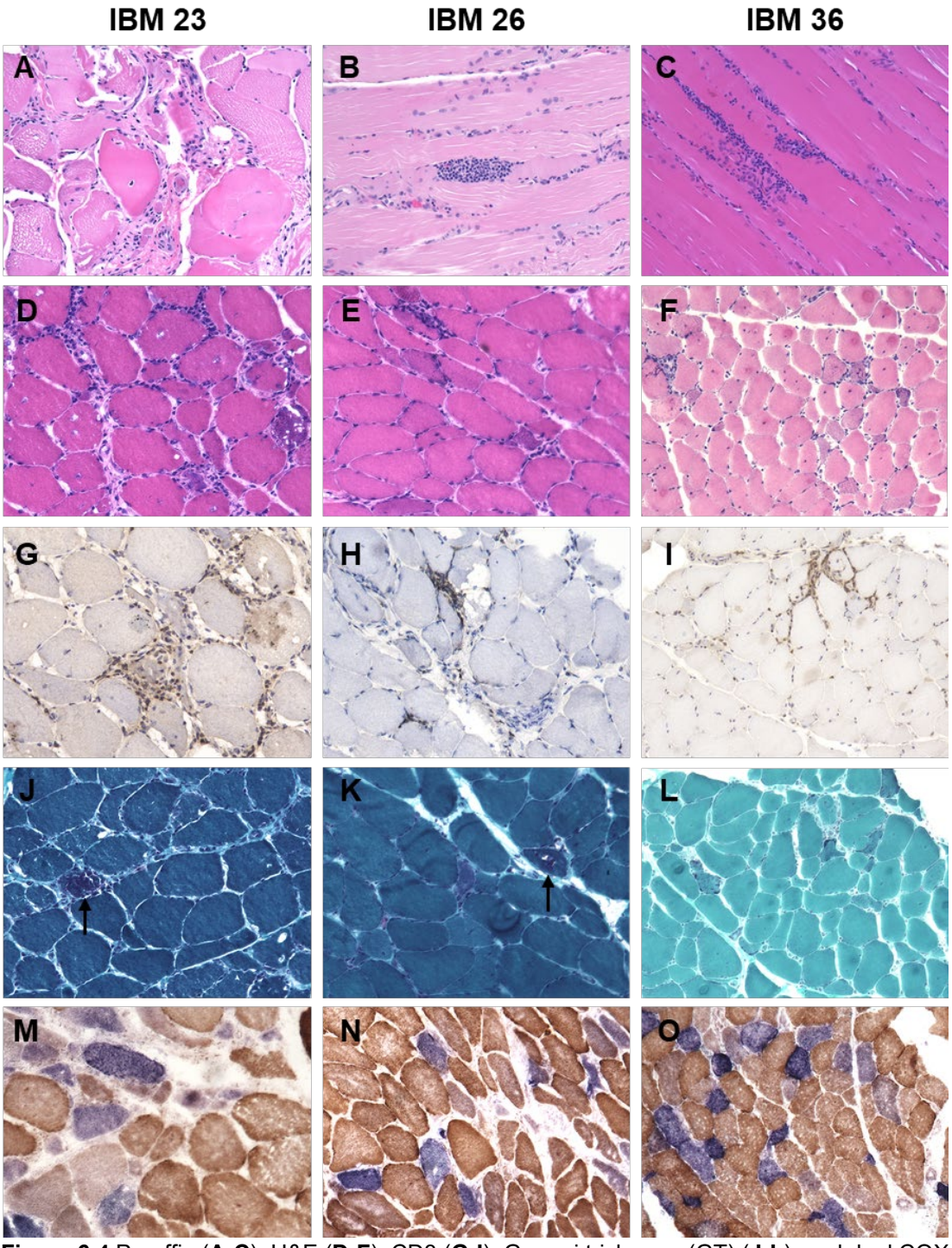

Figure 6.4 Paraffin (**A-C**), H&E (**D-F**), CD3 (**G-I**), Gomori trichrome (GT) (**J-L**), and dual COX-SDH (M-O) stains showing representative histology from IBM cases 23, 26, And 36. All biopsies show endomysial inflammation and primary invasion (**A-I**). In addition, all biopsies show innumerable COX deficient fibers (**M-O**). The IBM cases 23 and 26 show rimmed vacuoles (**J,K arrows**), but vacuoles are absent in IBM case 36 (**L**).

OKT3 successfully eliminates T cells from xenografts, but myofiber regeneration is unaffected

Xenografted mice are treated weekly via intraperitoneal injection with 10mg/kg OKT3 as this treatment regimen has been shown to effectively ablate human T cells *in vivo* (Wunderlich et al. 2014). OKT3 dramatically reduced the number of CD3+ T cells at both 2-month ($p = 0.0286$) and 4-month ($p < 0.0001$) timepoints (**Figure 6.5A-E**). Untreated IBM xenografts show numerous foci of endomysial inflammation and high numbers of CD3+ T cells (**Figure 6.5A,B**), whereas OKT3 treated xenografts show very low numbers of scattered CD3+ T cells (**Figure 6.5 C,D**).

Although treatment with OKT3 was highly effective in depleting T cells, myofiber regeneration was unchanged between control and treatment groups (**Figure 6.6**). The number of regenerated fibers, their median CSA, and the fiber density of the xenografts are not significantly different (**Figure 6.6 E,F,H**). In addition, OKT3 treatment did not impact the number of eMHC+ fibers (**Figure 6.6G**), indicating that the process of myofiber maturation was unchanged (Schiaffino et al. 2015). The human biopsies display fiber size variability as expected for IBM patients (**Figure 6.7 A,C,E**), and the myofiber CSA distributions do not differ between OKT3 treated and untreated xenografts (**Figure 6.7B,D,F**). In healthy muscle, the inflammatory response to muscle injury is a highly complex and coordinated process involving cells from both the innate and adaptive immune system (Tidball 2017). Fortunately, these data demonstrate that the presence of T cells within IBM xenografts does not significantly impair myofiber regeneration in our model and allows us to examine if aspects of IBM pathology are influenced by the presence or absence of T cells.

Figure 6.5 OKT3 eliminates T cells from IBM Xenografts

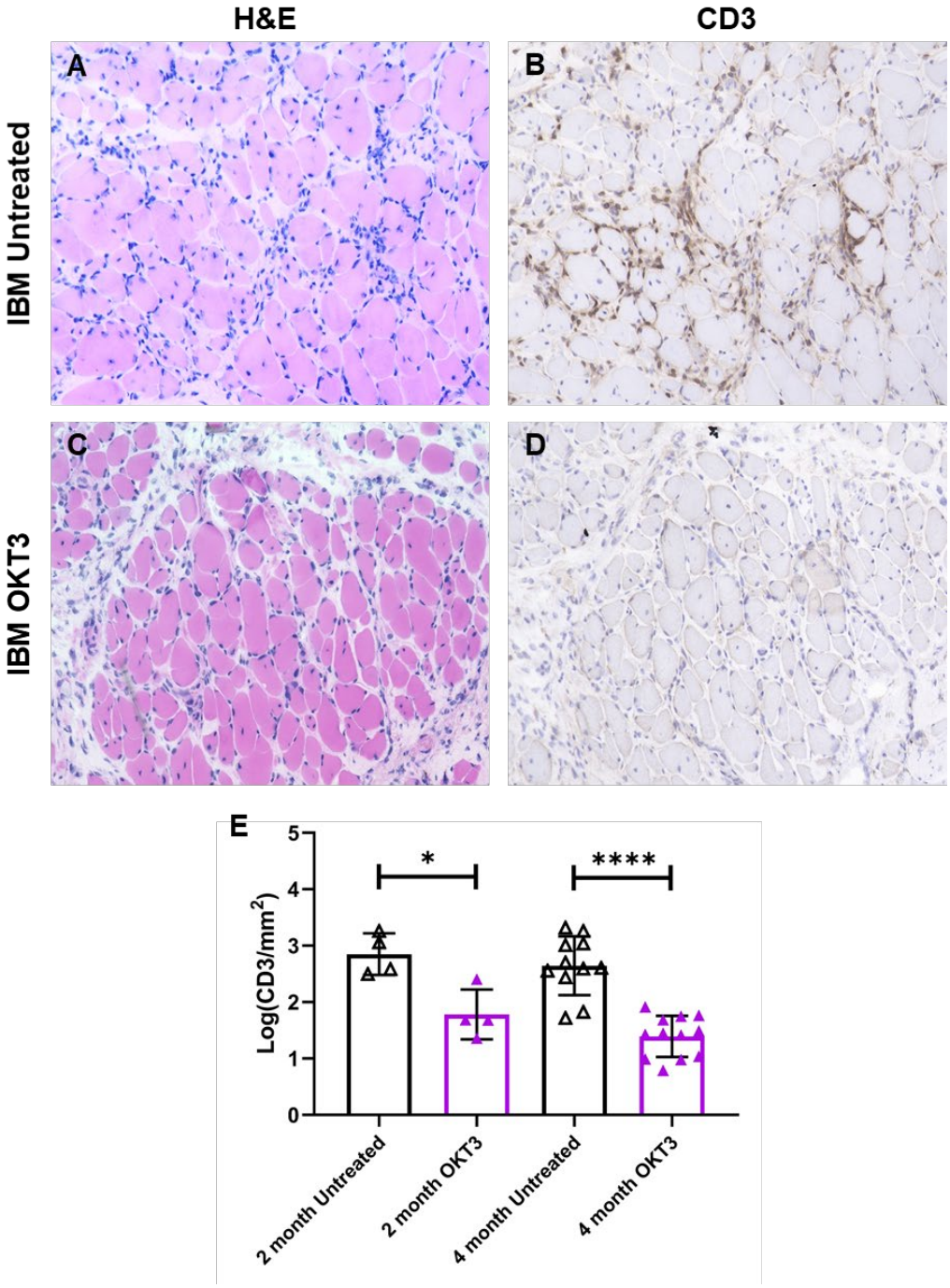

Figure 6.5 Representative H&E (**A,C**) and CD3 (**B,D**) stains of 4-month untreated (**A,B**) and OKT3 treated (**C,D**) xenografts from IBM case 26. Quantification of the number of CD3+ T cells over the xenograft area (**E**) shows the number of T cells is significantly reduced both at 2 months ($p=0.0286$) and 4 months ($p<0.0001$) by OKT3 treatment. For all graphs, each point denotes one xenograft (2 month untreated n = 4 , 2 month OKT3 n = 4 , 4 month untreated n = 11, 4 month OKT3 n = 12) and Mann-Whitney U test was used to determine p-values (*$p<0.05$, ****$p<0.0001$).

Figure 6.6 Myofiber regeneration is unaffected by T cells

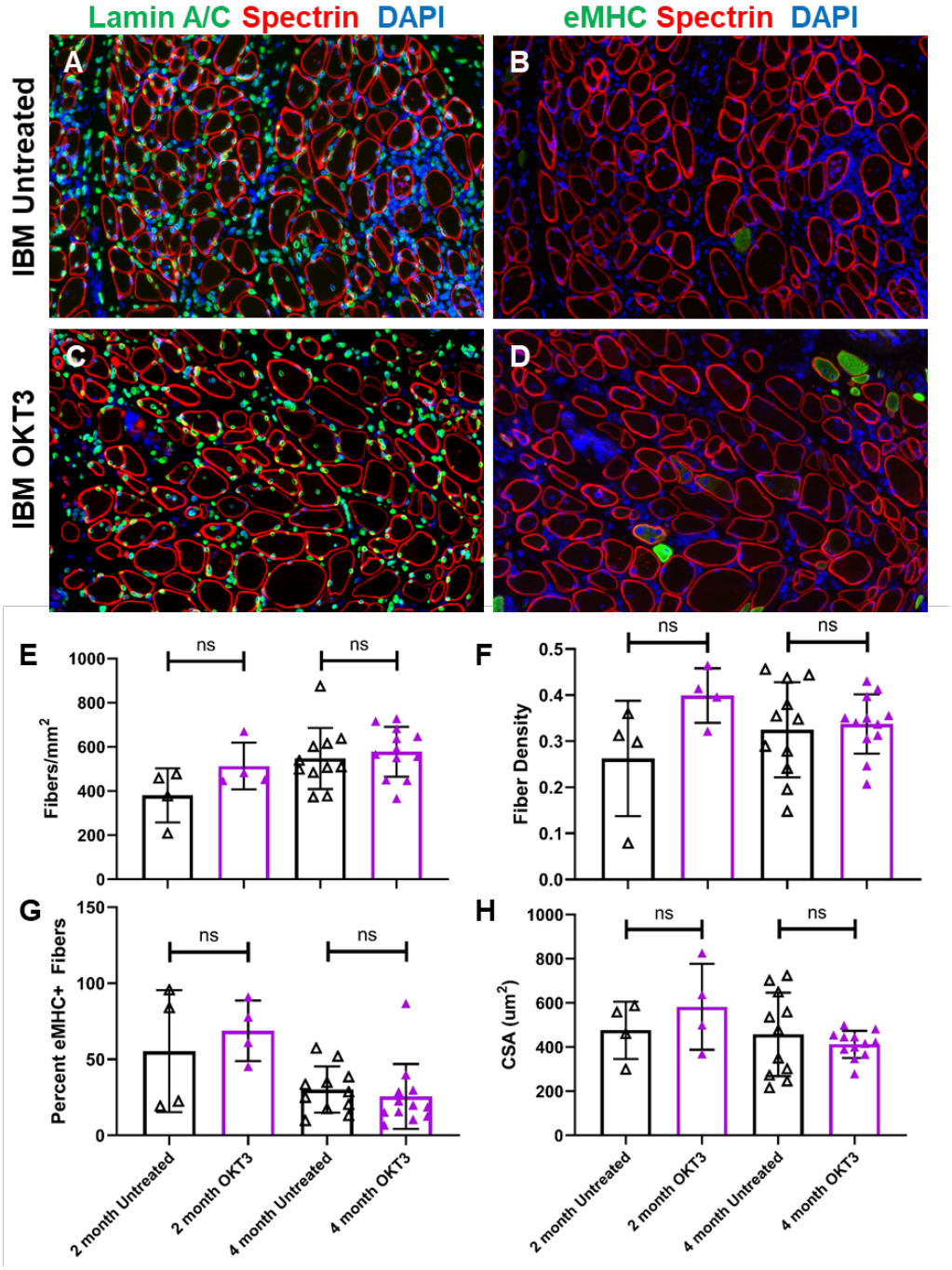

Figure 6.6 Representative lamin A/C (green), spectrin (red), eMHC (green), and DAPI (blue) stains of 4-month untreated (**A,B**) and OKT3 treated (**C,D**) xenografts from IBM case 36. Quantification of the number of fibers over the xenograft area (**E**), fiber density (**F**), percent of eMHC+ fibers (**G**), and median fiber CSA (**H**) show OKT3 treatment did not significantly impact regeneration or fiber morphology. For all graphs, each point denotes one xenograft (2 month untreated n = 4 , 2 month OKT3 n = 4 , 4 month untreated n = 11, 4 month OKT3 n = 12) and Mann-Whitney U test was used to test for significance (ns, not significant).

Figure 6.7 The distribution of myofiber CSA is unchanged by OKT3 treatment

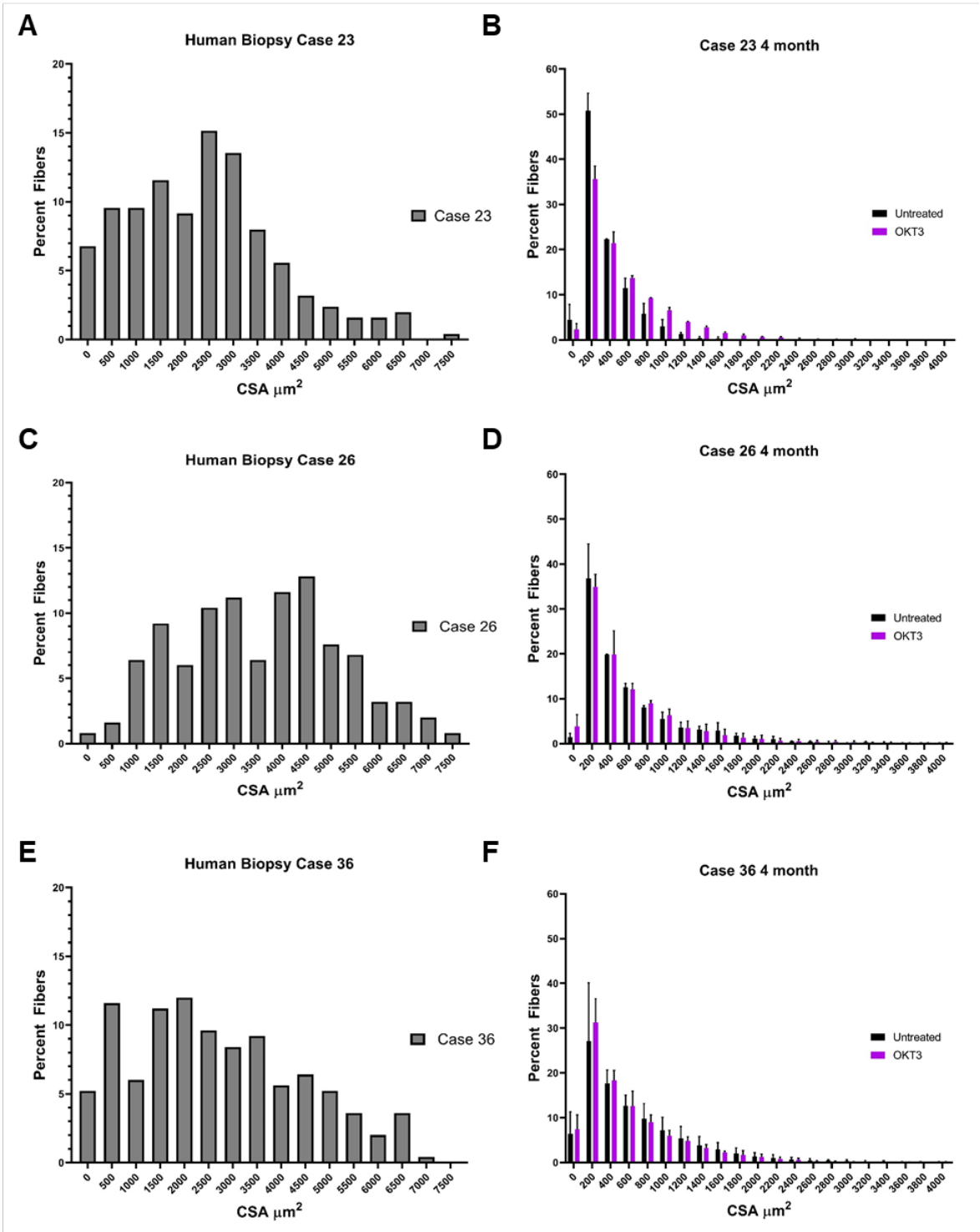

Figure 6.7 Histograms of the cross-sectional area (CSA) of the Case 23 (**A,B**), Case 26 (**C,D**), and Case 36 (**E,F**) human biopsies and the 4-month untreated and OKT3 treated xenografts. The distribution of the CSAs of the untreated and OKT3 treated xenografts are similar and are skewed right.

T cells drive mitochondrial pathology in IBM Xenografts

Dual COX/SDH staining was carried out on all 4-month xenograft samples from cases 23, 26, and 36 (**Figure 6.8A,B**). The untreated xenografts have an average of 3.27 COX-deficient fibers and the OKT3 treated xenografts had an average of 1.55 COX-deficient fibers, which was a significant decrease ($p = 0.0291$) (**Figure 6.8C**). These data indicate that T cells are driving mitochondrial pathology in IBM xenografts. Indeed, we find that the number of COX-deficient fibers is significantly correlated to the number of CD3+ T cells in IBM xenografts ($p = 0.0203$) (**Figure 6.8D**). These data support previous work demonstrating positive correlations between the number of COX-deficient muscle fibers and the severity of inflammation in IBM patient biopsies (Rygiel et al. 2015). Interestingly, this relationship is not observed in control myositis xenografts that show comparable levels of inflammation.

Figure 6.8 T cell-mediated inflammation drives mitochondrial pathology

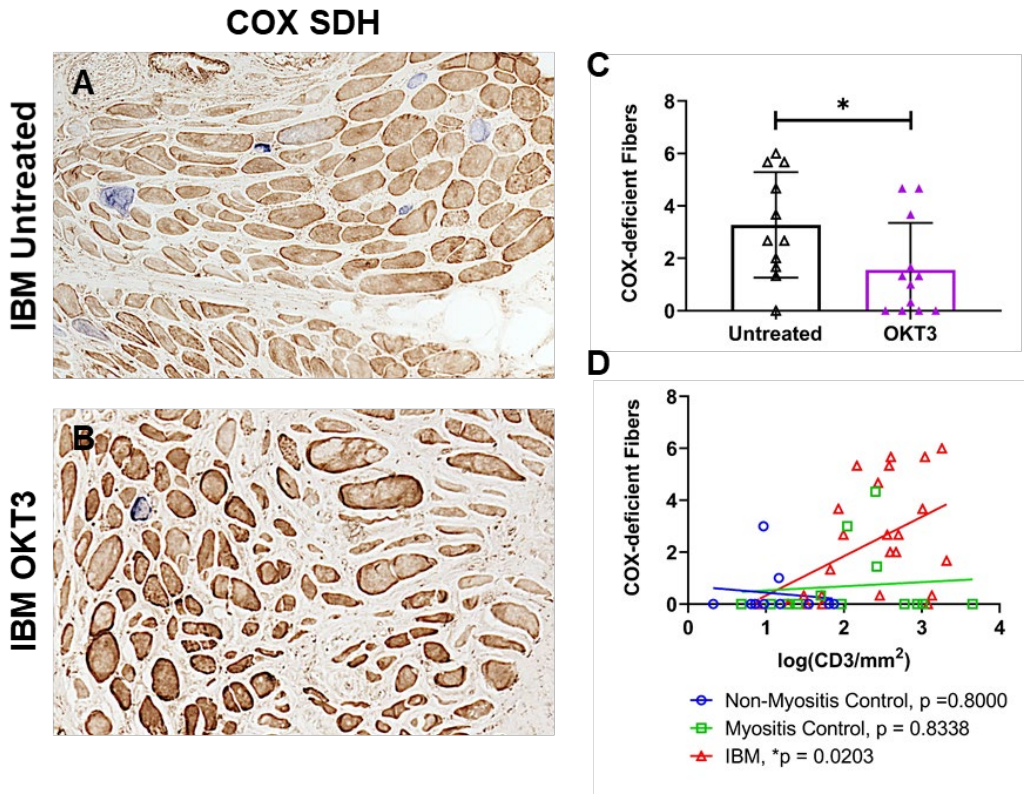

Figure 6.8 Dual COX-SDH stain of untreated (**A**) and OKT3 treated (**B**) 4-month IBM xenografts from IBM case 36. COX-deficient fibers appear light to dark blue. (**C**) Quantification of the number of COX-deficient fibers in 4-month xenografts, each point denotes one xenograft (untreated n = 11, OKT3 n =12). Mann-Whitney test was used to determine significance (*p ≤ 0.05). (**D**) Correlation of the number of CD3+ T cells to the number of COX-deficient fibers in 4-month xenografts, each point denotes one xenograft (non-myositis control n=12 , myositis control n=13, IBM n=25). Spearman rank correlation was used to determine all p-values (*p ≤ 0.05).

Chapter 7: Discussion and Future Directions

Human Skeletal Muscle Xenografts are a novel way to model IBM

The intertwined degenerative and inflammatory pathological features of IBM have fueled the debate underlying the pathogenesis of the disease and have stymied attempts to create comprehensive laboratory models (Keller, Schmidt, and Lünemann 2017; Greenberg 2019). Skeletal muscle xenografts provide an exciting new avenue to model both inherited and acquired muscle diseases (Zhang et al. 2014; Britson et al. 2019). These xenografts can recapitulate the complex genetic and epigenetic abnormalities that exist in human disease that may never be reproducible in other animal models, and xenografts form a complete *in vivo* system for modeling disease. There was an initial concern that IBM patient muscle would not be competent to form xenografts as some studies suggest muscle regeneration may be impaired in IBM. First, *in vitro* studies have shown that myoblasts isolated from IBM patients proliferate at a slower rate than age-matched controls, and show telomere shortening, indicative of premature senescence (Morosetti et al. 2010). In addition, skeletal muscle regeneration is highly regulated by the immune system, and the chronic inflammation in IBM has been suggested to negatively influence muscle regeneration (Loell and Lundberg 2011; reviewed in: Tidball 2017; Sass et al. 2018; Howard et al. 2020). Finally, aging itself diminishes the regenerative capacity of skeletal muscle, resulting in the loss of muscle mass and

strength observed in elderly populations termed sarcopenia (Suetta et al. 2013; Dodds et al. 2015; Joanisse et al. 2017).

In contrast to these studies suggesting muscle regeneration may be impaired in IBM, one study showed an increased expression of myogenic regulatory factor myogenin in IBM patient satellite cells and reported higher numbers of satellite cells and regenerating fibers in IBM patient biopsies in comparison to age-matched controls (Wanschitz et al. 2013). Our data show that IBM patient muscle can robustly regenerate in NRG host mice to form skeletal muscle xenografts. In fact, IBM xenografts showed significantly higher fiber density and increased median CSA in comparison to non-myositis control xenografts. These results show that our xenograft approach to modeling IBM is feasible despite previous studies showing reduced proliferation of IBM myoblasts, the persistent chronic inflammation in IBM xenografts, and the significantly elevated age of the IBM patients in our xenograft study in comparison to controls.

Importantly, several degenerative and inflammatory pathological features of IBM are recapitulated in this xenograft model. First, rare fibers with p62 aggregates are observed in 10-month IBM xenografts, but not in 10-month myositis control xenografts. It has been reported that the combination of p62 and TDP-43 staining is both sensitive and specific for IBM, and these two markers are seen aggregated in 12% of patient myofibers (Dubourg et al. 2011; Hiniker et al. 2013). Although these aggregates are rarely seen in other inflammatory myopathies, they are frequently observed in neurodegenerative diseases such as amyotrophic lateral sclerosis (ALS) and Alzheimer's disease (AD), which lends support to the idea that IBM is primarily a degenerative disease (Cortese et al. 2014; Chornenkyy, Fardo, and Nelson 2019). In our neuromuscular biopsy laboratory,

we have difficulty detecting TDP-43 cytoplasmic aggregates and loss of nuclear TDP-43 in IBM muscle biopsies, and as a result, we are unable to reliably quantify sarcoplasmic TDP-43 aggregation in IBM xenografts. However, a sensitive way to detect nuclear loss of TDP-43 is through the assessment of cryptic exon expression (Jonathan P. Ling 2015; Jeong et al. 2017). One of the normal functions of TDP-43 is to act as a splice repressor of these cryptic exons, and their incorporation in mRNA transcriptions can be detected using a simple RT-PCR assay (Jonathan P. Ling 2015; Jeong et al. 2017). Of note, cryptic exon incorporation can be detected in hippocampal samples from AD patients lacking TDP-43 aggregation, suggesting that nuclear depletion of TDP-43 precedes cytoplasmic aggregation (Sun et al. 2017).

As expected, the majority of IBM patient biopsies and none of the control patient biopsies showed cryptic exon expression. In addition, cryptic exon expression was detected within 8-month and 10-month IBM xenografts from three different IBM cases, but not in non-myositis control xenografts. Interestingly, cryptic exon incorporation is not observed in 4-month IBM xenografts, but is detected 8 months after the xenograft surgery suggesting this phenotype develops over time. It has been reported that TDP-43 has a role in normal muscle regeneration through the formation of cytoplasmic, amyloid-like “myo-granules,” which associate with sarcomeric mRNAs and localize to sites of sarcomere formation (Vogler et al. 2018). These myo-granules form in healthy muscle following injury and are readily cleared as myofibers matures. However, purified myo-granules can seed the formation of amyloid-like fibrils *in vitro* (Vogler et al. 2018). It is hypothesized that the normal formation and resolution of these myo-granules is disturbed in muscle disease, leading to the formation of stable aggregates, which may drive disease pathology (Cutler et al. 2019). The potential role these myo-granules play

in the development of IBM is an intriguing avenue for future studies with this xenograft model.

In addition to these degenerative features, IBM xenografts also show mitochondrial pathology in the form of significantly elevated numbers of COX-deficient fibers, as well as endomysial inflammation. IBM xenografts show elevation of MHC-I, which corresponds to the presence of CD3+ T cells within IBM xenografts. In addition, examples of primary invasion of non-necrotic fibers are observed in xenografts from several different IBM patients, but invasion is not observed in xenografts from myositis control patients despite showing similar levels of endomysial inflammation. Further studies reveal that T cells in IBM xenografts are proliferative, antigen-experienced, and oligoclonal, which mirror immune cell populations described in IBM patients (reviewed in:Greenberg 2019). The antigen or multiple antigens driving the clonal expansion of T cells in IBM patients are still unknown. The xenograft model may enrich for these clonal populations and facilitate antigen discovery.

Overall, our xenograft model of IBM is the first comprehensive laboratory model of the disease to model both degenerative and inflammatory features of the disease and represents a significant step forward in IBM research.

The IBM xenograft model can be used for mechanistic studies and pre-clinical testing

Based on recent successes with patient-derived tumor xenograft models, we hypothesize that treatment efficacy results in our IBM xenograft model are more likely to translate to trials in patients than in vitro models or mouse models of IBMPFD (Kim et al.

2005; Rubio-Viqueira and Hidalgo 2009; Sako et al. 2010; Roberts et al. 2014; Ahmed et al. 2016; Izumchenko et al. 2017). Due to the extensive endomysial inflammation present in IBM xenografts including examples of primary invasion, we aimed to determine if reducing this inflammation would have an impact on the features of IBM pathology observed in this model.

Although proponents of a primarily degenerative pathomechanism of IBM point to the lack of effectiveness of immunomodulatory therapies in IBM, there are a few clinical trials that suggest T cell ablation can benefit IBM patients. A pilot trial of alemtuzumab, a humanized monoclonal antibody targeting CD52 present on lymphocytes, was performed in 13 IBM patients and suggested that progression of weakness was reduced and that post-treatment biopsies showed a reduction in endomysial lymphocytes (Dalakas et al. 2009). However, this study is controversial and the conclusions have been challenged (Greenberg 2010a). In addition, dual treatment with anti-T lymphocyte globulin (ATG) and methotrexate in a small patient population showed statistically significant efficacy in comparison to treatment with methotrexate alone (Lindberg et al. 2003). It is also worth noting several studies have found that intravenous immunoglobulin (IVIG) may be beneficial for patients with dysphagia (Dalakas et al. 1997; Dobloug et al. 2012). Thus, depletion of T cells continues to be a possible therapeutic strategy.

Our initial attempts to remove inflammatory cells via *ex vivo* irradiation proved to be detrimental to control xenografts. Therefore, a more targeted approach using a monoclonal CD3 antibody (OKT3) was adopted. OKT3 binds to the epsilon chain of CD3, effectively blocking T cell receptor function and causing ablation of T cells *in vivo*

following treatment (Norman 1995; Kjer-Nielsen et al. 2004; Wunderlich et al. 2014). OKT3 treatment significantly reduced T cells in IBM xenografts, but this did not impact xenograft regeneration or fiber morphology. One of the more striking findings of these OKT3 experiments was the positive relationship between the number of COX-deficient fibers and the number of T cells in IBM xenografts, which has also been observed in patient biopsies (Rygiel et al. 2015). This relationship was not observed in control xenografts, and this phenotype could be significantly ameliorated by ablating T cells with OKT3. To our knowledge, this is the first demonstration that T cells are driving mitochondrial pathology in IBM. Our data is also supported by recent work showing that exposing primary myotubes derived from non-myopathic patient samples to pro-inflammatory cytokines such as interferon-gamma (IFN-γ) and interleukin-1beta (IL-1β) can result in decreased COX protein levels (Chinoy and Lilleker 2019: P123). This is an exciting step forward in IBM research and demonstrates this xenograft model of IBM can be used to carry out mechanistic studies to better understand disease pathogenesis and perform therapeutic testing.

Future Directions

Moving forward, our immediate goals are to fully characterize the human immune cells present within IBM xenografts, to compare xenografts to patient biopsies using RNA-sequencing (RNA-seq), and to better understand the dynamics underlying cryptic exon expression. We will be expanding on the TCR sequencing data by analyzing our patient biopsies and comparing them to xenografts. We hypothesize that all the xenografts from a single patient will be enriched for a subset of T cell clones shared with the original biopsy if the observed proliferation is antigen driven. Alternatively, xenografts from the same patient may show variable populations of T cells more indicative of a bottleneck. In

addition, flow cytometry will allow us to better understand the specific subsets of immune cells present within the xenografts. We have been able to show that IBM xenografts contain both CD8+CD57+ and CD4+CD57+, antigen experienced cells. Recently, highly differentiated, cytotoxic KLRG1+ T cells have been proposed as a potential therapeutic target in IBM (Greenberg et al. 2019), and our preliminary data show KLRG1+ T cells within xenografts. We aim to assess if this population of cells is affected by OKT3 treatment using flow cytometry and immunohistochemistry. Going forward, we are obtaining peripheral blood mononuclear cells (PBMCs) from patients at the time of biopsy so that we can compare the antigen-specificity and function of T cells from patient blood with those present in the biopsied muscle and xenograft.

It will be informative to examine the subsets of nonlymphocytic cells as well. For instance, it has been recently reported that CD74, CD163, and STAT1 are highly expressed in muscle biopsies of sIBM patients and these proteins were found to localize to macrophages (Roos et al. 2019). We are currently assessing different populations of human immune cells including macrophages, B cells, NK cells, and dendritic cells in all our xenograft experiments as we have done previously. Another interesting area to explore in the future is the role of the host (mouse) innate immune system in muscle regeneration in the xenograft model. Our preliminary flow cytometry experiments performed in collaboration with the Villalta laboratory suggest that there are many mouse macrophages present within the human xenografts, presumably to phagocytose degenerating human myofibers, but the role that they are playing in both control and IBM xenografts is unknown.

Recent RNA sequencing of myositis patients has shown activation of the interferon 1 (IFN1) pathway in patients with DM, antisynthetase syndrome (AS), IMNM, and IBM, as well as robust activation of the interferon 2 (IFN2) pathway in AS, IBM, and DM but not in IMNM (Pinal-Fernandez et al. 2019). In addition, a study comparing Jo-1 associated myositis patients to IBM patients using RNA sequencing followed by pathway analysis found the top canonical pathways altered in both Jo-1 and IBM were oxidative phosphorylation and mitochondrial dysfunction (Hamann et al. 2017). These studies demonstrate the usefulness of using transcriptomic analysis to understand similarities and differences between subsets of myositis, and to identify biological pathways of interest. We aim to perform RNA sequencing to compare xenografts with the initial muscle biopsy to determine how closely xenografts resemble the initial biopsy and to characterize cytokine expression and determine if there are any muscle-specific changes in gene expression.

In addition, we will expand our understanding of the dynamics underlying cryptic exon expression by analyzing additional xenograft samples and timepoints. Currently, it appears that only biopsies with cryptic exon expression result in xenografts with cryptic exon expression. We do not yet know whether the variability in cryptic exon detection is due to assay variability, heterogeneity of muscle biopsies, or whether the presence or absence of cryptic exon detection or defines specific subtypes of IBM. If the latter, cryptic exon detection may be a useful disease biomarker and may suggest that there is a factor intrinsic to the skeletal muscle niche regulating TDP-43 pathology. Our data also indicate that cryptic exon incorporation is only detectable at late timepoints, although we have yet to fully examine the time course of cryptic exon expression. In addition, it is possible that there is earlier expression, but that our RT-PCR assay is not sensitive

enough to detect it. Ligation *in situ* Hybridization (LISH) is a technique we plan to use for more sensitive detection of cryptic exons, and we may potentially adapt LISH to visualize cryptic exons within patient biopsies and xenograft samples (Credle et al. 2017). This method uses T4 RNA Ligase 2 to efficiently join adjacent chimeric RNA–DNA probe pairs hybridized *in situ* on fixed RNA target sequences, which allows for multiplexed measurement of multiple targets and would allow us to analyze several TDP-43 target genes simultaneously.

Finally, although the dramatic reduction of inflammatory cells via OKT3 did not significantly improve regeneration, these samples allow us to examine about how the presence of lymphocytes in IBM muscle impact some of the pathological phenotypes we've observed in the IBM xenograft model. Beyond the exciting results showing the role of inflammation in mitochondrial pathology, we also want to test how eliminating T cells impacts cryptic exon expression within xenografts. These experiments will help advance our understanding of how the immune system influences IBM pathology.

References

Afzali, A. M., T. Ruck, H. Wiendl, and S. G. Meuth. 2017. 'Animal models in idiopathic inflammatory myopathies: How to overcome a translational roadblock?', *Autoimmun Rev*, 16: 478-94.

Ahmed, Mhoriam, Pedro M. Machado, Adrian Miller, Charlotte Spicer, Laura Herbelin, Jianghua He, Janelle Noel, Yunxia Wang, April L. McVey, Mamatha Pasnoor, Philip Gallagher, Jeffrey Statland, Ching-hua Lu, Bernadett Kalmar, Stefen Brady, Huma Sethi, George Samandouras, Matt Parton, Janice L. Holton, Anne Weston, Lucy Collinson, J. Paul Taylor, Giampietro Schiavo, Michael G. Hanna, Richard J. Barohn, Mazen M. Dimachkie, and Linda Greensmith. 2016. 'Targeting protein homeostasis in sporadic inclusion body myositis', *Science Translational Medicine*, 8: 28-31.

Albayda, J., L. Christopher-Stine, C. O. Bingham Iii, J. J. Paik, E. Tiniakou, S. Billings, O. M. Uy, and P. Burlina. 2018. 'Pattern of muscle involvement in inclusion body myositis: a sonographic study', *Clin Exp Rheumatol*, 36: 996-1002.

Alexanderson, H. 2018. 'Exercise in Myositis', *Curr Treatm Opt Rheumatol*, 4: 289-98.

Alexanderson, Helene, and Ingrid E. Lundberg. 2012. 'Exercise as a therapeutic modality in patients with idiopathic inflammatory myopathies', *Current Opinion in Rheumatology*, 24: 201-07.

Amato, Anthony A., Kumaraswamy Sivakumar, Namita Goyal, William S. David, Mohammad Salajegheh, Jens Praestgaard, Estelle Lach-Trifilieff, Anne Ulrike Trendelenburg, Didier Laurent, David J. Glass, Ronenn Roubenoff, Brian S. Tseng, and Steven A. Greenberg. 2014. 'Treatment of sporadic inclusion body myositis with bimagrumab', *Neurology*, 83: 2239-46.

Amemiya, K. 2000. 'Clonal restriction of T-cell receptor expression by infiltrating lymphocytes in inclusion body myositis persists over time: Studies in repeated muscle biopsies', *Brain*, 123: 2030-39.

Amlani, A., M. Y. Choi, M. Tarnopolsky, L. Brady, A. E. Clarke, I. Garcia-De La Torre, M. Mahler, H. Schmeling, C. E. Barber, M. Jung, and M. J. Fritzler. 2019. 'Anti-NT5c1A Autoantibodies as Biomarkers in Inclusion Body Myositis', *Front Immunol*, 10: 745.

Amoasii, L., J. C. W. Hildyard, H. Li, E. Sanchez-Ortiz, A. Mireault, D. Caballero, R. Harron, T. R. Stathopoulou, C. Massey, J. M. Shelton, R. Bassel-Duby, R. J. Piercy, and E. N. Olson. 2018. 'Gene editing restores dystrophin expression in a canine model of Duchenne muscular dystrophy', *Science*, 362: 86-91.

Ansari, B., E. Salort-Campana, A. Ogier, D. A. Le Troter Ph, B. De Sainte Marie, M. Guye, E. Delmont, A. M. Grapperon, A. Verschueren, D. Bendahan, and S. Attarian. 2020. 'Quantitative muscle MRI study of patients with sporadic inclusion body myositis', *Muscle Nerve*, epub ahead of print.

Arnardottir, Snjolaug, Helene Alexanderson, Ingrid E. Lundberg, and Kristian Borg. 2003. 'Sporadic inclusion body myositis: pilot study on the effects of a home exercise program on muscle function, histopathology, and inflammatory reaction', *J Rehabil Med*, 35: 31-35.

Badrising, U. A., M. L. Maat-Schieman, M. D. Ferrari, A. H. Zwinderman, J. A. Wessels, F. C. Breedveld, P. A. van Doorn, B. G. van Engelen, J. E. Hoogendijk, C. J. Howeler, A. E. de Jager, F. G. Jennekens, P. J. Koehler, M. de Visser, A. Viddeleer, J. J. Verschuuren, and A. R. Wintzen. 2002. 'Comparison of weakness progression in inclusion body myositis during treatment with methotrexate or placebo', *Ann Neurol*, 51: 369-72.

Badrising, U. A., G. M. Schreuder, M. J. Giphart, K. Geleijns, J. J. Verschuuren, A. R. Wintzen, M. L. Maat-Schieman, P. van Doorn, B. G. van Engelen, C. G. Faber, J. E. Hoogendijk, A. E. de Jager, P. J. Koehler, M. de Visser, S. G. van Duinen, and I. B. M. Study Group Dutch. 2004. 'Associations with autoimmune disorders and HLA class I and II antigens in inclusion body myositis', *Neurology*, 63: 2396-98.

Baixauli, Francesc, Carlos López-Otín, and Maria Mittelbrunn. 2014. 'Exosomes and autophagy: Coordinated mechanisms for the maintenance of cellular fitness', *Frontiers in Immunology*, 5: 1-6.

Barretina, J., G. Caponigro, N. Stransky, K. Venkatesan, A. A. Margolin, S. Kim, C. J. Wilson, J. Lehar, G. V. Kryukov, D. Sonkin, A. Reddy, M. Liu, L. Murray, M. F. Berger, J. E. Monahan, P. Morais, J. Meltzer, A. Korejwa, J. Jane-Valbuena, F. A. Mapa, J. Thibault, E. Bric-Furlong, P. Raman, A. Shipway, I. H. Engels, J. Cheng, G. K. Yu, J. Yu, P. Aspesi, Jr., M. de Silva, K. Jagtap, M. D. Jones, L. Wang, C. Hatton, E. Palescandolo, S. Gupta, S. Mahan, C. Sougnez, R. C. Onofrio, T. Liefeld, L. MacConaill, W. Winckler, M. Reich, N. Li, J. P. Mesirov, S. B. Gabriel, G. Getz, K. Ardlie, V. Chan, V. E. Myer, B. L. Weber, J. Porter, M. Warmuth, P. Finan, J. L. Harris, M. Meyerson, T. R. Golub, M. P. Morrissey, W. R. Sellers, R. Schlegel, and L. A. Garraway. 2012. 'The Cancer Cell Line Encyclopedia enables predictive modelling of anticancer drug sensitivity', *Nature*, 483: 603-7.

Barretina, J. 2019. 'Addendum: The Cancer Cell Line Encyclopedia enables predictive modelling of anticancer drug sensitivity', *Nature*, 565: E5-E6.

Behl, Christian. 2011. 'BAG3 and friends: Co-chaperones in selective autophagy during aging and disease', *Autophagy*, 7: 795-98.

Benatar, Michael, Joanne Wuu, Catalina Fernandez, Conrad C. Weihl, Heather Katzen, Julie Steele, Bjorn Oskarsson, and J. Paul Taylor. 2013. 'Motor neuron involvement in multisystem proteinopathy: Implications for ALS', *Neurology*, 80: 1874-80.

Bengtsson, Niclas E., John K. Hall, Guy L. Odom, Michael P. Phelps, Colin R. Andrus, R. David Hawkins, Stephen D. Hauschka, Joel R. Chamberlain, and Jeffrey S. Chamberlain. 2017. 'Corrigendum: Muscle-specific CRISPR/Cas9 dystrophin gene editing ameliorates pathophysiology in a mouse model for Duchenne muscular dystrophy', *Nature communications*, 8: 16007-07.

Benveniste, Olivier, Werner Stenzel, David Hilton, Jones Marco, Sandri Olivier, and Baziel G. M. Van Engelen. 2015. 'Amyloid deposits and inflammatory infiltrates in sporadic inclusion body myositis : the inflammatory egg comes before the degenerative chicken', *Acta Neuropathol*, 129: 611-24.

Bhatt, P. S., C. Tzoulis, N. Balafkan, H. Miletic, G. T. T. Tran, P. S. Sanaker, and L. A. Bindoff. 2019. 'Mitochondrial DNA depletion in sporadic inclusion body myositis', *Neuromuscul Disord*, 29: 242-46.

Biferali, B., D. Proietti, C. Mozzetta, and L. Madaro. 2019. 'Fibro-Adipogenic Progenitors Cross-Talk in Skeletal Muscle: The Social Network', *Front Physiol*, 10: 1074.

Bolotin, D. A., S. Poslavsky, I. Mitrophanov, M. Shugay, I. Z. Mamedov, E. V. Putintseva, and D. M. Chudakov. 2015. 'MiXCR: software for comprehensive adaptive immunity profiling', *Nat Methods*, 12: 380-1.

Bottai, M., A. Tjarnlund, G. Santoni, V. P. Werth, C. Pilkington, M. de Visser, L. Alfredsson, A. A. Amato, R. J. Barohn, M. H. Liang, J. A. Singh, R. Aggarwal, S. Arnardottir, H. Chinoy, R. G. Cooper, K. Danko, M. M. Dimachkie, B. M. Feldman, I. Garcia-De La Torre, P. Gordon, T. Hayashi, J. D. Katz, H. Kohsaka, P. A. Lachenbruch, B. A. Lang, Y. Li, C. V. Oddis, M. Olesinka, A. M. Reed, L. Rutkowska-Sak, H. Sanner, A. Selva-O'Callaghan, Y. Wook Song, J. Vencovsky, S. R. Ytterberg, F. W. Miller, L. G. Rider, I. E. Lundberg, the Euromyositis register International Myositis Classification Criteria Project consortium, Study the Juvenile Dermatomyositis Cohort Biomarker, and Repository. 2017. 'EULAR/ACR classification criteria for adult and juvenile idiopathic inflammatory myopathies and their major subgroups: a methodology report', *RMD Open*, 3: e000507.

Brady, S., W. Squier, and D. Hilton-Jones. 2013. 'Clinical assessment determines the diagnosis of inclusion body myositis independently of pathological features', *J Neurol Neurosurg Psychiatry*, 84: 1240-6.

Britson, K. A., A. D. Black, K. R. Wagner, and T. E. Lloyd. 2019. 'Performing Human Skeletal Muscle Xenografts in Immunodeficient Mice', *J Vis Exp*, 151: 10.3791/59966.

Britson, K. A., S. Y. Yang, and T. E. Lloyd. 2018. 'New Developments in the Genetics of Inclusion Body Myositis', *Curr Rheumatol Rep*, 20: 26.
Broccolini, Aldobrando, and Massimiliano Mirabella. 2015. 'Hereditary inclusion-body myopathies', *Biochimica et Biophysica Acta (BBA) - Molecular Basis of Disease*, 1852: 644-50.
Cai, Huaying, Ichiro Yabe, Kazunori Sato, Takahiro Kano, Masakazu Nakamura, Hideki Hozen, and Hidenao Sasaki. 2012. 'Clinical, pathological, and genetic mutation analysis of sporadic inclusion body myositis in Japanese people', *Journal of Neurology*, 259: 1913-22.
Callan, Aoife, Gorana Capkun, Vijayalakshmi Vasanthaprasad, Rita Freitas, and Merrilee Needham. 2017. 'A Systematic Review and Meta-Analysis of Prevalence Studies of Sporadic Inclusion Body Myositis', *Journal of Neuromuscular Diseases*, 4: 127-37.
Carpenter, S., G. Karpati, I. Heller, and A. Eisen. 1978. 'Inclusion body myositis: a distinct variety of idiopathic inflammatory myopathy', *Neurology*, 28: 8-17.
Carrillo, N., M. C. Malicdan, and M. Huizing. 2018. 'GNE Myopathy: Etiology, Diagnosis, and Therapeutic Challenges', *Neurotherapeutics*, 15: 900-14.
Catalan-Garcia, M., G. Garrabou, C. Moren, M. Guitart-Mampel, A. Hernando, A. Diaz-Ramos, I. Gonzalez-Casacuberta, D. L. Juarez, M. Bano, J. Enrich-Bengoa, S. Emperador, J. C. Milisenda, P. Moreno, E. Tobias, A. Zorzano, J. Montoya, F. Cardellach, and J. M. Grau. 2016. 'Mitochondrial DNA disturbances and deregulated expression of oxidative phosphorylation and mitochondrial fusion proteins in sporadic inclusion body myositis', *Clinical Science*, 130: 1741-51.
Chahin, N., and A. G. Engel. 2008. 'Correlation of muscle biopsy, clinical course, and outcome in PM and sporadic IBM', *Neurology*, 70: 418-24.
Chang, Ya Chu, Wan Tzu Hung, Yun Chin Chang, Henry C. Chang, Chia Lin Wu, Ann Shyn Chiang, George R. Jackson, and Tzu Kang Sang. 2011. 'Pathogenic VCP/TER94 alleles are dominant actives and contribute to neurodegeneration by altering cellular ATP level in a drosophila IBMPFD model', *PLoS Genetics*, 7: e1001288.
Chen, J. C., O. D. King, Y. Zhang, N. P. Clayton, C. Spencer, B. M. Wentworth, C. P. Emerson, Jr., and K. R. Wagner. 2016. 'Morpholino-mediated Knockdown of DUX4 Toward Facioscapulohumeral Muscular Dystrophy Therapeutics', *Mol Ther*, 24: 1405-11.
Chinoy, Hector, and James B. Lilleker. 2019. 'Abstracts of scientific contributions to GCOM 2019: Berlin, Germany. 27 - 30 March 2019.' in, *BMC Rheumatol*.
Chornenkyy, Y., D. W. Fardo, and P. T. Nelson. 2019. 'Tau and TDP-43 proteinopathies: kindred pathologic cascades and genetic pleiotropy', *Lab Invest*, 99: 993-1007.
Chou, S. M. 1967. 'Myxovirus-like structures in a case of human chronic polymyositis', *Science*, 158: 1453-5.
Cortese, Andrea, Vincent Plagnol, Stefen Brady, Roberto Simone, Tammaryn Lashley, Abraham Acevedo-Arozena, Rohan De Silva, Linda Greensmith, Janice Holton, Michael G. Hanna, Elizabeth M. C. Fisher, and Pietro Fratta. 2014. 'Widespread RNA metabolism impairment in sporadic inclusion body myositis TDP43-proteinopathy', *Neurobiology of Aging*, 35: 1491-8.
Cox, F. M., V. Delgado, J. J. Verschuuren, B. E. Ballieux, J. J. Bax, A. R. Wintzen, and U. A. Badrising. 2010. 'The heart in sporadic inclusion body myositis: a study in 51 patients', *J Neurol*, 257: 447-51.
Cox, F. M., M. Reijnierse, C. S. van Rijswijk, A. R. Wintzen, J. J. Verschuuren, and U. A. Badrising. 2011. 'Magnetic resonance imaging of skeletal muscles in sporadic inclusion body myositis', *Rheumatology (Oxford)*, 50: 1153-61.
Credle, J. J., C. Y. Itoh, T. Yuan, R. Sharma, E. R. Scott, R. E. Workman, Y. Fan, F. Housseau, N. J. Llosa, W. R. Bell, H. Miller, S. X. Zhang, W. Timp, and H. B. Larman. 2017. 'Multiplexed analysis of fixed tissue RNA using Ligation in situ Hybridization', *Nucleic Acids Res*, 45: e128.

Custer, Sara K., Manuela Neumann, Hongbo Lu, Alexander C. Wright, and J. Paul Taylor. 2010. 'Transgenic mice expressing mutant forms VCP/p97 recapitulate the full spectrum of IBMPFD including degeneration in muscle, brain and bone', *Human Molecular Genetics*, 19: 1741-55.
Cutler, A. A., T. E. Ewachiw, G. A. Corbet, R. Parker, and B. B. Olwin. 2019. 'Myo-granules Connect Physiology and Pathophysiology', *J Exp Neurosci*, 13: 1179069519842157.
Dahlbom, K., C. Lindberg, and A. Oldfors. 2002. 'Inclusion body myositis: morphological clues to correct diagnosis', *Neuromuscul Disord*, 12: 853-7.
Dalakas, M. C., B. Sonies, J. Dambrosia, E. Sekul, E. Cupler, and K. Sivakumar. 1997. 'Treatment of inclusion-body myositis with IVIg: a double-blind, placebo-controlled study', *Neurology*, 48: 712-6.
Dalakas, Marinos C. 2015. 'Inflammatory Muscle Diseases', *The New England Journal of Medicine*, 373: 393-94.
Dalakas, Marinos C., Goran Rakocevic, Jens Schmidt, Mohammad Salajegheh, Beverly McElroy, Michael O. Harris-Love, Joseph A. Shrader, Ellen W. Levy, James Dambrosia, Robert L. Kampen, David A. Bruno, and Allan D. Kirk. 2009. 'Effect of Alemtuzumab (CAMPATH 1-H) in patients with inclusion-body myositis', *Brain*, 132: 1536-44.
Dobloug, C., R. Walle-Hansen, J. T. Gran, and O. Molberg. 2012. 'Long-term follow-up of sporadic inclusion body myositis treated with intravenous immunoglobulin: a retrospective study of 16 patients', *Clin Exp Rheumatol*, 30: 838-42.
Dobrolecki, L. E., S. D. Airhart, D. G. Alferez, S. Aparicio, F. Behbod, M. Bentires-Alj, C. Brisken, C. J. Bult, S. Cai, R. B. Clarke, H. Dowst, M. J. Ellis, E. Gonzalez-Suarez, R. D. Iggo, P. Kabos, S. Li, G. J. Lindeman, E. Marangoni, A. McCoy, F. Meric-Bernstam, H. Piwnica-Worms, M. F. Poupon, J. Reis-Filho, C. A. Sartorius, V. Scabia, G. Sflomos, Y. Tu, F. Vaillant, J. E. Visvader, A. Welm, M. S. Wicha, and M. T. Lewis. 2016. 'Patient-derived xenograft (PDX) models in basic and translational breast cancer research', *Cancer Metastasis Rev*, 35: 547-73.
Dodds, R. M., H. C. Roberts, C. Cooper, and A. A. Sayer. 2015. 'The Epidemiology of Sarcopenia', *J Clin Densitom*, 18: 461-6.
Douglas, P. M., and D. M. Cyr. 2010. 'Interplay between protein homeostasis networks in protein aggregation and proteotoxicity', *Biopolymers*, 93: 229-36.
Dubourg, Odile, J. Wanschitz, T. Maisonobe, A. Béhin, Y. Allenbach, S. Herson, and O. Benveniste. 2011. 'Diagnostic value of markers of muscle degeneration in sporadic inclusion body myositis', *Acta Myologica*, 30: 103-08.
Dzangue-Tchoupou, G., K. Mariampillai, L. Bolko, D. Amelin, W. Mauhin, A. Corneau, C. Blanc, Y. Allenbach, and O. Benveniste. 2019. 'CD8+T-bet+ cells as a predominant biomarker for inclusion body myositis', *Autoimmun Rev*, 18: 325-33.
Elkina, Yulia, Stephan von Haehling, Stefan D. Anker, and Jochen Springer. 2011. 'The role of myostatin in muscle wasting: An overview', *Journal of Cachexia, Sarcopenia and Muscle*, 2: 143-51.
Falcke, S. E., P. F. Ruhle, L. Deloch, R. Fietkau, B. Frey, and U. S. Gaipl. 2018. 'Clinically Relevant Radiation Exposure Differentially Impacts Forms of Cell Death in Human Cells of the Innate and Adaptive Immune System', *Int J Mol Sci*, 19: 3574.
Farup, J., L. Madaro, P. L. Puri, and U. R. Mikkelsen. 2015. 'Interactions between muscle stem cells, mesenchymal-derived cells and immune cells in muscle homeostasis, regeneration and disease', *Cell Death Dis*, 6: e1830.
Felice, K. J., and W. A. North. 2001. 'Inclusion body myositis in Connecticut: observations in 35 patients during an 8-year period', *Medicine (Baltimore)*, 80: 320-7.
Fergusson, D. 2009. 'Inappropriate referencing in research', *BMJ*, 339: b2049.
Finkel, Richard S., Eugenio Mercuri, Basil T. Darras, Anne M. Connolly, Nancy L. Kuntz, Janbernd Kirschner, Claudia A. Chiriboga, Kayoko Saito, Laurent Servais, Eduardo Tizzano, Haluk Topaloglu, Már Tulinius, Jacqueline Montes, Allan M. Glanzman, Kathie Bishop, Z. John Zhong, Sarah Gheuens, C. Frank Bennett, Eugene Schneider, Wildon

Farwell, and Darryl C. De Vivo. 2017. 'Nusinersen versus Sham Control in Infantile-Onset Spinal Muscular Atrophy', *New England Journal of Medicine*, 377: 1723-32.
Fouad, Y. A., and C. Aanei. 2017. 'Revisiting the hallmarks of cancer', *Am J Cancer Res*, 7: 1016-36.
Fox, S. A., B. K. Ward, P. D. Robbins, F. L. Mastaglia, and N. R. Swanson. 1996. 'Inclusion body myositis: investigation of the mumps virus hypothesis by polymerase chain reaction', *Muscle Nerve*, 19: 23-8.
Freret, M., L. Drouot, A. Obry, S. Ahmed-Lacheheb, C. Dauly, S. Adriouch, P. Cosette, F. J. Authier, and O. Boyer. 2013. 'Overexpression of MHC class I in muscle of lymphocyte-deficient mice causes a severe myopathy with induction of the unfolded protein response', *Am J Pathol*, 183: 893-904.
Fyhr, I. M., A. R. Moslemi, A. A. Mosavi, C. Lindberg, A. Tarkowski, and A. Oldfors. 1997. 'Oligoclonal expansion of muscle infiltrating T cells in inclusion body myositis', *J Neuroimmunol*, 79: 185-9.
Gabellini, D., M. R. Green, and R. Tupler. 2002. 'Inappropriate gene activation in FSHD: a repressor complex binds a chromosomal repeat deleted in dystrophic muscle', *Cell*, 110: 339-48.
Gang, Qiang, Concei o Bettencourt, Pedro M. Machado, Stefen Brady, Janice L. Holton, Alan M. Pittman, Deborah Hughes, Estelle Healy, Matthew Parton, David Hilton-Jones, Perry B. Shieh, Merrilee Needham, Christina Liang, Edmar Zanoteli, Leonardo Valente de Camargo, Boel De Paepe, Jan De Bleecker, Aziz Shaibani, Michela Ripolone, Raffaella Violano, Maurizio Moggio, Richard J. Barohn, Mazen M. Dimachkie, Marina Mora, Renato Mantegazza, Simona Zanotti, Andrew B. Singleton, Michael G. Hanna, Henry Houlden, Conceicao Bettencourt, April L. McVey, Mamatha Pasnoor, Melanie Glenn, Omar Jawdat, Jeffrey Statland, Gabrielle Rico, Frank Mastaglia, Marinos C. Dalakas, Angie Biba, Hector Chinoy, James B. Lilleker, Janine Lamb, Hazel Platt, Robert G. Cooper, James A. L. Miller, Mark Roberts, Elizabeth Househam, David Hilton, Aditya Shivane, Amy Bartlett, John T. Kissel, Heidi Runk, Matthew Wicklund, David S. Saperstein, and Lynette R. McKinney. 2016. 'Rare variants in SQSTM1 and VCP genes and risk of sporadic inclusion body myositis', *Neurobiology of Aging*, 47: 218.e1-18.e9.
Gang, Qiang, Conceição Bettencourt, Henry Houlden, Michael G. Hanna, and Pedro M. Machado. 2015. 'Genetic advances in sporadic inclusion body myositis', *Current Opinion in Rheumatology*, 27: 586-94.
Gang, Qiang, Conceicao Bettencourt, Pedro M. Machado, Zoe Fox, Stefen Brady, Estelle Healy, Matt Parton, Janice L. Holton, David Hilton-Jones, Perry B. Shieh, Edmar Zanoteli, Boel De Paepe, Jan De Bleecker, Aziz Shaibani, Michela Ripolone, Raffaella Violano, Maurizio Moggio, Richard J. Barohn, Mazen M. Dimachkie, Marina Mora, Renato Mantegazza, Simona Zanotti, Michael G. Hanna, and Henry Houlden. 2015. 'The effects of an intronic polymorphism in TOMM40 and APOE genotypes in sporadic inclusion body myositis', *Neurobiology of Aging*, 36: 1766.e1-66.e3.
Garlepp, M. J., B. Laing, P. J. Zilko, W. Ollier, and F. L. Mastaglia. 1994. 'HLA associations with inclusion body myositis', *Clinical and experimental immunology*, 98: 40-5.
Giebel, Sebastian, Leszek Miszczyk, Krzysztof Slosarek, Leila Moukhtari, Fabio Ciceri, Jordi Esteve, Norbert-Claude Gorin, Myriam Labopin, Arnon Nagler, Christoph Schmid, and Mohamad Mohty. 2014. 'Extreme Heterogeneity of Myeloablative Total Body Irradiation Techniques in Clinical Practice A Survey of the Acute Leukemia Working Party of the European Group for Blood and Marrow Transplantation', *Cancer*, 120: 2760-65.
Glaubitz, S., R. Zeng, and J. Schmidt. 2020. 'New insights into the treatment of myositis', *Ther Adv Musculoskelet Dis*, 12: 1759720X19886494.
Gonzalez, Michael A., Shawna M. Feely, Fiorella Speziani, Alleene V. Strickland, Matt Danzi, Chelsea Bacon, Youjin Lee, Tsui Fen Chou, Susan H. Blanton, Conrad C. Weihl, Stephan Zuchner, and Michael E. Shy. 2014. 'A novel mutation in VCP causes Charcot-Marie-Tooth Type 2 disease', *Brain*, 137: 2897-902.

Greenberg, S. A. 2009. 'How citation distortions create unfounded authority: analysis of a citation network', *BMJ*, 339: b2680.
Greenberg, S. A. 2010a. 'Comment on alemtuzumab and inclusion body myositis', *Brain*, 133: e135.
Greenberg, S. A. 2010b. 'Theories of the pathogenesis of inclusion body myositis', *Curr Rheumatol Rep*, 12: 221-8.
Greenberg, S. A. 2014. 'Cytoplasmic 5'-nucleotidase autoantibodies in inclusion body myositis: Isotypes and diagnostic utility', *Muscle Nerve*, 50: 488-92.
Greenberg, S. A. 2017. 'Unfounded Claims of Improved Functional Outcomes Attributed to Follistatin Gene Therapy in Inclusion Body Myositis', *Mol Ther*, 25: 2235-37.
Greenberg, S. A. 2019. 'Inclusion body myositis: clinical features and pathogenesis', *Nat Rev Rheumatol*, 15: 257-72.
Greenberg, S. A., E. M. Bradshaw, J. L. Pinkus, G. S. Pinkus, T. Burleson, B. Due, L. Bregoli, K. C. O'Connor, and A. A. Amato. 2005. 'Plasma cells in muscle in inclusion body myositis and polymyositis', *Neurology*, 65: 1782-7.
Greenberg, S. A., J. L. Pinkus, A. A. Amato, T. Kristensen, and D. M. Dorfman. 2016. 'Association of inclusion body myositis with T cell large granular lymphocytic leukaemia', *Brain*, 139: 1348-60.
Greenberg, S. A., J. L. Pinkus, S. W. Kong, C. Baecher-Allan, A. A. Amato, and D. M. Dorfman. 2019. 'Highly differentiated cytotoxic T cells in inclusion body myositis', *Brain*, 142: 2590-604.
Griggs, R. C., V. Askanas, S. DiMauro, a Engel, G. Karpati, J. R. Mendell, and L. P. Rowland. 1995. 'Inclusion body myositis and myopathies', *Annals of Neurology*, 38: 705-13.
Guimaraes, J. B., E. Zanoteli, T. M. Link, L. V. de Camargo, L. Facchetti, L. Nardo, and Adrc Fernandes. 2017. 'Sporadic Inclusion Body Myositis: MRI Findings and Correlation With Clinical and Functional Parameters', *AJR Am J Roentgenol*, 209: 1340-47.
Gulati, Adarsh K. 1987. 'The effect of X-irradiation on skeletal muscle regeneration in the adult rat', *Journal of the Neurological Sciences Tel*, 78404: 111-20.
Guttsches, Anne Katrin, Stefen Brady, Kathryn Krause, Alexandra Maerkens, Julian Uszkoreit, Martin Eisenacher, Anja Schreiner, Sara Galozzi, Janine Mertens-Rill, Martin Tegenthoff, Janice L. Holton, Matthew B. Harms, Thomas E. Lloyd, Matthias Vorgerd, Conrad C. Weihl, Katrin Marcus, and Rudolf A. Kley. 2017. 'Proteomics of rimmed vacuoles define new risk allele in inclusion body myositis', *Annals of Neurology*, 81: 227-39.
Hall, Eric J, and James G Kereiakes. 2001. 'Effects of Ionizing Radiation on Cells.' in Nicholas Sperelakis (ed.), *Cell Physiology Source Book: A Molecular Approach* (Elsevier: Academic Press).
Hamann, P. D., B. T. Roux, J. A. Heward, S. Love, N. J. McHugh, S. W. Jones, and M. A. Lindsay. 2017. 'Transcriptional profiling identifies differential expression of long non-coding RNAs in Jo-1 associated and inclusion body myositis', *Sci Rep*, 7: 8024.
Hanna, M. G., U. A. Badrising, O. Benveniste, T. E. Lloyd, M. Needham, H. Chinoy, M. Aoki, P. M. Machado, C. Liang, K. A. Reardon, M. de Visser, D. P. Ascherman, R. J. Barohn, M. M. Dimachkie, J. A. L. Miller, J. T. Kissel, B. Oskarsson, N. C. Joyce, P. Van den Bergh, J. Baets, J. L. De Bleecker, C. Karam, W. S. David, M. Mirabella, S. P. Nations, H. H. Jung, E. Pegoraro, L. Maggi, C. Rodolico, M. Filosto, A. I. Shaibani, K. Sivakumar, N. A. Goyal, M. Mori-Yoshimura, S. Yamashita, N. Suzuki, M. Katsuno, K. Murata, H. Nodera, I. Nishino, C. D. Romano, V. S. L. Williams, J. Vissing, L. Z. Auberson, M. Wu, A. de Vera, D. A. Papanicolaou, A. A. Amato, and Resilient Study Group. 2019. 'Safety and efficacy of intravenous bimagrumab in inclusion body myositis (RESILIENT): a randomised, double-blind, placebo-controlled phase 2b trial', *Lancet Neurol*, 18: 834-44.
Hansen, Jakob, Claus Brandt, Anders R. Nielsen, Pernille Hojman, Martin Whitham, Mark A. Febbraio, Bente K. Pedersen, and Peter Plomgaard. 2011. 'Exercise induces a marked increase in plasma follistatin: Evidence that follistatin is a contraction-induced hepatokine', *Endocrinology*, 152: 164-71.

Hay, M., D. W. Thomas, J. L. Craighead, C. Economides, and J. Rosenthal. 2014. 'Clinical development success rates for investigational drugs', *Nat Biotechnol*, 32: 40-51.
Hermanns, B., M. Molnar, and J. M. Schroder. 2000. 'Peripheral neuropathy associated with hereditary and sporadic inclusion body myositis: confirmation by electron microscopy and morphometry', *J Neurol Sci*, 179: 92-102.
Hiniker, Annie, Brianne H. Daniels, Han S. Lee, and Marta Margeta. 2013. 'Comparative utility of LC3, p62 and TDP-43 immunohistochemistry in differentiation of inclusion body myositis from polymyositis and related inflammatory myopathies', *Acta Neuropathol Commun*, 1: 1-29.
Hogarth, M. W., A. Defour, C. Lazarski, E. Gallardo, J. Diaz Manera, T. A. Partridge, K. Nagaraju, and J. K. Jaiswal. 2019. 'Fibroadipogenic progenitors are responsible for muscle loss in limb girdle muscular dystrophy 2B', *Nat Commun*, 10: 2430.
Hokkoku, K., M. Sonoo, M. Higashihara, E. Stalberg, and T. Shimizu. 2012. 'Electromyographs of the flexor digitorum profundus muscle are useful for the diagnosis of inclusion body myositis', *Muscle Nerve*, 46: 181-6.
Hollemann, David, Herbert Budka, Wolfgang N. Löscher, Genya Yanagida, Michael B. Fischer, and Julia V. Wanschitz. 2008. 'Endothelial and Myogenic Differentiation of Hematopoietic Progenitor Cells in Inflammatory Myopathies', *Journal of Neuropathology and Experimental Neurology*, 67: 711-19.
Hoogendijk, J. E., A. A. Amato, B. R. Lecky, E. H. Choy, I. E. Lundberg, M. R. Rose, J. Vencovsky, M. de Visser, and R. A. Hughes. 2004. '119th ENMC international workshop: trial design in adult idiopathic inflammatory myopathies, with the exception of inclusion body myositis, 10-12 October 2003, Naarden, The Netherlands', *Neuromuscul Disord*, 14: 337-45.
Houser, S. M., L. H. Calabrese, and M. Strome. 1998. 'Dysphagia in patients with inclusion body myositis', *Laryngoscope*, 108: 1001-5.
Howard, E. E., S. M. Pasiakos, C. N. Blesso, M. A. Fussell, and N. R. Rodriguez. 2020. 'Divergent Roles of Inflammation in Skeletal Muscle Recovery From Injury', *Front Physiol*, 11: 87.
Hruz, T., O. Laule, G. Szabo, F. Wessendorp, S. Bleuler, L. Oertle, P. Widmayer, W. Gruissem, and P. Zimmermann. 2008. 'Genevestigator v3: a reference expression database for the meta-analysis of transcriptomes', *Adv Bioinformatics*, 2008: 420747.
Huizing, M., N. Carrillo-Carrasco, M. C. Malicdan, S. Noguchi, W. A. Gahl, S. Mitrani-Rosenbaum, Z. Argov, and I. Nishino. 2014. 'GNE myopathy: new name and new mutation nomenclature', *Neuromuscul Disord*, 24: 387-9.
Ikenaga, Chiseko, Akatsuki Kubota, Masato Kadoya, Kenichiro Taira, Naohiro Uchio, Ayumi Hida, Meiko Hashimoto Maeda, Yu Nagashima, Hiroyuki Ishiura, Kenichi Kaida, Jun Goto, Shoji Tsuji, and Jun Shimizu. 2017. 'Clinicopathologic features of myositis patients with CD8-MHC-1 complex pathology', *Neurology*, 89: 1060-68.
Ikezoe, K., H. Furuya, H. Arahata, M. Nakagawa, T. Tateishi, N. Fujii, and J. Kira. 2009. 'Amyloid-beta accumulation caused by chloroquine injections precedes ER stress and autophagosome formation in rat skeletal muscle', *Acta Neuropathol*, 117: 575-82.
Izumchenko, E., K. Paz, D. Ciznadija, I. Sloma, A. Katz, D. Vasquez-Dunddel, I. Ben-Zvi, J. Stebbing, W. McGuire, W. Harris, R. Maki, A. Gaya, A. Bedi, S. Zacharoulis, R. Ravi, L. H. Wexler, M. O. Hoque, C. Rodriguez-Galindo, H. Pass, N. Peled, A. Davies, R. Morris, M. Hidalgo, and D. Sidransky. 2017. 'Patient-derived xenografts effectively capture responses to oncology therapy in a heterogeneous cohort of patients with solid tumors', *Ann Oncol*, 28: 2595-605.
Jensen, K. Y., M. Jacobsen, H. D. Schroder, P. Aagaard, J. L. Nielsen, A. N. Jorgensen, E. Boyle, R. D. Bech, S. Rosmark, L. P. Diederichsen, and U. Frandsen. 2019. 'The immune system in sporadic inclusion body myositis patients is not compromised by blood-flow restricted exercise training', *Arthritis Res Ther*, 21: 293.

Jeong, Y. H., J. P. Ling, S. Z. Lin, A. N. Donde, K. E. Braunstein, E. Majounie, B. J. Traynor, K. D. LaClair, T. E. Lloyd, and P. C. Wong. 2017. 'Tdp-43 cryptic exons are highly variable between cell types', *Mol Neurodegener*, 12: 13.

Jin, Y., Y. Shen, X. Su, N. Weintraub, and Y. Tang. 2019. 'CRISPR/Cas9 Technology in Restoring Dystrophin Expression in iPSC-Derived Muscle Progenitors', *J Vis Exp*, 151: 10.3791/59432.

Joanisse, S., J. P. Nederveen, T. Snijders, B. R. McKay, and G. Parise. 2017. 'Skeletal Muscle Regeneration, Repair and Remodelling in Aging: The Importance of Muscle Stem Cells and Vascularization', *Gerontology*, 63: 91-100.

Johari, M., M. Arumilli, J. Palmio, M. Savarese, G. Tasca, M. Mirabella, N. Sandholm, H. Lohi, P. Hackman, and B. Udd. 2017. 'Association study reveals novel risk loci for sporadic inclusion body myositis', *European Journal of Neurology*, 24: 572-77.

Johnson, Janel O., Jessica Mandrioli, Michael Benatar, Yevgeniya Abramzon, Vivianna M. Van Deerlin, John Q. Trojanowski, J. Raphael Gibbs, Maura Brunetti, Susan Gronka, Joanne Wuu, Jinhui Ding, Leo McCluskey, Maria Martinez-Lage, Dana Falcone, Dena G. Hernandez, Sampath Arepalli, Sean Chong, Jennifer C. Schymick, Jeffrey Rothstein, Francesco Landi, Yong Dong Wang, Andrea Calvo, Gabriele Mora, Mario Sabatelli, Maria Rosaria Monsurrò, Stefania Battistini, Fabrizio Salvi, Rossella Spataro, Patrizia Sola, Giuseppe Borghero, Giuliana Galassi, Sonja W. Scholz, J. Paul Taylor, Gabriella Restagno, Adriano Chiò, and Bryan J. Traynor. 2010. 'Exome Sequencing Reveals VCP Mutations as a Cause of Familial ALS', *Neuron*, 68: 857-64.

Johnson, Liam G., Kelly E. Collier, Dylan J. Edwards, Danielle L. Philippe, Peter R. Eastwood, Susan E. Walters, Gary W. Thickbroom, and Frank L. Mastaglia. 2009. 'Improvement in aerobic capacity after an exercise program in sporadic inclusion body myositis', *Journal of Clinical Neuromuscular Disease*, 10: 178-84.

Jonathan P. Ling, Olga Pletnikova Juan C. Troncoso Philip C. Wong. 2015. 'TDP-43 repression of nonconserved cryptic exons is compromised in ALS-FTD', *Science*, 349: 650-5.

Jones, R. A., C. Harrison, S. L. Eaton, M. Llavero Hurtado, L. C. Graham, L. Alkhammash, O. A. Oladiran, A. Gale, D. J. Lamont, H. Simpson, M. W. Simmen, C. Soeller, T. M. Wishart, and T. H. Gillingwater. 2017. 'Cellular and Molecular Anatomy of the Human Neuromuscular Junction', *Cell Rep*, 21: 2348-56.

Joshi, P. R., M. Vetterke, A. Hauburger, P. Tacik, G. Stoltenburg, and F. Hanisch. 2014. 'Functional relevance of mitochondrial abnormalities in sporadic inclusion body myositis', *J Clin Neurosci*, 21: 1959-63.

Ju, Jeong Sun, Rodrigo A. Fuentealba, Sara E. Miller, Erin Jackson, David Piwnica-Worms, Robert H. Baloh, and Conrad C. Weihl. 2009. 'Valosin-containing protein (VCP) is required for autophagy and is disrupted in VCP disease', *Journal of Cell Biology*, 187: 875-88.

Jung, J., H. S. Seol, and S. Chang. 2018. 'The Generation and Application of Patient-Derived Xenograft Model for Cancer Research', *Cancer Res Treat*, 50: 1-10.

Kallajoki, M., T. Hyypia, P. Halonen, C. Orvell, B. K. Rima, and H. Kalimo. 1991. 'Inclusion body myositis and paramyxoviruses', *Hum Pathol*, 22: 29-32.

Keller, Christian W., Jens Schmidt, and Jan D. Lünemann. 2017. 'Immune and myodegenerative pathomechanisms in inclusion body myositis', *Annals of Clinical and Translational Neurology*, 4: 422-45.

Keshishian, A., S. A. Greenberg, N. Agashivala, O. Baser, and K. Johnson. 2018. 'Health care costs and comorbidities for patients with inclusion body myositis', *Curr Med Res Opin*, 34: 1679-85.

Kieran, D., B. Kalmar, J. R. Dick, J. Riddoch-Contreras, G. Burnstock, and L. Greensmith. 2004. 'Treatment with arimoclomol, a coinducer of heat shock proteins, delays disease progression in ALS mice', *Nat Med*, 10: 402-5.

Kim, J., H.H. Wu, A.D. Lander, K.M. Lyons, M.M. Matzuk, and A.L. Calof. 2005. 'GDF11 Controls the Timing of Progenitor Cell Competence in Developing Retina', *Science*, 308: 1927-30.

Kim, Kwangwoo, So Young Bang, Hye Soon Lee, Yukinori Okada, Buhm Han, Woei Yuh Saw, Yik Ying Teo, and Sang Cheol Bae. 2014. 'The HLA-DRβ1 amino acid positions 11-13-26 explain the majority of SLE-MHC associations', *Nature communications*, 5: 5902.
Kimonis, Virginia E., Erin Fulchiero, Jouni Vesa, and Giles Watts. 2008. 'VCP disease associated with myopathy, Paget disease of bone and frontotemporal dementia: Review of a unique disorder', *Biochimica et Biophysica Acta - Molecular Basis of Disease*, 1782: 744-48.
Kjer-Nielsen, L., M. A. Dunstone, L. Kostenko, L. K. Ely, T. Beddoe, N. A. Mifsud, A. W. Purcell, A. G. Brooks, J. McCluskey, and J. Rossjohn. 2004. 'Crystal structure of the human T cell receptor CD3 epsilon gamma heterodimer complexed to the therapeutic mAb OKT3', *Proc Natl Acad Sci U S A*, 101: 7675-80.
Klaips, C. L., G. G. Jayaraj, and F. U. Hartl. 2018. 'Pathways of cellular proteostasis in aging and disease', *J Cell Biol*, 217: 51-63.
Koo, J. H., E. B. Kang, and J. Y. Cho. 2019. 'Resistance Exercise Improves Mitochondrial Quality Control in a Rat Model of Sporadic Inclusion Body Myositis', *Gerontology*, 65: 240-52.
Koppers, Max, Marka M. van Blitterswijk, Lotte Vlam, Paulina A. Rowicka, Paul W. J. van Vught, Ewout J. N. Groen, Wim G. M. Spliet, JooYeon Engelen-Lee, Helenius J. Schelhaas, Marianne de Visser, Anneke J. van der Kooi, W. Ludo van der Pol, R. Jeroen Pasterkamp, Jan H. Veldink, and Leonard H. van den Berg. 2012. 'VCP mutations in familial and sporadic amyotrophic lateral sclerosis', *Neurobiology of Aging*, 33: 837.e7-37.e13.
Kota, Janaiah, Chalonda R. Handy, Amanda M. Haidet, Chrystal L. Montgomery, Amy Eagle, Louise R. Rodino-Klapac, Danielle Tucker, Christopher J. Shilling, Walter R. Therlfall, Christopher M. Walker, Steven E. Weisbrode, Paul M. L. Janssen, K. Reed Clark, Zarife Sahenk, Jerry R. Mendell, and Brian K. Kaspar. 2009. 'Follistatin gene delivery enhances muscle growth and strength in nonhuman primates', *Science Translational Medicine*, 1: 1-8.
Krupke, D. M., D. A. Begley, J. P. Sundberg, J. E. Richardson, S. B. Neuhauser, and C. J. Bult. 2017. 'The Mouse Tumor Biology Database: A Comprehensive Resource for Mouse Models of Human Cancer', *Cancer Res*, 77: e67-e70.
Kung, P., G. Goldstein, E. L. Reinherz, and S. F. Schlossman. 1979. 'Monoclonal antibodies defining distinctive human T cell surface antigens', *Science*, 206: 347-9.
Larman, H. Benjamin, Mohammad Salajegheh, Remedios Nazareno, Theresa Lam, John Sauld, Hanno Steen, Sek Won Kong, Jack L. Pinkus, Anthony A. Amato, Stephen J. Elledge, and Steven A. Greenberg. 2013. 'Cytosolic 5′-nucleotidase 1A autoimmunity in sporadic inclusion body myositis', *Annals of Neurology*, 73: 408-18.
Lee, J., D. H. Jo, J. H. Kim, C. S. Cho, J. E. Han, Y. Kim, H. Park, S. H. Yoo, Y. S. Yu, H. E. Moon, H. R. Park, D. G. Kim, and S. H. Paek. 2019. 'Development of a patient-derived xenograft model of glioblastoma via intravitreal injection in mice', *Exp Mol Med*, 51: 43.
Lemmers, R. J., P. J. van der Vliet, R. Klooster, S. Sacconi, P. Camano, J. G. Dauwerse, L. Snider, K. R. Straasheijm, G. J. van Ommen, G. W. Padberg, D. G. Miller, S. J. Tapscott, R. Tawil, R. R. Frants, and S. M. van der Maarel. 2010. 'A unifying genetic model for facioscapulohumeral muscular dystrophy', *Science*, 329: 1650-3.
Leung, Doris G., Harold A. Taylor, Amanda S. Lindy, Monica J. Basehore, and Andrew L. Mammen. 2014. 'A case of progressive quadriceps weakness and elevated creatine kinase level mimicking inclusion body myositis', *Arthritis Care and Research*, 66: 328-33.
Li, CKc, P. Knopp, H. Moncrieffe, B. Singh, S. Shah, K. Nagaraju, H. Varsani, B. Gao, and L. R. Wedderburn. 2009. 'Overexpression of MHC Class I Heavy Chain Protein in Young Skeletal Muscle Leads to Severe Myositis : Implications for Juvenile Myositis', *Am J Pathol*, 175: 1030-40.
Li, Songqing, Peipei Zhang, Brian D. Freibaum, Nam Chul Kim, Regina Maria Kolaitis, Amandine Molliex, Anderson P. Kanagaraj, Ichiro Yabe, Mishie Tanino, Shinya Tanaka, Hidenao Sasaki, Eric D. Ross, J. Paul Taylor, and Hong Joo Kim. 2016. 'Genetic interaction of

hnRNPA2B1 and DNAJB6 in a Drosophila model of multisystem proteinopathy', *Human Molecular Genetics*, 25: 936-50.
Limaye, Vidya S., Sue Lester, Peter Blumbergs, and Steven A. Greenberg. 2016. 'anti-cN1A Antibodies in South Australian Patients with Inclusion Body Myositis', *Muscle and Nerve*, 53: 653-54.
Lindberg, C., E. Trysberg, A. Tarkowski, and A. Oldfors. 2003. 'Anti-T-lymphocyte globulin treatment in inclusion body myositis: a randomized pilot study', *Neurology*, 61: 260-2.
Lindberg, Christopher, Anders Oldfors, and Andrzej Tarkowski. 1994. 'Restricted use of T cell receptor V genes in endomysial infiltrates of patients with inflammatory myopathies', *European Journal of Immunology*, 24: 2659-63.
Lindgren, Ulrika, Sara Roos, Carola Hedberg Oldfors, Ali Reza Moslemi, Christopher Lindberg, and Anders Oldfors. 2015. 'Mitochondrial pathology in inclusion body myositis', *Neuromuscular Disorders*, 25: 281-8.
Lloyd, Thomas E., Lisa Christopher-Stine, Iago Pinal-Fernandez, Eleni Tiniakou, Michelle Petri, Alan Baer, Sonye K. Danoff, Katherine Pak, Livia A. Casciola-Rosen, and Andrew L. Mammen. 2016. 'Cytosolic 5′-Nucleotidase 1A As a Target of Circulating Autoantibodies in Autoimmune Diseases', *Arthritis Care and Research*, 68: 66-71.
Lloyd, Thomas E., Andrew L. Mammen, Anthony A. Amato, Michael D. Weiss, Merrilee Needham, and Steven A. Greenberg. 2014. 'Evaluation and construction of diagnostic criteria for inclusion body myositis', *Neurology*, 83: 426-33.
Loell, I., and I. E. Lundberg. 2011. 'Can muscle regeneration fail in chronic inflammation: a weakness in inflammatory myopathies?', *J Intern Med*, 269: 243-57.
Loughlin, M. 1993. *Muscle biopsy. A laboratory investigation* (Butterworth-Heinemann Oxford).
Majounie, Elisa, Bryan J. Traynor, Adriano Chiò, Gabriella Restagno, Jessica Mandrioli, Michael Benatar, J. Paul Taylor, and Andrew B. Singleton. 2012. 'Mutational analysis of the VCP gene in Parkinson's disease', *Neurobiology of Aging*, 33: 209.e1-09.e2.
Malecova, B., S. Gatto, U. Etxaniz, M. Passafaro, A. Cortez, C. Nicoletti, L. Giordani, A. Torcinaro, M. De Bardi, S. Bicciato, F. De Santa, L. Madaro, and P. L. Puri. 2018. 'Dynamics of cellular states of fibro-adipogenic progenitors during myogenesis and muscular dystrophy', *Nat Commun*, 9: 3670.
Mastaglia, F. L. 2009. 'Sporadic inclusion body myositis: Variability in prevalence and phenotype and influence of the MHC', *Acta Myologica*, 28: 66-71.
Mastaglia, F. L., A. Rojana-udomsart, I. James, M. Needham, T. J. Day, L. Kiers, J. A. Corbett, A. M. Saunders, M. W. Lutz, and A. D. Roses. 2013. 'Polymorphism in the TOMM40 gene modifies the risk of developing sporadic inclusion body myositis and the age of onset of symptoms', *Neuromuscular Disorders*, 23: 969-74.
Masuda, Shinya, Tsubasa Hisamatsu, Daiki Seko, Yoshishige Urata, Shinji Goto, Tao Sheng Li, and Yusuke Ono. 2015. 'Time- and dose-dependent effects of total-body ionizing radiation on muscle stem cells', *Physiological Reports*, 3: 1-8.
Mayeuf-Louchart, A., D. Hardy, Q. Thorel, P. Roux, L. Gueniot, D. Briand, A. Mazeraud, A. Bougle, S. L. Shorte, B. Staels, F. Chretien, H. Duez, and A. Danckaert. 2018. 'MuscleJ: a high-content analysis method to study skeletal muscle with a new Fiji tool', *Skelet Muscle*, 8: 25.
Maykel, J., J. H. Liu, H. Li, L. D. Shultz, D. L. Greiner, and J. Houghton. 2014. 'NOD-scidIl2rg (tm1Wjl) and NOD-Rag1 (null) Il2rg (tm1Wjl) : a model for stromal cell-tumor cell interaction for human colon cancer', *Dig Dis Sci*, 59: 1169-79.
Mendell, Jerry R., Samiah Al-Zaidy, Richard Shell, W. Dave Arnold, Louise R. Rodino-Klapac, Thomas W. Prior, Linda Lowes, Lindsay Alfano, Katherine Berry, Kathleen Church, John T. Kissel, Sukumar Nagendran, James L'Italien, Douglas M. Sproule, Courtney Wells, Jessica A. Cardenas, Marjet D. Heitzer, Allan Kaspar, Sarah Corcoran, Lyndsey Braun, Shibi Likhite, Carlos Miranda, Kathrin Meyer, K. D. Foust, Arthur H. M. Burghes, and Brian K. Kaspar. 2017. 'Single-Dose Gene-Replacement Therapy for Spinal Muscular Atrophy', *New England Journal of Medicine*, 377: 1713-22.

Mendell, Jerry R., Zarife Sahenk, Samiah Al-Zaidy, Louise R. Rodino-Klapac, Linda P. Lowes, Lindsay N. Alfano, Katherine Berry, Natalie Miller, Mehmet Yalvac, Igor Dvorchik, Melissa Moore-Clingenpeel, Kevin M. Flanigan, Kathleen Church, Kim Shontz, Choumpree Curry, Sarah Lewis, Markus McColly, Mark J. Hogan, and Brian K. Kaspar. 2017. 'Follistatin Gene Therapy for Sporadic Inclusion Body Myositis Improves Functional Outcomes', *Molecular Therapy*, 25: 870-79.

Mendell, Jerry R., Zarife Sahenk, Vinod Malik, Ana M. Gomez, Kevin M. Flanigan, Linda P. Lowes, Lindsay N. Alfano, Katherine Berry, Eric Meadows, Sarah Lewis, Lyndsey Braun, Kim Shontz, Maria Rouhana, Kelly Reed Clark, Xiomara Q. Rosales, Samiah Al-Zaidy, Alessandra Govoni, Louise R. Rodino-Klapac, Mark J. Hogan, and Brian K. Kaspar. 2015. 'A Phase 1/2a Follistatin Gene Therapy Trial for Becker Muscular Dystrophy', *Molecular Therapy*, 23: 192-201.

Meyer, Hemmo, and Conrad C. Weihl. 2014. 'The VCP/p97 system at a glance: connecting cellular function to disease pathogenesis', *Journal of Cell Science*, 127: 3877-83.

Mladenov, E., S. Magin, A. Soni, and G. Iliakis. 2016. 'DNA double-strand-break repair in higher eukaryotes and its role in genomic instability and cancer: Cell cycle and proliferation-dependent regulation', *Semin Cancer Biol*, 37-38: 51-64.

Mohannak, N., G. Pattison, K. Hird, and M. Needham. 2019. 'Dysphagia in Patients with Sporadic Inclusion Body Myositis: Management Challenges', *Int J Gen Med*, 12: 465-74.

Molberg, O., and C. Dobloug. 2016. 'Epidemiology of sporadic inclusion body myositis', *Curr Opin Rheumatol*, 28: 657-60.

Montagne, Janelle M., Xuwen Alice Zheng, Iago Pinal-Fernandez, Jose C. Milisenda, Lisa Christopher-Stine, Thomas E. Lloyd Lloyd, Andrew L. Mammen, and H. Benjamin Larman. 2018. 'Ultra-Efficient Short Read Sequencing of Immune Receptor Repertoires', *bioRxiv*.

Morgan, J. E., G. R. Coulton, and T. A. Partridge. 1989. 'Mdx muscle grafts retain the mdx phenotype in normal hosts', *Muscle Nerve*, 12: 401-9.

Morosetti, R., A. Broccolini, C. Sancricca, C. Gliubizzi, T. Gidaro, P. A. Tonali, E. Ricci, and M. Mirabella. 2010. 'Increased aging in primary muscle cultures of sporadic inclusion-body myositis', *Neurobiol Aging*, 31: 1205-14.

Moussa, C. E., Q. Fu, P. Kumar, A. Shtifman, J. R. Lopez, P. D. Allen, F. LaFerla, D. Weinberg, J. Magrane, T. Aprahamian, K. Walsh, K. M. Rosen, and H. W. Querfurth. 2006. 'Transgenic expression of beta-APP in fast-twitch skeletal muscle leads to calcium dyshomeostasis and IBM-like pathology', *FASEB J*, 20: 2165-7.

MRC, (Medical Research Council). 1976. "Aids to the investigation of the peripheral nervous system." In. London: Her Majesty's Stationary Office.

Mueller, A. L., and R. J. Bloch. 2019. 'Skeletal muscle cell transplantation: models and methods', *J Muscle Res Cell Motil*, epub ahead of print.

Müntzing, K., C. Lindberg, A. R. Moslemi, and A. Oldfors. 2003. 'Inclusion body myositis: Clonal expansions of muscle-infiltrating T cells persist over time', *Scandinavian Journal of Immunology*, 58: 195-200.

Naddaf, E., R. J. Barohn, and M. M. Dimachkie. 2018. 'Inclusion Body Myositis: Update on Pathogenesis and Treatment', *Neurotherapeutics*, 15: 995-1005.

Nagaraju, K., N. Raben, L. Loeffler, T. Parker, P. J. Rochon, E. Lee, C. Danning, R. Wada, C. Thompson, G. Bahtiyar, J. Craft, R. Hooft van Huijsduijnen, and P. Plotz. 2000. 'Conditional up-regulation of MHC class I in skeletal muscle leads to self-sustaining autoimmune myositis and myositis-specific autoantibodies', *Proceedings of the National Academy of Sciences*, 97: 9209-14.

Nalbandian, A., K. J. Llewellyn, M. Badadani, H. Z. Yin, C. Nguyen, V. Katheria, G. Watts, J. Mukherjee, J. Vesa, V. Caiozzo, T. Mozaffar, J. H. Weiss, and V. E. Kimonis. 2013. 'A progressive translational mouse model of human valosin-containing protein disease: the VCP(R155H/+) mouse', *Muscle Nerve*, 47: 260-70.

Namekawa, T., K. Ikeda, K. Horie-Inoue, and S. Inoue. 2019. 'Application of Prostate Cancer Models for Preclinical Study: Advantages and Limitations of Cell Lines, Patient-Derived Xenografts, and Three-Dimensional Culture of Patient-Derived Cells', *Cells*, 8: 74.

Navone, N. M., W. M. van Weerden, R. L. Vessella, E. D. Williams, Y. Wang, J. T. Isaacs, H. M. Nguyen, Z. Culig, G. van der Pluijm, C. A. Rentsch, R. B. Marques, C. M. A. de Ridder, L. Bubendorf, G. N. Thalmann, W. N. Brennen, F. R. Santer, P. L. Moser, P. Shepherd, E. Efstathiou, H. Xue, D. Lin, J. Buijs, T. Bosse, A. Collins, N. Maitland, M. Buzza, M. Kouspou, A. Achtman, R. A. Taylor, G. Risbridger, and E. Corey. 2018. 'Movember GAP1 PDX project: An international collection of serially transplantable prostate cancer patient-derived xenograft (PDX) models', *Prostate*, 78: 1262-82.

Needham, Merrilee, Alastair Corbett, Timothy Day, Frank Christiansen, Vicki Fabian, and Frank L. Mastaglia. 2008. 'Prevalence of sporadic inclusion body myositis and factors contributing to delayed diagnosis', *Journal of Clinical Neuroscience*, 15: 1350-53.

Needham, Merrilee, I. James, A. Corbett, T. Day, F. Christiansen, B. Phillips, and F. L. Mastaglia. 2008. 'Sporadic inclusion body myositis: Phenotypic variability and influence of HLA-DR3 in a cohort of 57 Australian cases', *Journal of Neurology, Neurosurgery and Psychiatry*, 79: 1056-60.

Nishino, H., A. G. Engel, and B. K. Rima. 1989. 'Inclusion body myositis: the mumps virus hypothesis', *Ann Neurol*, 25: 260-4.

No, Daniel, Yadira Valles-Ayoub, Rosangela Carbajo, Zeshan Khokher, Lucia Sandoval, Beth Stein, Mark Andrew Tarnopolsky, Tahseen Mozaffar, Babak Darvish, Marvin Pietruszka, and Daniel Darvish. 2013. 'Novel GNE mutations in autosomal recessive hereditary inclusion body myopathy patients', *Genetic testing and molecular biomarkers*, 17: 376-82.

Nogalska, Anna, Chiara Terracciano, Carla D'Agostino, W. King Engel, and Valerie Askanas. 2009. 'p62/SQSTM1 is overexpressed and prominently accumulated in inclusions of sporadic inclusion-body myositis muscle fibers, and can help differentiating it from polymyositis and dermatomyositis', *Acta Neuropathologica*, 118: 407-13.

Norman, D. J. 1995. 'Mechanisms of action and overview of OKT3', *Ther Drug Monit*, 17: 615-20.

O'Hanlon, T. P., M. C. Dalakas, P. H. Plotz, and F. W. Miller. 1994. 'The alpha beta T-cell receptor repertoire in inclusion body myositis: diverse patterns of gene expression by muscle-infiltrating lymphocytes', *J Autoimmun*, 7: 321-33.

Oh, T. H., K. A. Brumfield, T. L. Hoskin, K. A. Stolp, J. A. Murray, and J. R. Bassford. 2007. 'Dysphagia in inflammatory myopathy: clinical characteristics, treatment strategies, and outcome in 62 patients', *Mayo Clin Proc*, 82: 441-7.

Oldfors, A., N. G. Larsson, C. Lindberg, and E. Holme. 1993. 'Mitochondrial DNA deletions in inclusion body myositis', *Brain*, 116: 325-36.

Oldfors, A., A. R. Moslemi, L. Jonasson, M. Ohlsson, G. Kollberg, and C. Lindberg. 2006. 'Mitochondrial abnormalities in inclusion-body myositis', *Neurology*, 66: S49-S55.

Paix, A., D. Antoni, W. Waissi, M. P. Ledoux, K. Bilger, L. Fornecker, and G. Noel. 2018. 'Total body irradiation in allogeneic bone marrow transplantation conditioning regimens: A review', *Crit Rev Oncol Hematol*, 123: 138-48.

Paltiel, A. D., E. Ingvarsson, D. K. Lee, R. L. Leff, R. J. Nowak, K. D. Petschke, S. Richards-Shubik, A. Zhou, M. Shubik, and K. C. O'Connor. 2015. 'Demographic and clinical features of inclusion body myositis in North America', *Muscle Nerve*, 52: 527-33.

Pandya, J. M., A. E. Fasth, M. Zong, S. Arnardottir, L. Dani, E. Lindroos, V. Malmstrom, and I. E. Lundberg. 2010. 'Expanded T cell receptor Vbeta-restricted T cells from patients with sporadic inclusion body myositis are proinflammatory and cytotoxic CD28null T cells', *Arthritis Rheum*, 62: 3457-66.

Pankiv, Serhiy, Endalkachew A. Alemu, Andreas Brech, Jack Ansgar Bruun, Trond Lamark, Aud Øvervatn, Geir Bjørkøy, and Terje Johansen. 2010. 'FYCO1 is a Rab7 effector that binds to LC3 and PI3P to mediate microtubule plus end - Directed vesicle transport', *Journal of Cell Biology*, 188: 253-69.

Perel, P., I. Roberts, E. Sena, P. Wheble, C. Briscoe, P. Sandercock, M. Macleod, L. E. Mignini, P. Jayaram, and K. S. Khan. 2007. 'Comparison of treatment effects between animal experiments and clinical trials: systematic review', *BMJ*, 334: 197.

Phillips, B. A., L. A. Cala, G. W. Thickbroom, A. Melsom, P. J. Zilko, and F. L. Mastaglia. 2001. 'Patterns of muscle involvement in inclusion body myositis: clinical and magnetic resonance imaging study', *Muscle Nerve*, 24: 1526-34.

Pinal-Fernandez, I., M. Casal-Dominguez, A. Derfoul, K. Pak, P. Plotz, F. W. Miller, J. C. Milisenda, J. M. Grau-Junyent, A. Selva-O'Callaghan, J. Paik, J. Albayda, L. Christopher-Stine, T. E. Lloyd, A. M. Corse, and A. L. Mammen. 2019. 'Identification of distinctive interferon gene signatures in different types of myositis', *Neurology*, 93: e1193-e204.

Pluk, Helma, Bas J. A. Van Hoeve, Sander H. J. Van Dooren, Judith Stammen-Vogelzangs, Annemarie Van Der Heijden, Helenius J. Schelhaas, Marcel M. Verbeek, Umesh A. Badrising, Snjolaug Arnardottir, Karina Gheorghe, Ingrid E. Lundberg, Wilbert C. Boelens, Baziel G. Van Engelen, and Ger J. M. Pruijn. 2013. 'Autoantibodies to cytosolic 5′-nucleotidase 1A in inclusion body myositis', *Annals of Neurology*, 73: 397-407.

Pogoryelova, O., J. A. Gonzalez Coraspe, N. Nikolenko, H. Lochmuller, and A. Roos. 2018. 'GNE myopathy: from clinics and genetics to pathology and research strategies', *Orphanet J Rare Dis*, 13: 70.

Pubmed. 2020. 'PubMed: Inclusion Body Myositis Results by Year', National Center for Biotechnology Information, Accessed 02/02. https://www.ncbi.nlm.nih.gov/pubmed/.

Ramdas, S., and L. Servais. 2020. 'New treatments in spinal muscular atrophy: an overview of currently available data', *Expert Opin Pharmacother*, 21: 307-15.

Ranque-Francois, B., T. Maisonobe, E. Dion, J. C. Piette, M. P. Chauveheid, Z. Amoura, and T. Papo. 2005. 'Familial inflammatory inclusion body myositis', *Annals of the Rheumatic Diseases*, 64: 634-37.

Riederer, Ingo, Elisa Negroni, Maximilien Bencze, Annie Wolff, Ahmed Aamiri, James P. Di Santo, Suse D. Silva-Barbosa, Gillian Butler-Browne, Wilson Savino, and Vincent Mouly. 2012. 'Slowing Down Differentiation of Engrafted Human Myoblasts Into Immunodeficient Mice Correlates With Increased Proliferation and Migration', *Molecular Therapy*, 20: 146-54.

Rietveld, A., L. L. van den Hoogen, N. Bizzaro, S. L. M. Blokland, C. Dahnrich, J. E. Gottenberg, G. Houen, N. Johannsen, T. Mandl, A. Meyer, C. T. Nielsen, P. Olsson, J. van Roon, W. Schlumberger, B. G. M. van Engelen, C. G. J. Saris, and G. J. M. Pruijn. 2018. 'Autoantibodies to Cytosolic 5'-Nucleotidase 1A in Primary Sjogren's Syndrome and Systemic Lupus Erythematosus', *Front Immunol*, 9: 1200.

Ritson, Gillian P., Sara K. Custer, Brian D. Freibaum, Jake B. Guinto, Dyanna Geffel, Jennifer Moore, Waixing Tang, Matthew J. Winton, Manuela Neumann, Q. John, Virginia M. y Lee, Mark S. Forman, and J. Paul Taylor. 2010. 'TDP-43 mediates degeneration in a novel Drosophila model of disease causes by mutations in VCP/p97', 30: 7729-39.

Roberts, Kathryn G., Yongjin Li, Debbie Payne-Turner, Richard C. Harvey, Yung-Li Yang, Deqing Pei, Kelly McCastlain, Li Ding, Charles Lu, Guangchun Song, Jing Ma, Jared Becksfort, Michael Rusch, Shann-Ching Chen, John Easton, Jinjun Cheng, Kristy Boggs, Natalia Santiago-Morales, Ilaria Iacobucci, Robert S. Fulton, Ji Wen, Marcus Valentine, Cheng Cheng, Steven W. Paugh, Meenakshi Devidas, I. Ming Chen, Shalini Reshmi, Amy Smith, Erin Hedlund, Pankaj Gupta, Panduka Nagahawatte, Gang Wu, Xiang Chen, Donald Yergeau, Bhavin Vadodaria, Heather Mulder, Naomi J. Winick, Eric C. Larsen, William L. Carroll, Nyla A. Heerema, Andrew J. Carroll, Guy Grayson, Sarah K. Tasian, Andrew S. Moore, Frank Keller, Melissa Frei-Jones, James A. Whitlock, Elizabeth A. Raetz, Deborah L. White, Timothy P. Hughes, Jaime M. Guidry Auvil, Malcolm A. Smith, Guido Marcucci, Clara D. Bloomfield, Krzysztof Mrózek, Jessica Kohlschmidt, Wendy Stock, Steven M. Kornblau, Marina Konopleva, Elisabeth Paietta, Ching-Hon Pui, Sima Jeha, Mary V. Relling, William E. Evans, Daniela S. Gerhard, Julie M. Gastier-Foster, Elaine Mardis, Richard K. Wilson, Mignon L. Loh, James R. Downing, Stephen P.

Hunger, Cheryl L. Willman, Jinghui Zhang, and Charles G. Mullighan. 2014. 'Targetable Kinase-Activating Lesions in Ph-like Acute Lymphoblastic Leukemia', *New England Journal of Medicine*, 371: 1005-15.

Roda, Ricardo H., Alice B. Schindler, Craig Blackstone, Andrew L. Mammen, Andrea M. Corse, and Thomas E. Lloyd. 2014. 'Laing distal myopathy pathologically resembling inclusion body myositis', *Annals of Clinical and Translational Neurology*, 1: 1053-58.

Rodriguez Cruz, P. M., Y. B. Luo, J. Miller, R. C. Junckerstorff, F. L. Mastaglia, and V. Fabian. 2014. 'An analysis of the sensitivity and specificity of MHC-I and MHC-II immunohistochemical staining in muscle biopsies for the diagnosis of inflammatory myopathies', *Neuromuscul Disord*, 24: 1025-35.

Rohrer, Jonathan D., Jason D. Warren, David Reiman, James Uphill, Jonathan Beck, John Collinge, Martin N. Rossor, Adrian M. Isaacs, and Simon Mead. 2011. 'A novel exon 2 I27V VCP variant is associated with dissimilar clinical syndromes', *Journal of Neurology*, 258: 1494-96.

Rojana-udomsart, Arada, Ian James, Alison Castley, Merrilee Needham, Adrian Scott, Timothy Day, Lynette Kiers, Alastair Corbett, Carolyn Sue, Campbell Witt, Patricia Martinez, Frank Christiansen, and Frank Mastaglia. 2012. 'High-resolution HLA-DRB1 genotyping in an Australian inclusion body myositis (s-IBM) cohort: An analysis of disease-associated alleles and diplotypes', *Journal of Neuroimmunology*, 250: 77-82.

Roos, A., C. Preusse, D. Hathazi, H. H. Goebel, and W. Stenzel. 2019. 'Proteomic Profiling Unravels a Key Role of Specific Macrophage Subtypes in Sporadic Inclusion Body Myositis', *Front Immunol*, 10: 1040.

Rose, M. R., and ENMC. 2013. '188th ENMC International Workshop: Inclusion Body Myositis, 2-4 December 2011, Naarden, The Netherlands', *Neuromuscul Disord*, 23: 1044-55.

Rosenbohm, A., D. Buckert, J. Kassubek, W. Rottbauer, A. C. Ludolph, and P. Bernhardt. 2020. 'Sporadic inclusion body myositis: no specific cardiac involvement in cardiac magnetic resonance tomography', *J Neurol*: epub ahead of print.

Roses, Allen D., Michael W. Lutz, Donna G. Crenshaw, Iris Grossman, Ann M. Saunders, and W. Kirby Gottschalk. 2013. 'TOMM40 and APOE: Requirements for replication studies of association with age of disease onset and enrichment of a clinical trial', *Alzheimer's and Dementia*, 9: 132-6.

Rothwell, Simon, Robert G. Cooper, Ingrid E. Lundberg, Peter K. Gregersen, Michael G. Hanna, Pedro M. Machado, Megan K. Herbert, Ger J. M. Pruijn, James B. Lilleker, Mark Roberts, John Bowes, Michael F. Seldin, Jiri Vencovsky, Katalin Danko, Vidya Limaye, Albert Selva-O'Callaghan, Hazel Platt, Øyvind Molberg, Olivier Benveniste, Timothy R. D. J. Radstake, Andrea Doria, Jan De Bleecker, Boel De Paepe, Christian Gieger, Thomas Meitinger, Juliane Winkelmann, Christopher I. Amos, William E. Ollier, Leonid Padyukov, Annette T. Lee, Janine A. Lamb, Hector Chinoy, Christopher Denton, Karina Gheorghe, David Hilton-Jones, Patrick Kiely, and Herman Mann. 2017. 'Immune-Array Analysis in Sporadic Inclusion Body Myositis Reveals HLA–DRB1 Amino Acid Heterogeneity Across the Myositis Spectrum', *Arthritis and Rheumatology*, 69: 1090-99.

Rothwell, Simon, Robert G. Cooper, Ingrid E. Lundberg, Frederick W. Miller, Peter K. Gregersen, John Bowes, Jiri Vencovsky, Katalin Danko, Vidya Limaye, Albert Selva-O'Callaghan, Michael G. Hanna, Pedro M. Machado, Lauren M. Pachman, Ann M. Reed, Lisa G. Rider, Joanna Cobb, Hazel Platt, Øyvind Molberg, Olivier Benveniste, Pernille Mathiesen, Timothy Radstake, Andrea Doria, Jan De Bleecker, Boel De Paepe, Britta Maurer, William E. Ollier, Leonid Padyukov, Terrance P. O'Hanlon, Annette Lee, Christopher I. Amos, Christian Gieger, Thomas Meitinger, Juliane Winkelmann, Lucy R. Wedderburn, Hector Chinoy, Janine A. Lamb, and Consortium Myositis Genetics. 2016. 'Dense genotyping of immune-related loci in idiopathic inflammatory myopathies confirms HLA alleles as the strongest genetic risk factor and suggests different genetic background for major clinical subgroups', *Annals of the Rheumatic Diseases*, 75: 1558-66.

Rubio-Viqueira, B., and M. Hidalgo. 2009. 'Direct in vivo xenograft tumor model for predicting chemotherapeutic drug response in cancer patients', *Clinical Pharmacology & Therapeutics*, 85: 217-21.
Ruparelia, Avnika A., Viola Oorschot, Georg Ramm, and Robert J. Bryson-Richardson. 2016. 'FLNC myofibrillar myopathy results from impaired autophagy and protein insufficiency', *Human Molecular Genetics*, 25: 2131-42.
Rygaard, J., and C. O. Povlsen. 1969. 'Heterotransplantation of a human malignant tumour to "Nude" mice', *Acta Pathol Microbiol Scand*, 77: 758-60.
Rygiel, K. A., J. Miller, J. P. Grady, M. C. Rocha, R. W. Taylor, and D. M. Turnbull. 2015. 'Mitochondrial and inflammatory changes in sporadic inclusion body myositis', *Neuropathology and Applied Neurobiology*, 41: 288-303.
Sako, Dianne, Asya V. Grinberg, June Liu, Monique V. Davies, Roselyne Castonguay, Silas Maniatis, Amy J. Andreucci, Eileen G. Pobre, Kathleen N. Tomkinson, Travis E. Monnell, Jeffrey A. Ucran, Erik Martinez-Hackert, R. Scott Pearsall, Kathryn W. Underwood, Jasbir Seehra, and Ravindra Kumar. 2010. 'Characterization of the ligand binding functionality of the extracellular domain of activin receptor type IIB', *Journal of Biological Chemistry*, 285: 21037-48.
Salajegheh, M., G. Rakocevic, R. Raju, A. Shatunov, L. G. Goldfarb, and M. C. Dalakas. 2007. 'T cell receptor profiling in muscle and blood lymphocytes in sporadic inclusion body myositis', *Neurology*, 69: 1672-79.
Salajegheh, Mohammad, Theresa Lam, and Steven A. Greenberg. 2011. 'Autoantibodies against a 43 kDa muscle protein in inclusion body myositis', *PloS one*, 6: 5-7.
Salajegheh, Mohammad, Jack L. Pinkus, J. Paul Taylor, A. Amato, Remedios Nazareno, Robert H. Baloh, and A. Steven. 2009. 'Sarcoplasmic Redistribution of Nuclear TDP-43 in Inclusion Body Myositis', *Muscle and Nerve*, 40: 19-31.
Sass, F. A., M. Fuchs, M. Pumberger, S. Geissler, G. N. Duda, C. Perka, and K. Schmidt-Bleek. 2018. 'Immunology Guides Skeletal Muscle Regeneration', *Int J Mol Sci*, 19: 835.
Scherer, W. F., J. T. Syverton, and G. O. Gey. 1953. 'Studies on the propagation in vitro of poliomyelitis viruses. IV. Viral multiplication in a stable strain of human malignant epithelial cells (strain HeLa) derived from an epidermoid carcinoma of the cervix', *J Exp Med*, 97: 695-710.
Schiaffino, S., A. C. Rossi, V. Smerdu, L. A. Leinwand, and C. Reggiani. 2015. 'Developmental myosins: expression patterns and functional significance', *Skelet Muscle*, 5: 22.
Schindelin, J., I. Arganda-Carreras, E. Frise, V. Kaynig, M. Longair, T. Pietzsch, S. Preibisch, C. Rueden, S. Saalfeld, B. Schmid, J. Y. Tinevez, D. J. White, V. Hartenstein, K. Eliceiri, P. Tomancak, and A. Cardona. 2012. 'Fiji: an open-source platform for biological-image analysis', *Nat Methods*, 9: 676-82.
Schmidt, Jens. 2018. 'Current Classification and Management of Inflammatory Myopathies', *Journal of Neuromuscular Diseases*, 5: 109-29.
Scott, Adrian P., Nigel G. Laing, Frank Mastaglia, Marinos Dalakas, Merrilee Needham, and Richard J. N. Allcock. 2012. 'Investigation of NOTCH4 coding region polymorphisms in sporadic inclusion body myositis', *Journal of Neuroimmunology*, 250: 66-70.
Sekul, E. A., C. Chow, and M. C. Dalakas. 1997. 'Magnetic resonance imaging of the forearm as a diagnostic aid in patients with sporadic inclusion body myositis', *Neurology*, 48: 863-6.
Silva-Barbosa, Suse Dayse, Gillian S. Butler-Browne, James P. Di Santo, and Vincent Mouly. 2005. 'Comparative analysis of genetically engineered immunodeficient mouse strains as recipients for human myoblast transplantation', *Cell Transplantation*, 14: 457-67.
Sivakumar, Kumaraswamy, Christina Semino-Mora, and Marinos C. Dalakas. 1997. 'An inflammatory, familial, inclusion body myositis with autoimmune features and a phenotype identical to sporadic inclusion body myositis: Studies in three families', *Brain*, 120: 653-61.

Spector, S. A., J. T. Lemmer, B. M. Koffman, T. A. Fleisher, I. M. Feuerstein, B. F. Hurley, and M. C. Dalakas. 1997. 'Safety and efficacy of strength training in patients with sporadic inclusion body myositis', *Muscle & nerve*, 20: 1242-8.
Spina, S., A. D. Van Laar, J. R. Murrell, R. L. Hamilton, J. K. Kofler, F. Epperson, M. R. Farlow, O. L. Lopez, J. Quinlan, S. T. DeKosky, and B. Ghetti. 2013. 'Phenotypic variability in three families with valosin-containing protein mutation', *Eur J Neurol*, 20: 251-58.
Suetta, C., U. Frandsen, A. L. Mackey, L. Jensen, L. G. Hvid, M. L. Bayer, S. J. Petersson, H. D. Schroder, J. L. Andersen, P. Aagaard, P. Schjerling, and M. Kjaer. 2013. 'Ageing is associated with diminished muscle re-growth and myogenic precursor cell expansion early after immobility-induced atrophy in human skeletal muscle', *J Physiol*, 591: 3789-804.
Sun, M., W. Bell, K. D. LaClair, J. P. Ling, H. Han, Y. Kageyama, O. Pletnikova, J. C. Troncoso, P. C. Wong, and L. L. Chen. 2017. 'Cryptic exon incorporation occurs in Alzheimer's brain lacking TDP-43 inclusion but exhibiting nuclear clearance of TDP-43', *Acta Neuropathol*, 133: 923-31.
Suzuki, N., M. Mori-Yoshimura, S. Yamashita, S. Nakano, K. Y. Murata, Y. Inamori, N. Matsui, E. Kimura, H. Kusaka, T. Kondo, I. Higuchi, R. Kaji, M. Tateyama, R. Izumi, H. Ono, M. Kato, H. Warita, T. Takahashi, I. Nishino, and M. Aoki. 2016. 'Multicenter questionnaire survey for sporadic inclusion body myositis in Japan', *Orphanet J Rare Dis*, 11: 146.
Tawara, N., S. Yamashita, X. Zhang, M. Korogi, Z. Zhang, T. Doki, Y. Matsuo, S. Nakane, Y. Maeda, K. Sugie, N. Suzuki, M. Aoki, and Y. Ando. 2017. 'Pathomechanisms of anti-cytosolic 5'-nucleotidase 1A autoantibodies in sporadic inclusion body myositis', *Ann Neurol*, 81: 512-25.
Tidball, J. G. 2017. 'Regulation of muscle growth and regeneration by the immune system', *Nat Rev Immunol*, 17: 165-78.
Tracey, A. T., K. S. Murray, J. A. Coleman, and K. Kim. 2020. 'Patient-Derived Xenograft Models in Urological Malignancies: Urothelial Cell Carcinoma and Renal Cell Carcinoma', *Cancers (Basel)*, 12: E439.
Uruha, A., S. Noguchi, Y. K. Hayashi, R. S. Tsuburaya, T. Yonekawa, I. Nonaka, and I. Nishino. 2016. 'Hepatitis C virus infection in inclusion body myositis: A case-control study', *Neurology*, 86: 211-7.
Villalta, S. A., W. Rosenthal, L. Martinez, A. Kaur, T. Sparwasser, J. G. Tidball, M. Margeta, M. J. Spencer, and J. A. Bluestone. 2014. 'Regulatory T cells suppress muscle inflammation and injury in muscular dystrophy', *Sci Transl Med*, 6: 258ra142.
Vogler, T. O., J. R. Wheeler, E. D. Nguyen, M. P. Hughes, K. A. Britson, E. Lester, B. Rao, N. D. Betta, O. N. Whitney, T. E. Ewachiw, E. Gomes, J. Shorter, T. E. Lloyd, D. S. Eisenberg, J. P. Taylor, A. M. Johnson, B. B. Olwin, and R. Parker. 2018. 'TDP-43 and RNA form amyloid-like myo-granules in regenerating muscle', *Nature*, 563: 508-13.
Wang, Y., G. C. Melkani, J. A. Suggs, A. Melkani, W. A. Kronert, A. Cammarato, and S. I. Bernstein. 2012. 'Expression of the inclusion body myopathy 3 mutation in Drosophila depresses myosin function and stability and recapitulates muscle inclusions and weakness', *Mol Biol Cell*, 23: 2057-65.
Wanschitz, Julia V., Odile Dubourg, Emmanuelle Lacene, Michael B. Fischer, Romana Höftberger, Herbert Budka, Norma B. Romero, Bruno Eymard, Serge Herson, Gillian S. Butler-Browne, Thomas Voit, and Olivier Benveniste. 2013. 'Expression of myogenic regulatory factors and myo-endothelial remodeling in sporadic inclusion body myositis', *Neuromuscular Disorders*, 23: 75-83.
Watt, D. J., J. E. Morgan, M. A. Clifford, and T. A. Partridge. 1987. 'The movement of muscle precursor cells between adjacent regenerating muscles in the mouse', *Anat Embryol (Berl)*, 175: 527-36.
Watts, Giles D. J., Jill Wymer, Margaret J. Kovach, Sarju G. Mehta, Steven Mumm, Daniel Darvish, Alan Pestronk, Michael P. Whyte, and Virginia E. Kimonis. 2004. 'Inclusion body

myopathy associated with Paget disease of bone and frontotemporal dementia is caused by mutant valosin-containing protein', *Nature Genetics*, 36: 377-81.
Weihl, C. C., and A. L. Mammen. 2017. 'Sporadic inclusion body myositis – a myodegenerative disease or an inflammatory myopathy', *Neuropathology and Applied Neurobiology*, 43: 82-91.
Weihl, Conrad C., Robert H. Baloh, Youjin Lee, Tsui Fen Chou, Sara K. Pittman, Glenn Lopate, Peggy Allred, Jennifer Jockel-Balsarotti, Alan Pestronk, and Matthew B. Harms. 2015. 'Targeted sequencing and identification of genetic variants in sporadic inclusion body myositis', *Neuromuscular Disorders*, 25: 289-96.
Weihl, Conrad C., Sara E. Miller, Phyllis I. Hanson, and Alan Pestronk. 2007. 'Transgenic expression of inclusion body myopathy associated mutant p97/VCP causes weakness and ubiquitinated protein inclusions in mice', *Human Molecular Genetics*, 16: 919-28.
Wintzen, A. R., G. T. Bots, H. M. de Bakker, J. H. Hulshof, and G. W. Padberg. 1988. 'Dysphagia in inclusion body myositis', *J Neurol Neurosurg Psychiatry*, 51: 1542-5.
Wong, C. H., K. W. Siah, and A. W. Lo. 2019. 'Estimation of clinical trial success rates and related parameters', *Biostatistics*, 20: 273-86.
Wunderlich, Mark, Ryan A. Brooks, Rushi Panchal, Garrett W. Rhyasen, Gwenn Danet-Desnoyers, and James C. Mulloy. 2014. 'OKT3 prevents xenogeneic GVHD and allows reliable xenograft initiation from unfractionated human hematopoietic tissues', *Blood*, 123: e134-44.
Yunis, E. J., and F. J. Samaha. 1971. 'Inclusion body myositis', *Lab Invest*, 25: 240-8.
Zammit, P. S. 2017. 'Function of the myogenic regulatory factors Myf5, MyoD, Myogenin and MRF4 in skeletal muscle, satellite cells and regenerative myogenesis', *Semin Cell Dev Biol*, 72: 19-32.
Zhang, Y., O. D. King, F. Rahimov, T. I. Jones, C. W. Ward, J. P. Kerr, N. Liu, C. P. Emerson, Jr., L. M. Kunkel, T. A. Partridge, and K. R. Wagner. 2014. 'Human skeletal muscle xenograft as a new preclinical model for muscle disorders', *Hum Mol Genet*, 23: 3180-8.
Zhang, Z., W. Hu, L. Li, H. Ding, and H. Li. 2018. 'Therapeutic monoclonal antibodies and clinical laboratory tests: When, why, and what is expected?', *J Clin Lab Anal*, 32: e22307.

Curriculum Vita

Kyla A. Britson

The Johns Hopkins University School of Medicine
Department of Neurology
855 N Wolfe St., John G. Rangos Building, Rm 294
Baltimore, MD 21205
Email: kbritso1@jhmi.edu

Education

B.S.	2013	Major: Genetics, Cell Biology, and Development University of Minnesota-Twin Cities
Ph.D.	2020	Program in Cellular and Molecular Medicine Mentor: Thomas E. Lloyd

Professional Experience

09/2009 - 05/2013	Laboratory Technician, University of Minnesota: Lab of Dr. Paul Mermelstein
05/2011 - 08/2011	Summer Undergraduate Researcher, Michigan State University: Lab of Dr. Steven van Nocker
05/2012 - 08/2012	Summer Undergraduate Research Fellow, Mayo Clinic: Lab of Dr. Michael Berry
06/2013 - 06/2015	Research Technologist, Johns Hopkins University: Lab of Dr. Deborah Andrew
08/2015 - 03/2020	Doctoral thesis research, Johns Hopkins University: Lab of Dr. Thomas E. Lloyd

Fellowships and Funding

03/2019	Global Conference on Myositis Junior Fellowship funding totaling 850 EUR to attend conference
10/2019	World Muscle Society Fellowship funding totaling 1000 EUR to attend conference
07/2019-07/2020	The pathogenesis and treatment of inclusion body myositis in a xenograft model Myositis UK (Registered Charity No. 327791) Speed Funding Award, 15,000EUR Role: PI

Honors

2009 - 2013	College of Biological Science Deans List: fall and spring of 2009, 2010, 2011, 2012, and spring of 2013, University of Minnesota
2009 - 2010	Florence Sinclair Scholarship, University of Minnesota
2012 - 2013	College of Biological Sciences Annual Giving Scholarship, University of Minnesota
2013	Bachelor of Science with high distinction, University of Minnesota
2019	Best Oral Presentation, Global Conference on Myositis

Professional Memberships

2018 -	Member, The Myositis Association
2019-	Member, World Muscle Society

Publications, peer reviewed

Meitzen J, Luoma JI, Boulware MI, Hedges VL, Peterson BM, Tuomela K, Britson KA, Mermelstein PG. Palmitoylation of estrogen receptors is essential for neuronal membrane signaling. Endocrinology. (2013) 154(11): 4293-4304. doi: 10.1210/en.2013-1172

Meitzen J, Britson KA, Tuomela K, Mermelstein PG. The expression of select genes necessary for membrane-associated estrogen receptor signaling differ by sex in adult rat hippocampus. Steroids. (2017) doi: 10.1016/j.steroids.2017.09.012

Britson KA, Yang SY, Lloyd TE. New developments in the genetics of Inclusion Body Myositis. Current Rheumatology Reports. (2018) 20(5):26. doi: 10.1007/s11926-018-0738-0

Vogler TO, Wheeler JR, Nguyen ED, Hughes MP, Britson KA, Lester E, Rao B, Betta ND, Whitney ON, Ewachiw TE, Gomes E, Shorter J, Lloyd TE, Eisenberg DS, Taylor JP, Johnson AM, Olwin BB, Parker R. TDP-43 and RNA form amyloid-like myo-granules in regenerating muscle. Nature. 2018 Nov 22; 563(7732): 508-513. doi: 10.1038/s41586-018-0665-2.

Britson KA, Black AD, Wagner KR, Lloyd TE. Performing Human Skeletal Muscle Xenografts in Immunodeficient Mice. J. Vis. Exp. 2019 Sep 16; (151). doi: 10.3791/59966.

Publications, non-peer reviewed

Britson KA 2017-2020. Bi-Monthly Blog posts. *The Biomedical Odyssey Blog*. https://biomedicalodyssey.blogs.hopkinsmedicine.org/

Published abstracts presented at International Meetings

Britson KA, Russell K, Wagner KR, Ostrow LW, Lloyd TE. Human skeletal muscle xenografts to model sporadic inclusion body myositis. BMJ. 2018 June 15; FRI0415 (Annual European Congress of Rheumatology, Amsterdam).

Britson KA, Russell K,Tsao W, Montagne J, Larman HB, Wagner KR, Ostrow LW, Lloyd TE. Lloyd. Xenograft model of sporadic inclusion body myositis. Neuromuscular Disorders. 2019 Oct 29; S46P.17. (World Muscle Society conference).

Oral Presentations

GCOM 2019 Biannual Meeting
Title: Xenograft Model of Sporadic Inclusion Body Myositis
Authors: Britson KA, Russell K, Tsao W, Montagne J, Larman B, Wagner KR, Ostrow LW, Lloyd TE.
Date: 03/27/2019

GCOM 2019 Biannual Meeting Speed Funding Session
Title: The Pathogenesis and Treatment of Inclusion Body Myositis in a Xenograft Model
Author: Britson KA
Date: 03/28/2019

Poster Presentations

Cellular and Molecular Medicine Program Annual Retreat 2017
Title: Of Mice and Men and Flies: Investigating the Pathogenesis of Inclusion Body Myositis
Authors: Britson KA, Wagner KR, Lloyd TE.
Date: 9/14/2017

ASCB-EMBO Annual Meeting 2017
Title: Filamin and Valosin Containing Protein Interaction in Inclusion Body Myositis
Authors: Britson KA, Michelle H, Castro C, Aksentijevich I, Schiffenbaurer A, Mankodi A, Kastner D, Mammen A, Weihl CC, Siegel R, Lloyd TE.
Date: 12/3/2017

EULAR Annual Meeting 2018
Title: Human skeletal muscle xenografts to model sporadic inclusion body myositis.
Authors: Britson KA, Russell K, Wagner KR, Ostrow LW, Lloyd TE.
Date: 06/15/2018

WMS 2019 Annual Meeting
Title: Xenograft model of sporadic inclusion body myositis
Authors: Britson KA, Russell K, Tsao W, Montagne J, Larman B, Wagner KR, Ostrow LW, Lloyd TE.
Date: 10/2/2019

Service and Leadership

Leader and Co-founder of Hopkins Hikers, 08/2017 to Present
Johns Hopkins School of Medicine, Graduate Student Association recognized student organization - Baltimore, MD

As a co-founder and leader of Hopkins Hikers, I coordinate monthly hikes in the greater Baltimore area and organize the group's Meetup page. The goal of Hopkins Hikers is to bring together both avid and aspiring outdoor enthusiasts in the Johns Hopkins community and provide a platform to explore everything the greater Baltimore area has to offer.

Volunteer for Baltimore Animal Care and Rescue Shelter, 08/2015 to Present
BARCs - Baltimore, MD

Once a week, I provide care for animals located at satellite locations and promote their adoption.

Volunteer for Project Bridge, 06/2017 to 09/2019
Johns Hopkins School of Medicine, Graduate Student Association recognized student organization - Baltimore, MD

Project Bridge is a graduate student group that engages in a variety of community outreach programs with a focus on scientific communication. I work on both the "Science at the Market" and "Science Communication" subcommittees, which promote scientific discourse with the Baltimore community.

Violinist, 08/2013 to 05/2019
Hunt Valley Symphony Orchestra (HVSO) - Baltimore, MD

I have been performing with the HVSO since moving to Baltimore in 2013. The Hunt Valley Symphony Orchestra is a non-profit 501c3 organization that was created in 2013 with the vision of creating a professional level, non-profit community orchestra & chorale in the greater Baltimore area.